The modern sediments of Lake Oeschinen (Swiss Alps) as an archive for climatic and meteorological events

Master's Thesis

Faculty of Science

University of Bern

presented by

Fabian Mauchle

2010

Supervisor:

Prof. Dr. Martin Grosjean

Institute of Geography and Oeschger Centre for Climate Change Research

Advisor:

Dr. Mathias Trachsel

Institute of Geography and Oeschger Centre for Climate Change Research

Lake Oeschinen, Fabian Mauchle, 2010

Table of contents

Summary XI
Zusammenfassung XIII
1. Introduction 1
1.1. Research motivation and general objectives 1
1.2. State of knowledge 2
1.3. Research questions and working hypothesis 3
1.4. Project design 5
1.5. Thesis outline 5
2. Study site - Lake Oeschinen 7
2.1. Geographical setting 7
2.2. Physical characteristics of Lake Oeschinen 7
2.3. Climate 7
2.4. Geological setting 9
2.5. Hydrology 10
3. Material and Methods 11
3.1. Process study 11
3.1.1. Fieldwork – Collecting delta fan sediments 11
3.1.1.1. X-Ray powder diffraction (XRD) 11
3.1.2. Sediment traps 12
3.1.2.1. Grain size analysis – Laser diffraction 13
3.1.2.2. Mineralogy - X-ray diffraction smear slides 13
3.2. Recovery and analysis of the mastercore 13
3.2.1. Chronology 14
3.2.1.1. Radionuclide dating - ^{210}Pb and ^{137}Cs 14
3.2.1.2. Spheroidal carbonaceous particles (SCP) 14
3.2.2. Resin blocks and thin sections 15
3.2.3. Micro-X-ray fluorescence elemental mapping 15
3.2.4. X-ray fluorescence scans (XRF) 16
3.2.5. Establishment of the varve chronology and varve counts 16
3.3. Meteorological data 17
3.4. Statistical analyses 18
4. Results and Interpretation 19
4.1. Process study 19
4.1.1. Mineralogy of the creek deltas 19
4.1.2. Mineralogical and elemental signals from the catchment 21
4.2. Sediment traps 22
4.2.1. Particle flux 22
4.2.2. Mineralogy of trapped particles 22

4.3. Interpretation of interannual sedimentation processes 24
4.4. Hypothesis for varve formation 24
4.5. Sediment record – mastercore 26
4.5.1. Core description and sedimentary facies 26
4.5.2. Sediment chronology 30
4.5.2.1. ^{210}Pb and ^{137}Cs 30
4.5.2.2. Spheroidal carbonaceous particle counts 32
4.5.2.3. Varve counts 32
4.6. Comparison of varve thickness with instrumental data 34
4.6.1. Entire varve record AD 1907 - 1986 34
4.6.2. Varve record AD 1920 - 1986 34
5. Discussion 37
5.1. Chronology 37
5.2. Sediment composition and proxy interpretation 39
5.3. Working hypothesis – Climate controls on varve formation 40
5.4. Comparison with Leemann (1993) and other studies 42
6. Conclusions and Outlook 45
6.1. Conclusions 45
6.2. Outlook 46
Acknowledgements 47
References 48
Appendix A 53
Appendix B 64

List of figures

Figure 1: Study design of the Thesis. 4
Figure 2: Maps showing the location of the study site. 8
Figure 3: Geological map showing the regional setting of the catchment area of Lake Oeschinen 9
Figure 4: Map showing the alluvial fans (dotted areas) around the shoreline of Lake Oeschinen 11
Figure 5: X-ray diffractograms showing the mineralogy of the delta fan sediments 19
Figure 6: Mineralogy of the delta sediments around the shoreline of Lake Oeschinen. 20
Figure 7: Mineralogical and elemental signals from the catchment. 21
Figure 8: XRD diffractogram with qualitative mineralogical compositions of trapped particles 22
Figure 9: Sediment trap data from May 2007 to June 2008 23
Figure 10: Hypothetical varve formation. 25
Figure 11: Composite photographs of the freeze core Oeschi 07-3 27
Figure 12: Geochemical and mineralogical characteristics of facies A. 28
Figure 13 Photographs of 3 different varve types found in the sediment record 29
Figure 14 Photographs of the turbidites T10 and T12 29
Figure 15: Geochemical and mineralogical characteristics of facies B 30
Figure 16: ^{210}Pb and ^{137}Cs activities in the mastercore 31
Figure 17: Comparison of the CRS and ^{137}Cs-AD 1963-constrained CRS age-depth models. 31
Figure 18: SCP profile of the sediment core Oeschi 07-3 32
Figure 19: Varve counts of the top 50 cm of the mastercore 33
Figure 20: Comparison of the varve thickness (AD 1907 -1986) with cumulative summer precipitation . . 35
Figure 21: Chronology of the mastercore Oeschi 07-3. 38
Figure 22: Parameters that likely influenced varve formation from AD 1907-1986. 40
Figure 23: ^{210}Pb sampling 66

List of tables

Table 1: Subdivision of the catchment according to physical properties. 10
Table 2: Correlation coefficients r between different meteorological records. 17
Table 3: Coring locations 26
Table 4: Correlation coefficients r between varve thickness and summer precipitation 34
Table 5: Comparison of correlation coefficients r from Leemann (1993) and this study 42
Table A1: Raw sediment trap data 53
Table A2: Grain size data of trapped particles 53
Table A3: Raw XRD data from the delta sediments in alphabetical order. 54
Table B1: Raw ^{210}Pb and ^{137}Cs data 64
Table B2: Raw data SCP counts 67
Table B3: Varve thickness from AD 1907- 1986. 69

List of Abbreviations

AD	Anno Domini
cal	Calcite
chl	Chlorite
CIC	Constant Initial Concentration
CRS	Constant Rate of Supply
DF	Degrees of Freedom
dol	Dolomite
EAWAG	Swiss Federal Institute of Aquatic Science and Technology
ETH	Swiss Federal Institute of Technology
ill	Illite
IPCC	Intergovernmental Panel on Climate Change
JJA	June, July, August
K-fs	K-feldspar
LIA	Little Ice Age
LiF	Lithium fluoride
MJ	May, June
MJJA	May, June, July, August
MJJAS	May, June, July, August, September
NAO	North Atlantic Oscillation
pp	Precipitation
pl	Plagioclase
qz	Quartz
SCP	Spheroidal Carbonaceous Particle
SON	September, October, November
TT	Temperature
TIC	Total inorganic carbon
XRD	X-Ray Diffraction
XRF	X-Ray Fluorescence

Summary

Investigating paleoclimate archives, such as lake sediments, is fundamental for placing the period of human induced global warming into a long-term perspective. Due to their nearly seasonal resolution, annually layered sediments (varves) have great potential for transforming climate sensitive proxy data into quantitative estimates of past climatic conditions.

This Thesis investigates the varved sedimentary record of Lake Oeschinen (46°30'N, 7°44'E, 1580 m a.s.l.), which is located in the Bernese Alps. The aims of this study were to test the working hypothesis that varve thickness is primarily controlled by cumulative summer precipitation and to check whether physical proxy data could be used for the calibration against instrumental meteorological data.

A process-study was conducted to gain knowledge about varve formation in Lake Oeschinen by analyzing sediment trap data and the mineralogy of the shoreline and delta fan sediments. We used high-resolution XRF data from the top 50 cm of a sediment core for the identification of sedimentary facies. Varve thickness of an 80-yr long record (AD 1907-1986) was compared with meteorological parameters in order to detect the main climate factors that control sediment supply to Lake Oeschinen.

We identified the contrasts in the catchment geology and associated climate-sensitive erosional and sedimentation processes as the major factors that determine varve formation in Lake Oeschinen. The source of sedimentary particles could be traced using diagnostic mineralogical (calcite/quartz) and elemental ratios (Ca/Si): low Ca/Si ratios (~3.6) indicated that particles originated from the non-glaciated, northern catchment (Tertiary Flysch deposits). High Ca/Si ratios (~13.1), in contrast, denoted that the particles originated from the southern, glaciated catchment. Sediment analysis revealed that two different facies were present in the mastercore. Sedimentary facies A was characterized by rhythmically laminated sediments (varves) that alternately comprised sandy (summer) and clay-rich (winter) laminae. Facies A could be subdivided into 3 distinctive varve types that comprised one or multiple fining upward sequences (micro laminations) with low Ca/Si ratios. Particles in the summer laminae therefore mainly originate from the northern catchment (Flysch). Winter laminae, in contrast, comprised very fine-grained calcite particles (high Ca/Si ratios) that were probably eroded from the bedrock by the glaciers and released due to ice melt during summer. Ca/Si peaks (winter layers) denoted the boundaries between individual varves and were therefore fundamental for counting varves. Facies B represents graded event layers (turbidites) that were probably caused by heavy summer rainstorms.

Our results suggest that varve thickness in Lake Oeschinen was primarily controlled by cumulative summer precipitation (MJJA) ($r=0.64$ at $p< 0.05$, means for AD 1920-1986). Therefore, the working hypothesis was verified. However, the results also suggested that other low and high frequency climate signals are preserved in the varves.

The varve thickness time series provided by this Thesis is an ideal basis for further statistical analyses. A multivariate approach (e.g. principal component regression analysis) would help to achieve a more realistic estimate of the factors that control varve formation in Lake Oeschinen. Furthermore, the occurrence of 12 turbidites in the analyzed period (AD 1907 – 2007) showed that the catchment area of Lake Oeschinen is very sensitive to flood events. The sedimentary record of Lake Oeschinen has therefore great potential for reconstructing the frequency and intensities of flood events in the Bernese Alps throughout the mid- to late Holocene.

Zusammenfassung

Die Untersuchung von natürlichen Klimaarchiven wie Seesedimenten ist unverzichtbar für eine Einordnung der Zeitspanne des anthropogen verursachten Klimawandels in eine längerfristige zeitliche Perspektive. Jährlich geschichtete Seesedimente (Warven) bieten dank ihrer saisonalen bis jährlichen zeitlichen Auflösung die Möglichkeit, klima-sensitive Proxydaten als quantitative Messgrössen vergangener klimatischer Bedingungen auszudrücken.

In dieser Masterarbeit wurden die gewarvten Sedimente des Oeschinensees (46°30´N, 7°44´ E, 1580 m ü.M.) untersucht, welcher sich in den Berner Alpen befindet. Das Ziel dieser Studie war das Testen der Arbeitshypothese, dass die Warvendicke primär durch den kumulativen Sommerniederschlag gesteuert wird. Zudem sollte die Frage beantwortet werden, ob sich physische Proxydaten aus den Sedimenten für eine Kalibration mit instrumentellen meteorologischen Daten eignen.

Zu Beginn dieser Arbeit wurde eine Prozessstudie (Sedimentfallen und Analyse der Mineralogie von Deltasedimenten) durchgeführt, um die Warvenbildungsprozesse im Oeschinensee zu verstehen. Hochauflösende Röntgenfluoreszenz (XRF) Daten einer 50 cm langen Sedimentsequenz wurden für die Identifizierung sedimentärer Fazies verwendet. Eine 80 Jahre umfassende Zeitreihe der Mächtigkeiten einzelner Jahreslagen (AD 1907 – 1986) wurde anschliessend mit meteorologischen Parametern verglichen, um die Hauptfaktoren zu ermitteln, welche die Sediment-mobilisierenden Prozesse im Einzugsgebiet steuern.

Gegensätzliche geologische Einheiten im Einzugsgebiet und damit verbundene klima-sensitive Erosions- und Sedimentationsprozesse wurden als Hauptfaktoren erkannt, welche die Warvenbildung im Oeschinensee bestimmen. Die Herkunft von Sedimentpartikeln konnte mit diagnostischen Mineral- und Elementverhältnissen (z.B. Kalzit/Quarz und Ca/Si) abgeschätzt werden. Tiefe Ca/Si Verhältnisse (~3.6) zeigen an, dass die Partikel vom unvergletscherten, nördlichen Einzugsgebiet stammen (Tertiärer Flysch). Hohe Ca/Si Verhältnisse zeigen hingegen an, dass die Herkunft der Partikel dem südlichen, vergletscherten Einzugsgebiet zuzuschreiben ist. Die Sedimentanalysen haben aufgezeigt, dass im Sedimentkern zwei unterschiedliche sedimentäre Fazies vorkommen. Fazies A ist charakterisiert durch rhythmisch laminierte Sedimente (Warven) welche alternierend sandige (Sommer) und tonreiche (Winter) Laminae aufweisen. Fazies A konnte zudem in 3 weitere Subtypen unterteilt werden, welche durch eine einzige oder mehrere Kornverfeinerungssequenzen (fining upward sequences, Mikrolaminationen) sowie tiefe Ca/Si Verhältnissen charakterisiert sind. Sedimentpartikel in den Sommerlagen stammen deshalb hauptsächlich aus dem nördlichen Einzugsgebiet (Tertiärer Flysch). Die Winterlagen hingegen enthalten hauptsächlich feinkörnige Kalzitpartikel (hohe Ca/Si Verhältnisse) und sind deshalb als Sedimente anzusprechen, welche wahrscheinlich durch die Gletscher vom Felsuntergrund (mesozoische Sedimente) erodiert und durch die Eisschmelze im Sommer zum See transportiert wurden. Ca/Si peaks (Winterlagen) zeigen die Grenzen zwischen den einzelnen Warven an und sind deshalb unverzichtbar für die Warvenzählung. Fazies B repräsentiert gradierte Eventlagen (Turbidite), welche wahrscheinlich durch Starkniederschlagsereignisse im Einzugsgebiet ausgelöst wurden.

Unsere Ergebnisse verdeutlichen, dass die Warvendicke primär durch den kumulativen Sommerniederschlag (MJJA) gesteuert wird ($r=0.64$, $p<0.05$, AD 1920 – 1986). Unsere Arbeitshypothese konnte deshalb verifiziert werden. Unsere Resultate verdeutlichen aber auch, dass andere nieder- und hochfrequente Klimasignale in die Warven übertragen werden.

Die in dieser Arbeit präsentierte Zeitreihe mit den Warvendicken bietet eine ideale Ausgangslage für vertiefte statistische Analysen. Ein multivariater Ansatz (z.B. Principal Component Regression Analysis) würde eine genauere Abschätzung der unterschiedlichen Klimafaktoren erlauben, welche Einfluss auf die Warvenbildung im Oeschinensee nehmen. Das Vorkommen von 12 Turbiditen in der analysierten Zeitspanne von AD 1907-2007 hat zudem verdeutlicht, dass das Einzugsgebiet sensitiv auf Starkniederschlagsereignisse reagiert. Das sedimentäre Archiv des Oeschinensees hat deshalb ein grosses Potential für die Rekonstruktion der Frequenz und der Intensitäten von Flutereignissen im Berner Oberland während dem mittleren bis zum späten Holozän.

1. Introduction

1.1. Research motivation and general objectives

Considering our planet Earth as a complex system with many feedback mechanisms (e.g. water vapour, albedo and CO_2 feedbacks), it becomes obvious that even small perturbations can have large, long-term consequences (Lenton et al., 2008). Since the industrialization in the late 18th century, atmospheric concentrations of greenhouse gases (e.g. CO_2) have increased enormously from preindustrial 280 ppm to 379 ppm in AD 2005 (IPCC, 2007). Our Earth's climate, however, is a very sensitive system and critical thresholds, triggering a transition to a new state of the system, could be exceeded in the near future. Hence, frequencies of extreme weather events such as heavy precipitation events and heat waves are very likely going to change under current global warming (IPCC, 2007).

The anthropogenic effects on the Earth's climate, however, are superimposed on natural climate variability, which varies at decadal to millennial time scales (e.g. Mann et al., 1995). Instrumental records are only available since the 18th century, which coincides with the period of industrialization and release of CO_2 to the atmosphere. Thus, for understanding climate variability and feedback mechanisms, paleoclimate data help to place the instrumental record into a long-term perspective (Bradley, 2000). Here, natural archives such as ice cores, speleothems, tree rings and lake sediments are extremely valuable because they are climatically sensitive indicators. Such proxies are influenced by climate variables such as temperature and precipitation and are often representative of particular seasons.

Lake sediments, for instance, are highly suitable for climate reconstructions because lakes usually persist for long time periods, particles are continuously deposited, and annual layers (varves) are formed under specific conditions (Gierlowski-Kordesch and Kelts, 2000). The term "varve" was first introduced at the beginning of the 20th century by De Geer (1912) who investigated periodically layered sediments in the surroundings of Stockholm. De Geer (1912) reported that in these sediments, the deposit of each year could clearly be recognized and counted. De Geer (1912) established a geochronology based on varve counts that covered 12000 yr. In the late 19th and the beginning of the 20th century, however, it was not possible to prove that a pair of two or multiple laminae really represented an annual cycle of sedimentation. Only the development of physical dating methods (e.g. ^{210}Pb age-depth models and radiocarbon ages) during the 20th century enabled this hypothesis to be verified.

In general, varves are only formed in lakes that are located in environments with strong seasonal changes in environmental conditions (Last et al., 2001). Sedimentation patterns must allow an undisturbed deposition of laminae such as those that occur under anoxic conditions. Bioturbation, for instance, erases the pattern subsequently (Wetzel, 2001). Other factors that determine the formation of undisturbed seasonal laminae include the timing of the sediment input to the lake and autochthonous production of organic matter or inorganic precipitates such as calcite (Wetzel, 2001). Consequently, different varve types are distinguished (biochemical and clastic varves). In glacial environments, for instance, varves often have a bimodal pattern. Relatively coarse sediments are deposited in spring and summer due to snow and glacial melt. In contrast, finer clay particles are deposited during winter when the lake is ice covered (Wetzel, 2001).

For quantitative high-resolution climate reconstructions, varved sediments are highly suitable because varves allow the highest possible time-resolution (season to year) in long (centuries to millennia) proxy data time series (Lotter et al., 1997). Further-

more, it is commonly suggested that long-term and short-term responses to climatic change can be traced separately in varved lake sediments (Ohlendorf et al., 1997).

In the last decade, paleolimnology has profited from major developments in applied statistics. As a result, the research community has started to shift emphasis from qualitative, descriptive studies to being a quantitative, analytical science (Birks, 1998). Quantitative high-resolution climate reconstructions can be established with biological proxy data (e.g. chironomids, Larocque et al., 2009) using a calibration-in-space (e.g. transfer functions) approach and with geochemical proxies (e.g. diagnostic mineral ratios, Trachsel et al., 2008) using a calibration-in-time approach. Both approaches are based on the principle that environmental variables are related to indicators (proxies) preserved in recent sediments using statistical techniques (Smol, 2002). Importantly, these approaches make the assumption that the present-day relationships could be used to infer past environmental and climatic conditions. Thus, time series with both biological and geochemical, climate-sensitive proxies are calibrated against instrumental meteorological parameters (e.g. temperature and precipitation). These calibration sets have the potential to transform both biological and physical proxy data into quantitative estimates of past climatic and environmental conditions.

1.2. State of knowledge

In recent years, numerous studies were aimed at the calibration of glaciolacustrine varved sedimentary archives against instrumental climate data. Particularly, varved sedimentary records in the northern hemisphere have been investigated in northern America (e.g. Alaska, British Columbia, Washington and Yukon), Greenland, northern Europe (e.g. Norway and Sweden), Russia and the European Alps (e.g. Switzerland) (Hodder et al., 2007). Due to little land mass of the Southern Hemisphere between 40°S-60°S, clastic varves are only formed in a few lakes in South America (e.g. Lago Plomo, 47° S, 72° W, Julie Elbert, personal communication), and New Zealand (e.g. Lake Tekapo, 43°S, 170°E, Pickrill and Irwin, 1983).

In northern America, for instance, varve thickness has been linked with mean summer temperatures (e.g. Tomkins and Lamoureux, 2005), discharge (e.g. Menounos et al., 2005) and cumulative summer precipitation (e.g. Moore et al., 2001). Tomkins and Lamoureux (2005) found a link between varve thickness and mean summer temperatures (JJA) in the sedimentary record of Mirror Lake (r^2=0.55, $p < 0.01$, n=20), which is located in the Northwest Territories (62°N, 128°W). Similar relationships were reported by Moore et al. (2001) who investigated the varved sedimentary record of Lake Donard (Baffin Island, Canada, 66° N, 61° W). Moore et al. (2001) suggested that varve thickness was positively related with summer air temperatures (JJA) (r=0.57, p not reported, n=43). A weaker relationship was also found with cumulative summer precipitation (JJA) (r = 0.2, p not reported, n=43). In Duffey Lake (southern Coast Mountains of British Columbia, Canada, 50° N 122° W), varve thickness appeared to be positively correlated with discharge peaks (MJ) (r = 0.42, at p 0.05, n=72) and annual discharge peak (r = 0.6 – 0.74 at p 0.05, n = 43) (Menounos et al., 2005).

For the European Alps, the varved sediments of Lake Silvaplana (46°27'N, 9°48'E, 1800 m a.s.l.), a high Alpine proglacial lake in the Eastern Swiss Alps, are probably the best investigated sedimentary record. Physical and geochemical proxy data have been linked to meteorological parameters (e.g. temperature or precipitation) by several researchers (e.g. Leemann (1993), Ohlendorf (1997), Blass (2007a), and Trachsel et al. (2008)). Ohlendorf (1997) compared a 127 yr long varve record (AD 1864 – 1990) with meteorological parameters and found that the mass accumulation rate (MAR) was positively corre-

lated with the number of days with snow ($r^2 = 0.45$, p not reported), with cumulative summer precipitation (JJAS) ($r^2 = 0.3$, p not reported) and mean summer temperatures (MJJAS) ($r^2 = 0.19$, p not reported). Blass (2007a) found a strong relationship ($r = 0.7$, $p < 0.01$) between biogenic silica flux and autumn temperatures (SON) and developed a quantitative high-resolution autumn temperature reconstruction back to AD 1580. For the same period, Trachsel et al. (2008) created a mineralogy-based quantitative autumn, summer and annual precipitation, and summer temperature reconstruction.

For the Bernese Alps, however, no quantitative climate reconstruction has yet been developed. A study was conducted by Leemann (1993) at Lake Oeschinen (46°30'N, 7°44'E, 1580 m a.s.l.), which showed that the rhythmically laminated sediments represented annual layers. Due to the AD 1963 ^{137}Cs peak, the varve chronology could be verified. Furthermore, Leemann (1993) compared varve thickness from AD 1962 – 1982 with mean summer temperatures (JJAS), mean annual precipitation and winter precipitation from Adelboden (months were not reported). Leemann (1993) found that there was only a relationship with mean summer air temperatures ($r = 0.45$, $n = 21$, p is not reported).

Thus, varve thickness in Lake Oeschinen was assumed to be a function of mean summer air temperature and connected melting and erosional processes of the glaciers in the catchment. However, this varve-climate relationship was not tested for its significance (i.e. p values were not reported). As illustrated with studies from northern America and the Swiss Alps, the formation of clastic varves can be influenced by numerous climatic variables such as summer temperatures, cumulative summer precipitation or peaks in the discharge of the inflowing rivers.

Recent field observations in the catchment of Lake Oeschinen indicated that varve thickness was primarily controlled by cumulative summer precipitation. Particle load of the inflowing creeks appeared to be particularly high during spring snowmelt and summer rainstorms (Martin Grosjean, personal communication). Thus, the links between climate variables (e.g. temperature or precipitation) and sediment supply to Lake Oeschinen remained unclear and additional studies were needed.

Moreover, the potential of Lake Oeschinen for a regional, high-resolution climate reconstruction required investigation because only few natural archives (e.g. lake sediments) provide reliable proxy data that can be used for quantitative reconstructions of precipitation. Mankind is strongly dependent on the variability of precipitation (e.g. for agriculture), but so far only a few quantitative precipitation reconstructions have been developped. Thus, there is still a lack of well-calibrated proxy datasets of adequate quality, resolution and spatial distribution (Trachsel et al. 2008). As precipitation is spatially more heterogeneous than temperature, reconstructions of precipitation in high alpine areas are only valid for the catchment rather than for wider regions. Thus, there is the need for multiple precipitation reconstructions in order to understand climate variability across wider regions.

1.3. Research questions and working hypothesis

As seen in the previous section, varve-climate relationships of the sedimentary archive in Lake Oeschinen are unclear. Hence, the following research questions are addressed in this Thesis:

- ***How are varves formed and what are the mineralogical and geochemical features of varves formed in Lake Oeschinen?***

- ***Do comparisons of varve thickness with meteorological parameters (e.g. temperature and precipitation) reveal significant correlations?***

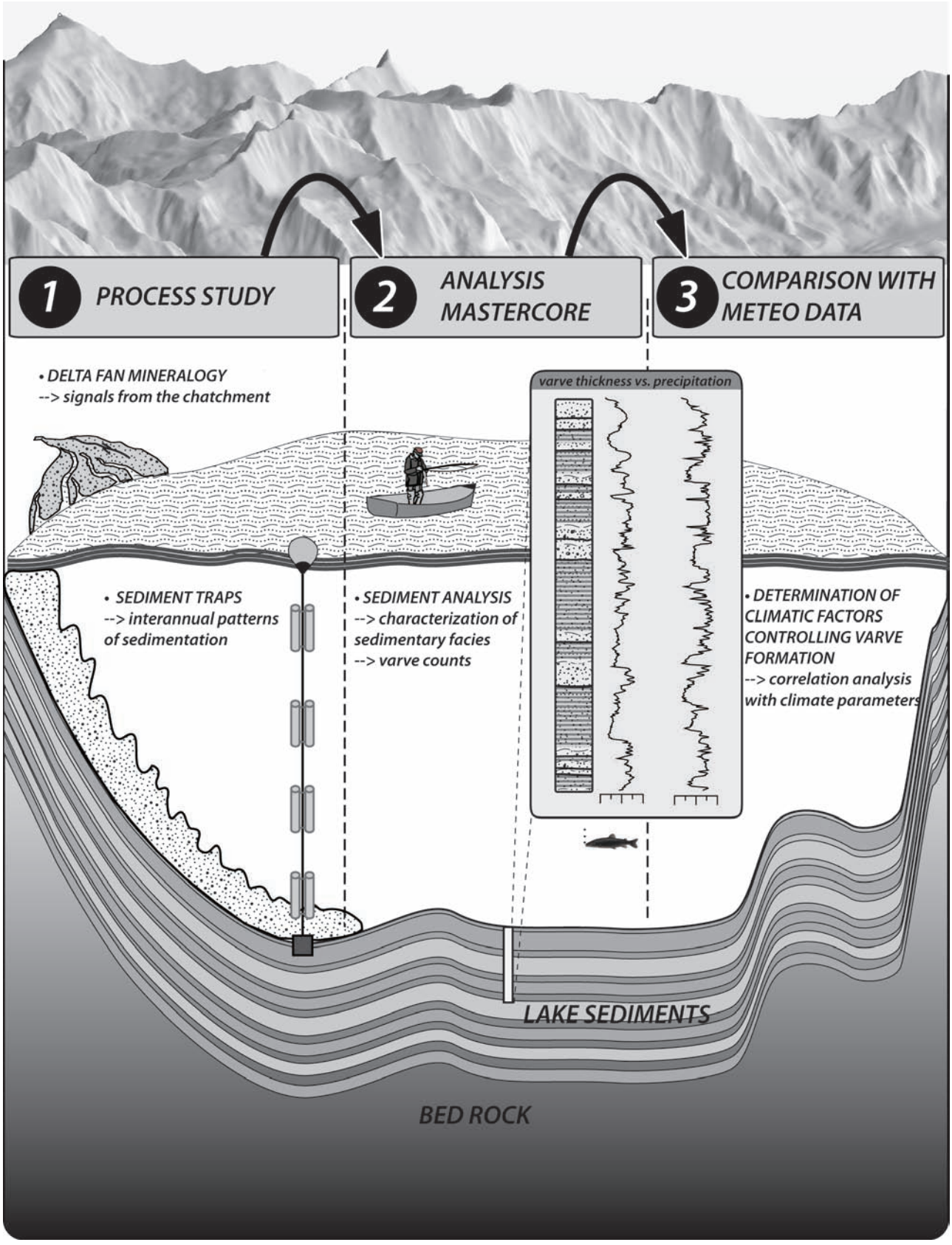

Figure 1: Study design of the Thesis. Note the three consecutive steps that included a process study (1), the analysis of the mastercore (2) and comparisons of physical proxy data with instrumental data (3). All steps were required for answering the research questions and testing the working hypothesis.

Furthermore, a critical working hypothesis was addressed:

- ***Varve thickness is primarily controlled by cumulative summer precipitation.***

1.4. Project design

In order to test the working hypothesis and answer the research questions, a careful project design was required. This study was therefore structured in 3 consecutive steps (Figure 1).

- Step 1 – Process study

First, a process study was conducted because sedimentary processes associated with varve formation remained unclear. The process study was aimed to gain knowledge about seasonal particle flux and the sediment source. Seasonally trapped particles and delta sediments were analyzed and interpreted. As a result, a hypothesis about varve formation was formulated.

- Step 2 – Analysis mastercore

Second, a sediment core (freeze core) was recovered from Lake Oeschinen. From the top 50 cm, sedimentary facies were analyzed and characterized using X-ray powder diffraction, Micro-X-ray fluorescence elemental mapping and X-ray fluorescence scans. Comparisons with the process study revealed if the varve hypothesis was verified. Importantly, a robust varve chronology was established using varve counts, an appropriate ^{210}Pb age-depth model, and independent chronomarker horizons (e.g. AD 1963 radiocaesium peak) for validation. Varve thickness was measured.

- Step 3 – Comparison with instrumental data

Third, a varve thickness time series was compared with instrumental data. Statistical analysis yielded information about the relationship between varve thickness and climate parameters (e.g. precipitation or temperature). Lastly, the working hypothesis was verified or assumptions about varve formation had to be rejected. Results were compared with preliminary studies from the literature.

1.5. Thesis outline

The Thesis is structured as follows: Chapter 1 gives an introduction to the scientific background and the potential of lake sediments for quantitative high-resolution climate reconstructions. The state of knowledge is summarized and both research questions and a working hypothesis are addressed. The study design, in particular, is highlighted. Chapter 2 introduces the reader to the study area. The geographical and geological setting is described. Information about hydrology and the climatic setting of the study area are given. Chapter 3 describes all the methods and materials used in this Thesis. Chapter 4 presents results and interpretations from the process study, analysis of the mastercore, and the comparisons with instrumental data. In Chapter 5, results are discussed and compared with preliminary findings from other studies. Major conclusions of this project are drawn in Chapter 6, together with an overview of possible forthcoming steps.

2. Study site - Lake Oeschinen

2.1. Geographical setting

Lake Oeschinen (46°30'N, 7°44'E, 1580 m a.s.l., Figure 2) is situated in the Swiss Alps, approximately 55 km south of Bern (Figure 2, A and B). The lake is located in a 4 km long, east-west oriented valley. The nearest settlement is Kandersteg which is located ~3 km E of Lake Oeschinen. The study area is very popular for both summer and winter tourism. Since AD 1948, a cable-car has connected Kandersteg with Alp Oeschinen. A hotel (Hotel Oeschinensee) was constructed in AD 1892 at the western shoreline of the lake.

2.2. Physical characteristics of Lake Oeschinen

Lake Oeschinen is a warm monomictic and oligotrophic lake formed by a landslide (Niklaus, 1967). The lake surface is frozen during the winter months (December to May). With the progression of summer, a thermal stratification is established; the thermocline is located ~20 m water depth. Water temperatures in the epilimnion can reach up to 16°C. Mixing only takes place in late autumn. Throughout the entire year, water temperatures in the hypolimnion are always in the range of 4.4 - 5.7° C (Leemann, 1993). The lake basin is topographically closed and therefore has an underground outflow (Figure 2, Oeschibach = number 6). The lake has a maximum depth of ~56 m, a maximum area of 1.18 km^2 and a volume of 37 Mio m^3. Moreover, annual lake level fluctuations average ~12 m. The lowest water levels occur before spring snowmelt in April. At this time, the area of the lake encompasses ~0.88 km^2 and all deltas are exposed around the shoreline. Due to snowmelt and glacial ice melt during summer, the water level is continuously rising and reaches a high stand in September (Niklaus, 1967).

2.3. Climate

Climate variability in the European Alps is influenced by the Atlantic weather systems, the Mediterranean Sea and the large Eurasian land mass. The North Atlantic Oscillation (NAO) is the dominant climate mode for Europe and particularly controls the weather in western and northern Europe in winter (Casty et al., 2005). During the winter season, air pressure over the European Alps appears to be dominated by the interplay between the Icelandic Low, the Azores subtropical high and the Siberian high. Both the transport of moist air from the Atlantic (westerlies) and dry cold air masses from the east are controlled by the relative strength of these pressure systems. In summer, Alpine weather is predominantly influenced by local heat lows and the Azores High spreading over the European continent. During spring and autumn cold fronts from the northwest and southeast are often deflected by the Alpine barrier. As a result, lee cyclogenesis takes place over the Gulf of Genoa that causes both föhn effects and heavy precipitation at the southern margin of the Alps (Wanner et al., 2003).

Local climate in the study area is classified after Köppen-Geiger to lie in a transition zone between warm temperate, fully humid, summer-warm (Cfb) and polar tundra climate (ET) (Kottek et al., 2006). Unfortunately, there is no meteorological station located at Lake Oeschinen. Mean annual temperatures, recorded in Adelboden (1320 m a.s.l., ~13 km W of Lake Oeschinen), average + 5.7°C (means for AD 1959 -2009). Lowest mean temperatures occur in January (-1.8°C) and maximum mean temperatures are measured in July (13.9°C). The highest amounts of precipitation, measured in Kandersteg (1176 m a.s.l., ~3 km W of Lake Oeschinen), occur in July (141 mm, means for AD 1900-2009) whereas in February, a minimum (69 mm) is measured. Total annual precipitation is 1173 mm (data from Meteo Schweiz).

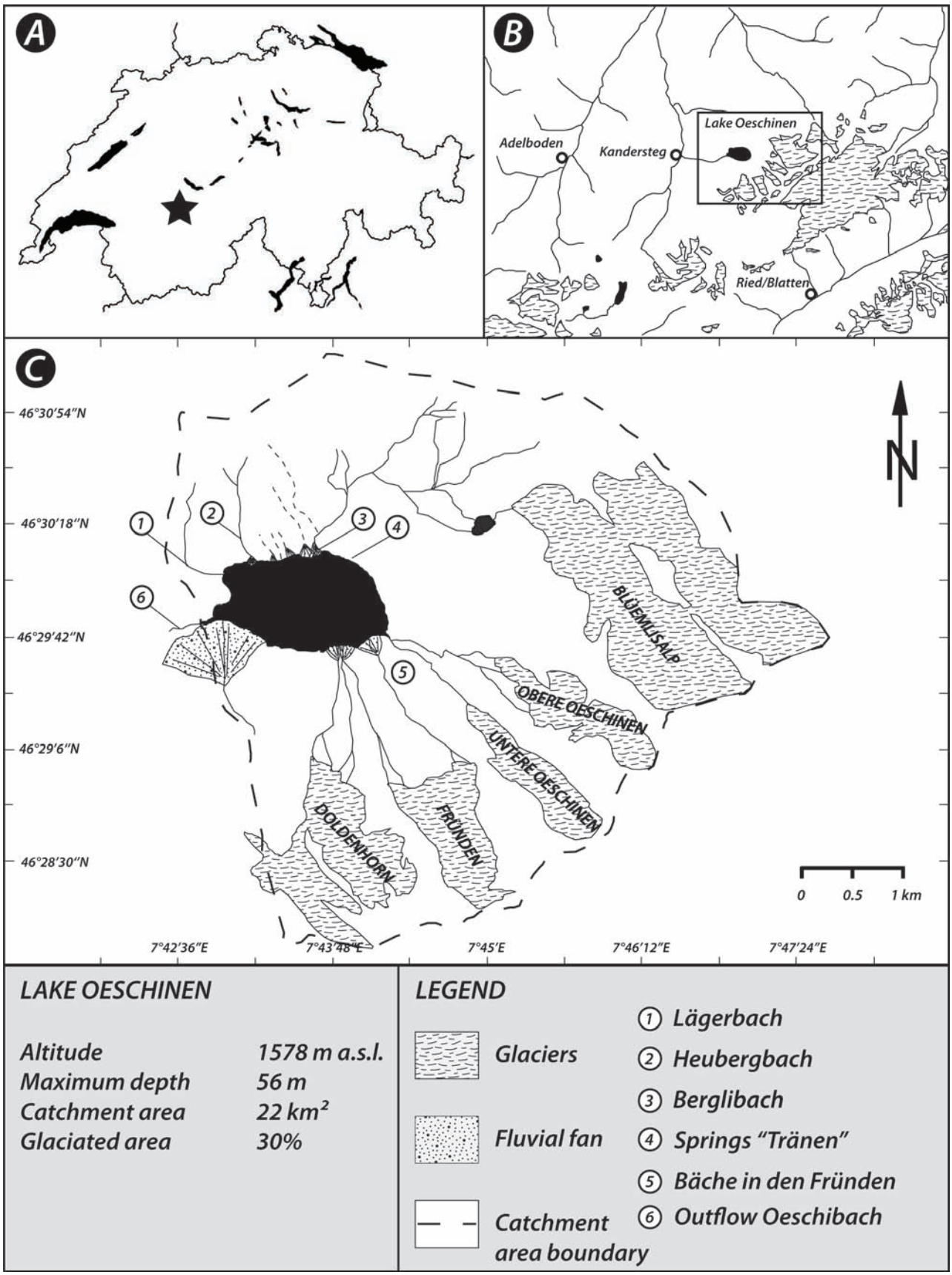

Figure 2: Maps showing the location of the study site. A) Overview map of Switzerland with the largest lakes and the location of the study area in the Bernese Alps (asterisk). B) Map showing the location of the study area (square), lakes (black areas), glacial cover (shaded areas), rivers (lines), and the meteorological stations in Kandersteg, Adelboden, and Ried/Blatten (circles). C) Map of Lake Oeschinen (dark) with its catchment area (dashed line), glacier extensions (shaded areas, status 2007), inflowing rivers (lines) and river deltas (dotted areas). Note the names of the rivers (numbered) that contribute to the inflow of the lake.

2.4. Geological setting

The study area is located along the northern margin of the Alps in the Helvetic nappes. Three tectonic nappes (Wildhorn, Gellihorn and Doldenhorn) build up the catchment of Lake Oeschinen. The highest mountains reach up to >3600 m a.s.l. (Figure 3).

The southern catchment is built up by the Doldenhorn nappe that comprises Mesozoic limestone. (Figure 3, Jurassic = blue, Cretaceous = green). These rocks were continuously deposited on the Tethyan carbonate platform at the continental margin of the European continent during the Jurassic and Cretaceous. In the northern catchment, the Doldenhorn nappe is overlain by the Gellihorn and the Wildhorn nappe. The Gellihorn nappe, in contrast to the Doldenhorn and Wildhorn nappe, comprises Tertiary Flysch deposits. Flysch are deep-marine mass flow deposits characterized by fining upward sequences. In the beginnings of the Alpine orogene, the Piemont Ocean started to subduct under the Adriatic margin. Consequently, a deep basin formed that was continuously filled with turbidites and other clastic sediments (Pfiffner, 2009). The Flysch units, found in the northern catchment of Lake Oeschinen, are characterized by sandstones

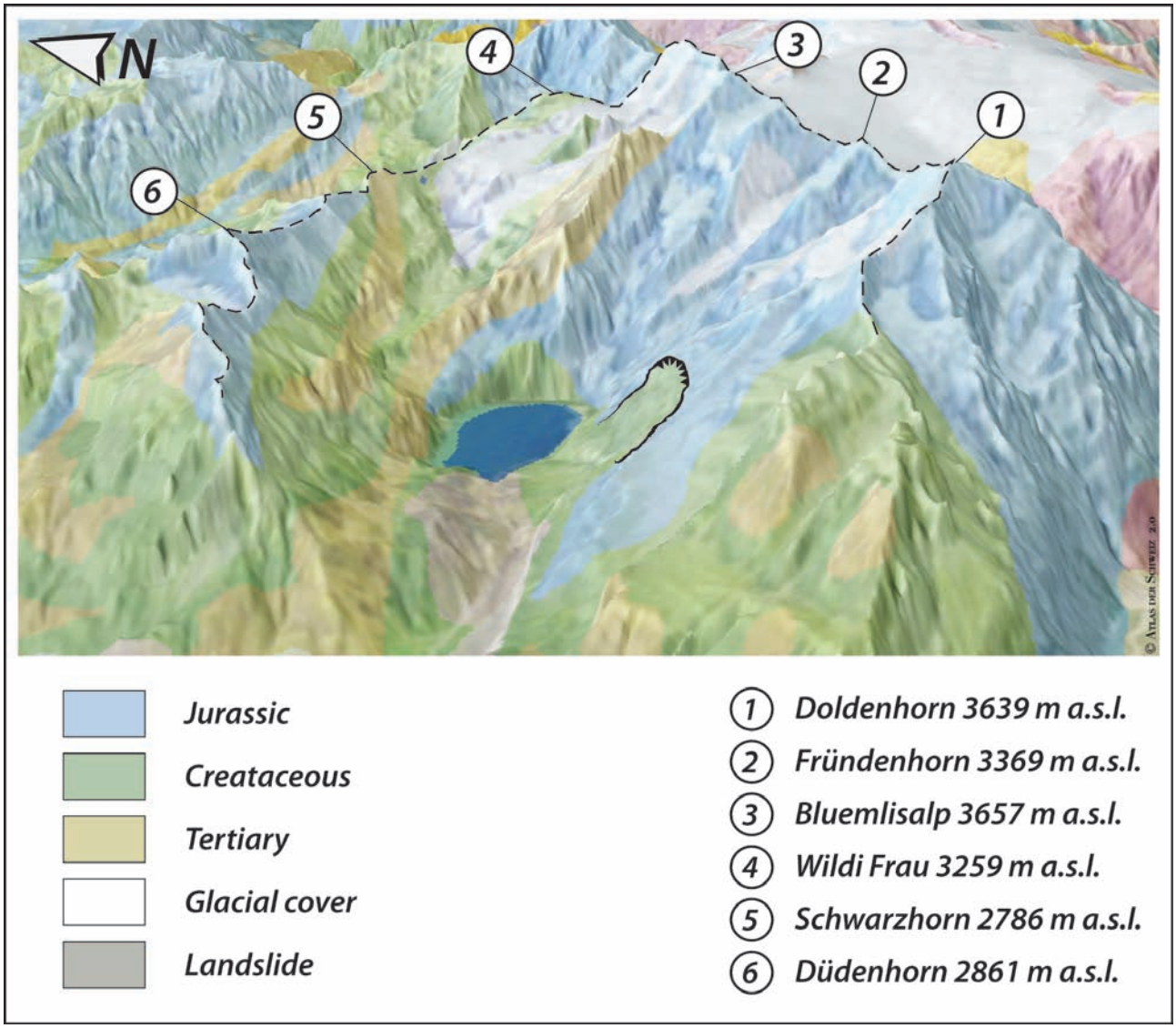

Figure 3: Geological map showing the regional setting of the catchment area of Lake Oeschinen (dashed line). Note that the southern catchment is mainly comprised of Jurassic sediments (light blue). In contrast, in the northern part of the catchment, all Tertiary Flysch deposits (yellow), Cretaceous (green) and Jurassic (blue) sediments are present. Area of rupture of the lake-damming landslide is located at the north-facing slopes (black triangles). (Figure modified after Atlas der Schweiz 2.0)

that are interbedded with various shaly and marly horizons (Suchy et al., 1997).

Importantly, in the youngest geological history of the Oeschinen valley, a landslide occurred that dammed the lake. The surface of rupture is located in the north-facing slopes at the border between Jurassic and Cretaceous limestone (Figure 3, black triangles). The landslide is not dated. However, its occurrence may date back to the early Holocene during a thermal and solar irradiation maximum (Niklaus, 1967; Tinner et al., 2005). Warm and wet climate during this period coincides with the occurrence of the main Kander valley rockfall (BP 9600), the Flims landslide (BP 8900 ± 700 yr) and possibly with the landslide that dams Lake Oeschinen.

2.5. Hydrology

The catchment has an area of 22 km^2. Around 30 % (status 1993) is covered by five glaciers (Doldenhorn, Fründen, Oeschinen, Vorderer Blüemlisalp and Blüemlisalp glacier) located south and east of the lake. The catchment can be sub-divided into the draining areas creeks from the S, creeks from the NE-N and creeks from the N. Table 1 lists physical properties of these subgroups such the individual areas (%), glaciological and geological features.

S (~40 % of the catchment) - Glacial melt water from the Doldenhorn, Fründen and Oeschinen glaciers is drained by the creeks "Bäche in den Fründen" (~40 % of the catchment). The creeks enter Lake Oeschinen at the southern shoreline and contribute to the inflow of the lake, particularly in summer (Niklaus, 1967).

NE-N (40 % of the catchment) - Another 40 % of the catchment is drained by the creek Berglibach. The largest glacier in the catchment, the Blüemlisalp glacier, is separated from the Doldenhorn, Fründen and Oeschinen glaciers by east-west oriented mountain ridge. Glacial melt water contributes to the inflow of the lake, particularly during summer. Moreover, in the AD 1950's, a moraine-dammed, proglacial lake has formed (46°30'18.34"N, 7°44'57.72"E, 2148 m a.s.l). Both glacial creeks and creeks from the N merge to form the creek Berglibach at Oberbergli (2020 m a.s.l.).

N (~20 % of the catchment) - The northern catchment is drained by numerous small creeks that are particularly active during snow melt and summer rainstorms. The slopes are steep and cut by gullies where enormous quantities of eroded sediments from the Tertiary Flysch have accumulated. Particularly during summer rainstorms, high energies are provided for the transport of these sediments to the lake.

Alluvial fans have accumulated at the northern and southern shoreline. Several springs are found in the catchment area, which is typical for karst environments.

Table 1: Subdivision of the catchment according to physical properties.

Draining area (groups)	*Area (% of entire catchment)*	*Glacial cover*	*Bedrock geology*
S (glacial rivers)	*~40%*	*3 glaciers (Doldenhorn, Fründen, Oeschinen)*	*Jurassic and Cretaceaous limestone*
NE-N	*~40 %*	*1 glacier (Blüemlisalp glacier), moraine-dammed proglacial lake*	*Cretaceous and Tertiary*
N	*~20 %*	-	*Jurassic, Cretaceous and Tertiary*

3. Material and Methods

3.1. Process study

3.1.1. Fieldwork – Collecting delta fan sediments

Delta samples were collected around the shoreline of Lake Oeschinen (Figure 4) in June 2008. Locations A – J are each represented by three samples. Furthermore, soils in the northern catchment are represented by location B. In October 2009, additional samples (locations K-Q) were collected from the glacial creek deltas at the southern shoreline. In contrast to previous fieldwork, each delta is only represented by one sample. From the proglacial lake, fed by the Blüemlisalp glacier, additional samples were recovered in June 2010. Due to low water levels in spring, lake sediments deposited near the shoreline could be collected (location R).

3.1.1.1. X-Ray powder diffraction (XRD)

X-ray diffraction is a technique used for the analysis of diffraction patterns of crystals (Manutchehr-Danai, 2009). The technique is based on the principle that an X-ray beam of a known wavelength is directed onto a crystals and its diffraction pattern depends on the three-dimensional arrangement of the crystal structure. A detailed description of the method is given in the textbook of Wenk and Bulakh (2004). In our study, X-ray powder diffraction was used for a quantitative determination of mineral proportions of the delta sediments. For a high quality XRD analysis, a reproducible sample preparation was essential. In general, the requirements of the sample preparation for XRD analyses are that the sample are homogeneous and representative of the

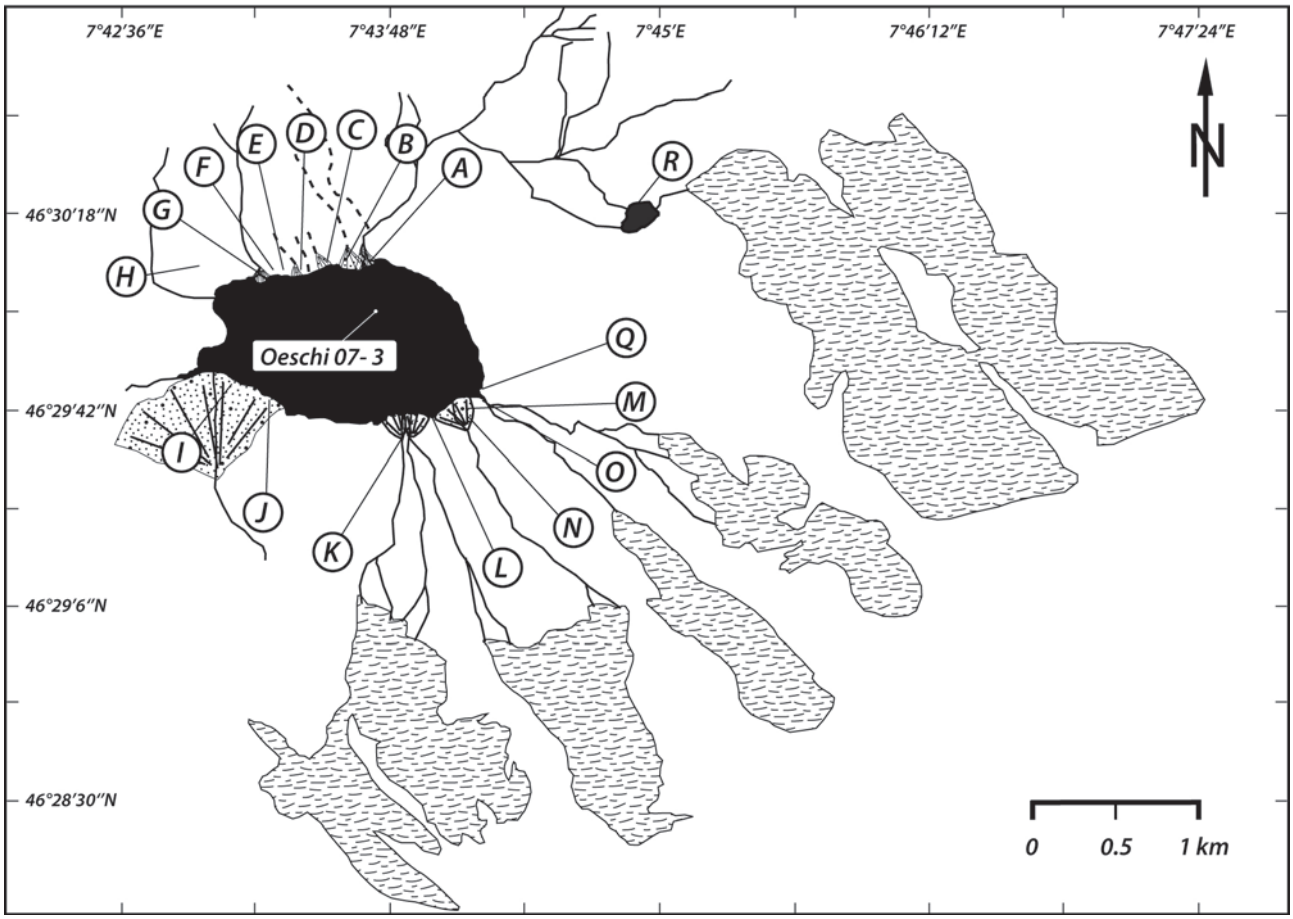

Figure 4: Map showing the alluvial fans (dotted areas) around the shoreline of Lake Oeschinen. The locations A-J are represented by 3 samples whereas at the locations K-R only one sample per location was collected. The coring spot, where the mastercore Oeschi 07-3 was recovered, is located between the proglacial deltas "Bäche in den Fründen".

source material (Denker et al., 2008). Furthermore, all particle size effects, orientation effects and the influence of the milling procedure had to be taken into account during the sample preparation.

Firstly, all samples were sieved through a 63 µm mesh in order to remove the sand fraction. Hydrogen peroxide (30 %) was used to decompose organic compounds. After washing the samples 3 times with distilled water, the samples were freeze-dried. Secondly, lithium fluoride (LiF) was added to act as an internal standard (ratio 1:10). 3 g sample and 0.3 g LiF are required for repeat determination. LiF was dried at 105°C overnight and stored in a desicator during sample preparation. Each mixture was homogenized in an achat mortar for 10 min to avoid particle size effects. Then, the sample was packed into a cavity holder. The crystals within the powder were disorientated with a stamp to minimize orientation effects. Finally, the samples were analyzed with a Philips PW 3710 at the Institute of Geological Sciences, University of Bern. The device uses Cu Kα radiation and scans from 4 to 60° 2θ with a step size of 0.02°. Measurements were performed at a generator voltage of 40 kV and a current of 30 mA.

Quartz (qz), calcite (cal), dolomite (dol), K-feldspar (kfs) and plagioclase (pl) were quantified using the software X'Pert Quantify. The quantification is based on the reference intensity ratio (RIR) method: The intensity of one or more peaks for each mineral is measured and compared with the peak intensity of the internal standard (LiF) (Hillier, 2000). Results are expressed as weight percent for the individual minerals. From the mineral proportions, elemental concentrations and elemental ratios were calculated.

Quantification of calcite is not precise for calcareous samples; proportions >100% are often indicated. This problem cannot be avoided because 10 of 12 synthetic reference samples used for calibration have proportions of calcite < 25 %. Hence, quantification errors remarkably increase with proportions of calcite > ~50%. The proportion of calcite (if > 100 % indicated) is calculated by the difference of 100 % - (sum quartz [%] + dolomite [%] + K-feldspar [%] + plagioclase [%]). To prove these results, total inorganic carbon (TIC) was measured with a Macro Vario elemental analyzer. In the catchment of Lake Oeschinen, inorganic carbon originates only from calcite and dolomite. Hence, the proportion calcite [%] is calculated by the formula:

$$\text{Calcite [\%]} = C_{\text{calcite}} \text{ [\%]} * (\text{molar mass}_{\text{calcite}} / \text{molar mass}_{\text{carbon in calcite}}),$$

where C_{calcite} [%] = TIC [%] - (dolomite [%] *(molar $\text{mass}_{\text{carbon in dolomite}}$ / molar $\text{mass}_{\text{dolomite}}$).

The proportion of clay minerals is calculated by the difference of 100% - (sum of calcite [%] + quartz [%] + dolomite [%] + K-feldspar [%] + plagioclase [%]). Individual proportions (e.g. [%] illite and chlorite) cannot be determined, but are qualitatively estimated using XRD diffractograms.

3.1.2. Sediment traps

Sediment traps (cylindrical, ø = 9 cm) were deployed at 4, 15, 30 and 45 m above lake ground. Vertical differences in sediment flux were determined in order to understand sediment transport processes within the water column. The buoy-carried traps were attached onto a rope anchored by a weight. As annual lake level fluctuations average 12 m, the depths have to be considered as depths above lake ground. The distance between the sediment traps and the lake surface was therefore changing during the observation period (30 May 2007 to 25 June 2008). Trapped particles were collected in four sampling intervals: 12 July (after 43 days), 20 September (after 70 days), 11 November (after 42 days), and 25 June (after 237 days). Due to ice cover in winter, only 3 sediment traps were deployed from November 2008 to June

2010. The trapped sediments were freeze-dried and weighed in order to calculate dry weights. Results are expressed as particle flux (mg dry sediment cm^{-2} day^{-1}).

3.1.2.1. Grain size analysis – Laser diffraction

Grain size analysis was conducted at the Paleolimnology Lab at ETH Zurich with a Malvern Mastersizer 2000S (Malvern Instruments Ltd). Using the laser diffraction technology, the device is able to measure the particle size distribution in the range of 0.02 µm to 2000 µm. The technology is based on the principle that suspended sediment particles are illuminated by a laser beam. As a result, the particles scatter the light in the forward direction at angles inversely proportional to their size (i.e. small particles scatter light in a wider angle than larger particles). The scattering is measured by photo detectors and resolved mathematically using a series of data fitting processes (Last, 2001).
However, using the laser diffraction technology, the clay content is systematically underestimated (Loizeau et al., 1994) and air bubbles in the circulation system reveal secondary peaks in the fraction ~500 -1000 µm.
All samples were pretreated with hydrogen peroxide (30 %) because the grain size fraction above 10 µm is overestimated without decomposition of organic compounds (Blass et al., 2005). Samples were placed in a water bath and heated at 80° C until the reaction was complete. The samples were then washed twice with distilled water. For the measurements, a well-homogenized sample aliquot of ~2 ml was directly pipeted from the original sample tubes and put in the suspension chamber of the Malvern Mastersizer 2000S. Every sample was measured three times. Grain size distributions are expressed in volume percent. Other statistical measures (e.g. mean, median and sorting) are given in µm.

3.1.2.2. Mineralogy - X-ray diffraction smear slides

Qualitative mineralogical compositions of the samples from the lowest sediment trap (4 m above lake ground) were determined. The samples were milled in an achat mortar. Organic compounds were removed with hydrogen peroxide (30 %). The samples were washed twice with distilled water. Three drops of ethylene glycol were added to each sample. Then, a sample aliquot was directly pipeted from the tubes onto the sample holder. Mineralogical composition was determined with a Philips PW 3710. Measurements were performed at a generator voltage of 40 kV and a current of 30 mA. The scans ranged from 4 to 40° 2θ with a step size of 0.02°. Due to preferred orientation of clay minerals (e.g. illite and chlorite) in the smear slides samples, results must only be regarded as a qualitative measure for mineralogical composition. Peak intensities were measured for calcite (at 29.5° 2θ) chlorite (at 12.6° 2θ), illite (at 8.9° 2θ), and quartz (at 26.7° 2θ). Finally, peak intensity ratios were calculated (e.g. calcite/illite).

3.2. Recovery and analysis of the mastercore

A freeze core was recovered from Lake Oeschinen in October 2007 using the in-situ freezing technique (Kulbe and Niederreiter, 2003). The coring was performed on a floating platform. The corer consisted of a high pressure resistant housing with a vacuum insulated jacket for chilled ethanol, adjustable stabilizing legs, an electrical pump and a freezing wedge of 100 cm length. The ethanol was cooled with liquid nitrogen down to ~-100°C and pumped to the coring wegde, stuck in the sediments. Within 30 - 45 minutes of freezing, the sediment core could be hauled up to the platform and prepared for storage in a cool room.

3.2.1. Chronology

3.2.1.1. Radionuclide dating - ^{210}Pb and ^{137}Cs

^{210}Pb dating is an important technique for dating recent (0-150 years) lake sediments in paleolimnology (Appleby, 2001). Within the natural ^{238}U decay series, ^{210}Pb (half life 22.3 yrs) is formed by the decay of the noble gas ^{222}Rn (half life 3.8 days). ^{210}Pb is supplied to lake sediments by two processes: on one hand, ^{210}Pb "supported" is directly formed within the sediments because ^{238}U and its daughter products naturally occur in bedrock. Thus, formation and decay of ^{210}Pb are in equilibrium. On the other hand, "unsupported ^{210}Pb" is formed in the atmosphere and removed by washout and dry deposition ($A_{unsupp} = A_{tot} - A_{supp}$). Unsupported ^{210}Pb is either directly deposited on the lake surface or reaches the lake indirectly via the catchment. After 6-7 half-lives, total activity within the sediments ($A_{tot} = A_{supp} + A_{unsupp}$) is in equilibrium with the in situ produced ^{210}Pb ($A_{tot} = A_{supp}$). The decay follows the equation. $A_{unsupp\ x} = A_{unsupp},0 * e^{(-\lambda * t)}$. The age, t, is calculated by $t = 1/\lambda * \ln (A_x / A_0)$. The initial concentration of the unsupported ^{210}Pb (A_0), however, is a function of both the deposition and the sedimentation rate $A_0 = (F / v)$, [dpm g^{-1}] with F = deposition rate [dpm cm^{-2} yr^{-2}] and v = sedimentation rate [g cm^{-2} yr^{-2}] (Håkanson and Jansson, 1983). As both variables (F and v) are unknown, assumptions are required for solving the equation.

Both the CIC (assuming a constant initial concentration, A_0 = constant) and the CRS model (assuming a constant rate of ^{210}Pb supply, F = constant) were calculated as described in Appleby (2001). Errors for the CRS model are calculated after Appleby (2001) and for the CIC model after Binford (1990). However, the models have to be validated with independent chronomarker horizons (e.g. AD 1963 and AD 1987 ^{137}Cs peak and historical flood events). The CRS model, furthermore, can be constrained by a chronomarker horizon (composite CRS model). The choice of the best model is often subjective and in most cases, a model is chosen that is best validated with ^{137}Cs stratigraphic markers (von Gunten et al., 2009a). Reasons for rejecting the CIC model, for example, include multiple age inversions. However, if atmospheric ^{210}Pb supply is not constant in time at a particular study site, the CIC model may yield more reliable ages (Appleby, 2001). Furthermore, the accuracy of the age-depth models is strongly determined by the initial sampling strategy. Sedimentary facies that represent only supported ^{210}Pb (e.g. turbidites) must not be used for the calculation of numerical ^{210}Pb age-depth models (Arnaud et al., 2002).

The mastercore (Oeschi 07-3) was sampled according to homogeneous sedimentary facies (for details see Appendix B, Table B1 and Figure 23). Attention was directed to event layers that were excluded from the data set. After freeze-drying the samples, water content was determined. The samples (~3 g) were put in 10 ml Milan test tubes and sent to EAWAG in Dübendorf. ^{210}Pb and ^{137}Cs activities were measured with a gamma-ray spectrometer. Results are expressed in Bq/kg dry sediment. All the CIC, CRS and the composite CRS models (constrained with the AD 1963 radiocaesium peak) were calculated and compared with the chronomarker horizons.

3.2.1.2. Spheroidal carbonaceous particles (SCP)

SCPs are soot particles formed by high-temperature (>1750 °C) fossil-fuel combustion. SCPs are deposited in lakes via atmospheric deposition. Reconstructions of past SCP fluxes since the beginning of industrialization are generally in agreement with the pollution history across wide regions (Rose, 2001). Thus, SCP profiles are very useful for paleolimnology because they provide independent time markers for sediment dating and information about the pollution history of regions. For European lakes, SCP

profiles are generally characterized by their first appearance in the early to mid 18th century, a rapid increase in the early to mid 20th century, and a peak in the AD 1970s (Rose, 2001).

The sample preparation mainly followed the procedure described in Renberg and Wik (1985). Hydrogen peroxide and hydrochloric acid were used to remove organic compounds and carbonate, respectively. Firstly, a sample aliquot of ~50 mg was placed into a 250 ml glass beaker. The exact weights of the tare and the sample were scaled. Secondly, 15 ml hydrogen peroxide (30 %) was added to the glass beaker in order to decompose organic matter. When the oxidation was finished, the glass beaker was filled with distilled water. The supernatant was carefully decanted when all particles had settled. Thirdly, 20 ml hydrochloric acid (10 %) was added in order to dissolve calcite and reduce iron oxides. The glass beaker was filled with distilled water. This procedure was repeated daily at least 4 times in order to dilute the hydrochloric acid. Lastly, the tare of an E-flask (200 ml) was weighed. The water in the glass beaker was carefully decanted until the 40 ml marker was reached. Then, the suspension was transferred to the E-flask. The new weight of the E-flask was scaled. The E-flask was shaken (~30 seconds) in order to homogenize the suspension. About 4-8 ml of the suspension was poured into a clean Petri dish (ø = 8 cm) until the whole bottom of the glass was covered with particles. The weight of the E-flask was immediately scaled again after pouring. As soon as the water evaporated, the sample was ready for SCP counts.

SCPs were counted under a light microscope at a magnification of 50 x. Typical properties such as surface morphology, size and color described in Griffin and Goldberg (1981) and Clark (unpublished) were used for identification of SCPs. In order to aid the counts, the Petri dish was put on a gridded paper with numbered units. The results of the SCP counts are expressed as number of particles per gram dry mass of sediment (SCPs g^{-1} dry sediment).

3.2.2. Resin blocks and thin sections

For establishing a reliable varve chronology, a sediment core has to be sampled without disturbances. Thus, the freeze-dry technique and the water-epoxy-exchange method was used to for the preparation of resin impregnated sediment block and thin sections (see Lotter and Lemcke, 1999). These methods are based on the principle that the pore water from the sediment is replaced by an epoxy resin. As a result, the resin impregnated sediments allow the investigation of microstructures as well as accurate counting and measuring of varves (Lotter and Lemcke, 1999). The mastercore (Oeschi 07-3) was cut in overlapping pieces (2 cm x ca. 13 cm) and put in aluminum trays. Then, the sediment blocks were freeze-dried and poured in resin (SPI-Chem™ Low Viscosity "Spurr" Kits). The resin-embedded sediment blocks were sent to Geoprep (Department of Environmental Sciences, University of Basel). Thin sections of the uppermost 50 cm sediment sequence were cut from the resin impregnated sediment blocks.

3.2.3. Micro-X-ray fluorescence elemental mapping

X-ray fluorescence is based on the emission of secondary fluorescent X-rays initiated by the bombardment of a material with a gamma ray beam. By the bombardment with high-energy gamma rays, an electron is lost from the inner shell (K shell) of the atom. Because the atom becomes unstable by this loss, the missing electron is replaced by another electron from a lower orbital. During this process, energy is released in the form of a fluorescent photon that is characteristic for the element (Beckhoff et al., 2006). Thus, X-ray fluorescence can be used for elemental analysis.

For paleolimnology, XRF elemental mapping offers a valuable tool, in particular for the study of lami-

nated sediments. The micro XRF technology can be applied for the identification of qualitative changes in elemental abundances associated with sediment laminations (Shanahan et al., 2008).

Both lines and areas can be scanned at ultra-high resolution (down to 50 µm). Using two-dimensional maps of a varved sediment sequence, elemental concentrations and visual information (e.g. thin sections) from individual laminae can be compared with each other. Thus, the elemental maps can be used for the verification of visual varve counts and for detailed studies of interannual changes in sedimentation.

In this study, an unambiguous varved sediment sequence (47.5 – 50 cm sediment depth) was chosen and scanned (resin impregnated sediment block) with an EAGLE III X-ray fluorescence device (µ-XRF; EDAX Inc., Mahwah, NJ, USA) at the Department of Geology, University of Geneva. Under vacuum conditions, the qualitative concentrations of light elements (e.g. Mg, Al, Si, Ca and Fe) were measured at 50 µm resolution. The results of the scanned lines are expressed in counts per second (cps). Maps were created for all detectable elements. Qualitative elemental concentrations are indicated by the intensity of different colors.

3.2.4. X-ray fluorescence scans (XRF)

The use of XRF core scanners has increasingly become popular in the past decade, because it allows non-destructive extraction of element intensities from sediment cores with a minimum of analytical effort (Weltje and Tjallingii, 2008). In contrast to conventional geochemical analyses, high-resolution data (down to 100 µm) can be achieved in short time periods (hours to days). As a result, detailed time-series of major elements are created, which can be applied to paleoclimate and paleoenvironmental interpretations (Zolitschka et al., 2002). The data output is expressed in qualitative elementary concentrations (counts per unit time per unit area), and cannot be linearly converted into quantitative measures. Weltje and Tjallingii (2008) reported that a universally applicable, robust procedure for converting core-scanner output to quantitative measures of sediment composition is still required.

Nevertheless, XRF scans were essential for this study because diagnostic elemental concentrations possibly enable the identification of sedimentary facies. The resin-impregnated sediment blocks (top 50 cm of the mastercore) were scanned with an AVAATECH X-Ray Fluorescence Core Scanner at ETH Zurich. The opening of the detector slit was adjusted to 12 mm in width. Qualitative elementary compositions were measured for light elements at 10 kV (e.g. Al, Si, K, Ca and Fe) and heavier elements at 30 kV (e.g. Zn, Br and Rb) at a resolution of 200 µm. According to the findings of the process study (chapter 4.1), diagnostic element ratios were calculated (e.g. Ca/Si) and used for identification of sedimentary facies. Importantly, the sediment blocks were put in aluminum trays for the sample preparation (see sectiion 3.2.2.). Al counts may have resulted from these trays and could therefore not be used for the calculation of diagnostic element ratios (e.g. Ca/Al).

3.2.5. Establishment of the varve chronology and varve counts

First, high-resolution digital images of the mastercore (top 50 cm) were created. The thin sections and the resin-impregnated blocks (including scale) were light-scanned at a maximum resolution of 1200 dpi with a CanoScan 8600F. Using Adobe Photoshop CS3, images were merged to a composite image.

Second, both the composite image and plots with the XRF data (Ca/Si) were imported into Adobe Illustrator CS3. Varves and event layers were classified according to visual information from the thin section and diagnostic elemental ratios derived from the process study (see sections 4.1) and character-

ization of sedimentary facies (see section 4.5.1). Importantly, the varve chronology was validated with the CRS ^{210}Pb age-depth model and chronomarker horizons (AD 1987 flood event and the AD 1963 radiocaesium peak). A bitmap file was then generated.

Third, the image was imported to the varve counting program WinGeol lamination tool. The software is able to semi-automatically detect and measure lamina thickness in natural archives that show internal growth variability (Meyer et al., 2006). The cell size of a pixel was calculated and adjusted before the measurements. On top of the digital image, a new vector layer with a polyline was created. The algorithms provided for layer identification are based on the analysis of RGB or grey scale curves obtained from digital images. Alternatively, layer boundaries can also be set manually. Numerous cracks in the thin sections, for example, inhibit the use of these algorithms. In this study, all nodes that mark the layer boundaries were set manually according to the previous varve classification. Data segments were classified into the categories: (1) data (varves); (2) no data (turbidites); and (3) links (linkage of consecutive sediment blocks). Finally, a text file was created with the thickness of the individual varves that could be used for statistical analysis.

3.3. Meteorological data

Instrumental data were available from different meteorological stations near the study area. Precipitation is measured in Kandersteg (7°40'E, 46°30'N, 1176 m a.s.l., ~3 km E of Lake Oeschinen), Adelboden (7°34'E, 46°30'N, 1320 m a.s.l, ~13 km E of Lake Oeschinen), Ried (07° 48´23´´E, 46°24´51´´N, 1500 m a.s.l., ~11 km S of Lake Oeschinen), and Blatten (07°49´16´´E, 46° 25´10´´N, 1535 m a.s.l. ~11 km S of Lake Oeschinen, see Figure 2, C).

However, the lengths of temperature and precipitation records differ. At the stations Ried and Blatten, instrumental data were only available since AD 1974 and 2001, respectively. In Adelboden, precipitation was recorded since AD 1901, but temperature was only recorded since AD 1959. Fortunately, a temperature record was available from Château-d'Oex (07°08´30´´E, 46°28´36´´N, 985 m a.s.l., ~86 km W of Lake Oeschinen) since AD 1887.

In Table 2, the different instrumental precipitation (top) and temperature (bottom) records were compared with each other. In general, the relationships between the temperature records appeared to be stronger than the among the precipitation records. However, all correlation coefficients (r) are significant at $p < 0.05$ (all data from Meteo Schweiz, https://gate.meteoswiss.ch/idaweb).

Table 2: Correlation coefficients (r) between different meteorological records. Top: Comparisons of cumulative summer precipitation MJJA and total annual precipitation records from the meteorological stations Kandersteg - Adelboden and Kandersteg - Ried. Bottom: Comparisons of the temperature records Adelboden - Château d'Oex and Adelboden - Ried. Both mean summer air temperatures JJAS and mean annual temperatures were compared between the different stations. Correlation coefficients (r) shown in bold are significant at p < 0.05.

Precipitation records	*pp MJJA (r)*	*total annual pp (r)*
Kandersteg - Adelboden (AD 1901 - 2007, n=107)	***0.70***	***0.73***
Kandersteg - Ried (AD 1974 - 1998, n=25)	***0.53***	***0.73***

Temperature records	*TT JJAS (r)*	*mean annual TT (r)*
Adelboden - Chateau d Oex (AD 1959 - 2007, n=49)	***0.95***	***0.94***
Adelboden - Ried (AD 1974 - 1998, n=25)	***0.98***	***0.98***

3.4. Statistical analyses

In order to evaluate the relationship between varve thickness and meteorological parameters, a correlation and regression analysis was conducted. Pearson correlation coefficients were calculated using the time series from the varve counts and meteorological parameters. The significance of the correlations was tested using a t-test. Due to dating uncertainties, the original time series was filtered with a 3 yr running mean. The effective number of samples was corrected according to Dawdy and Matalas (1964). The adjusted degrees of freedom (DF) were calculated using the following equation:

$$DF\ adj = (n-2) * \frac{(1 - ai * aj)}{(1 + ai * aj)}$$

DF_{adj} denotes the adjusted degrees of freedom, n the initial sample size, and ai and aj are the lag -1 autocorrelations of the two time series compared.

4. Results and Interpretation

4.1. Process study

4.1.1. Mineralogy of the creek deltas

The catchment geology was clearly reflected in the mineralogy of the creek deltas (Figure 6). Typical for the Helvetic nappes, calcite was the most abundant mineral followed by quartz, illite, chlorite, dolomite, K-feldspar and plagioclase. All data are given in Appendix A, Table A3.

The delta fan mineralogy is presented in separate groups: (1) streams from the north (Figure 6, sample locations C-G); (2) glacial streams from the south (sample locations K-Q); and (3) streams from the northeast (sample location A and R). Sample locations H, I and J do not represent fluvial delta fans, but represent unconsolidated sediments from the lake damming landslide. The mineralogy of the soils at the south-facing slopes is represented by sample location B.

Creeks from N - Sediments eroded from the northern slopes typically had a high proportion of quartz in the range of 22 to 45 % followed by clay minerals with an average proportion of ~25 %. Calcite was abundant with ~40 %. With the exception of location D, standard deviations for all minerals appeared to be low (< 6%) at the individual sample locations. At location D, standard deviations for clay minerals and quartz were higher ~13 %. Moreover, spatial variations were particularly observed for quartz and clay minerals: highest proportions of quartz (>40 %) and clay minerals (~38 %) were found at locations C/D and E, respectively.

Glacial creeks from S - Calcite, quartz and dolomite were the main minerals found at the southern shoreline. The mineralogy of the deltas was characterized by a high proportion of calcite (~88 %). Both quartz and dolomite had proportions around ~5 %. In contrast to the northern catchment, clay minerals were not found at the southern shoreline (Figure 5). Mineralogical compositions did not remarkably vary at the southern shoreline; standard deviations were < 4 % for all minerals.

Creeks from NE - The sediments of the Berglibach delta comprised the mineralogical signal of different source areas. Glacial sediments from the Blüemlisalp glacier (Cretaceous) and particles eroded from the north (Tertiary, Cretaceous and Jurassic) were deposited on the same delta; the mineralogical signal was mixed. The mineralogy was characterized

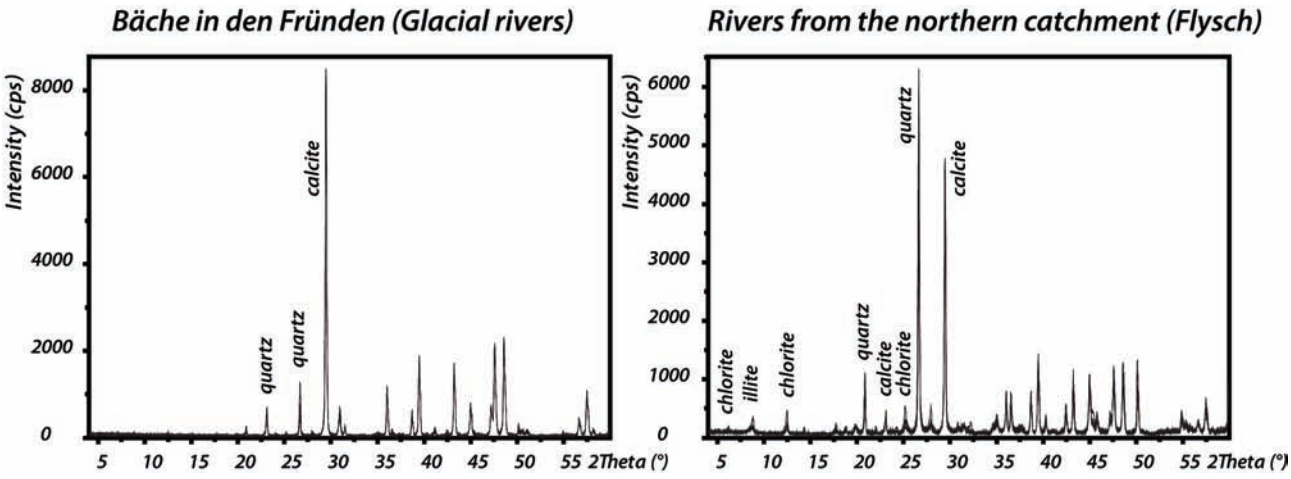

Figure 5: X-ray diffractograms showing the delta fan mineralogy of the rivers "Bäche in den Fründen" (left) and the rivers from N (right). Note that clay minerals (illite and chlorite) were absent at the glacial river deltas (for chlorite 12.6°2θ, for illite at 8.9°2θ). In contrast, both quartz and clay mineral were abundant at the northern shoreline.

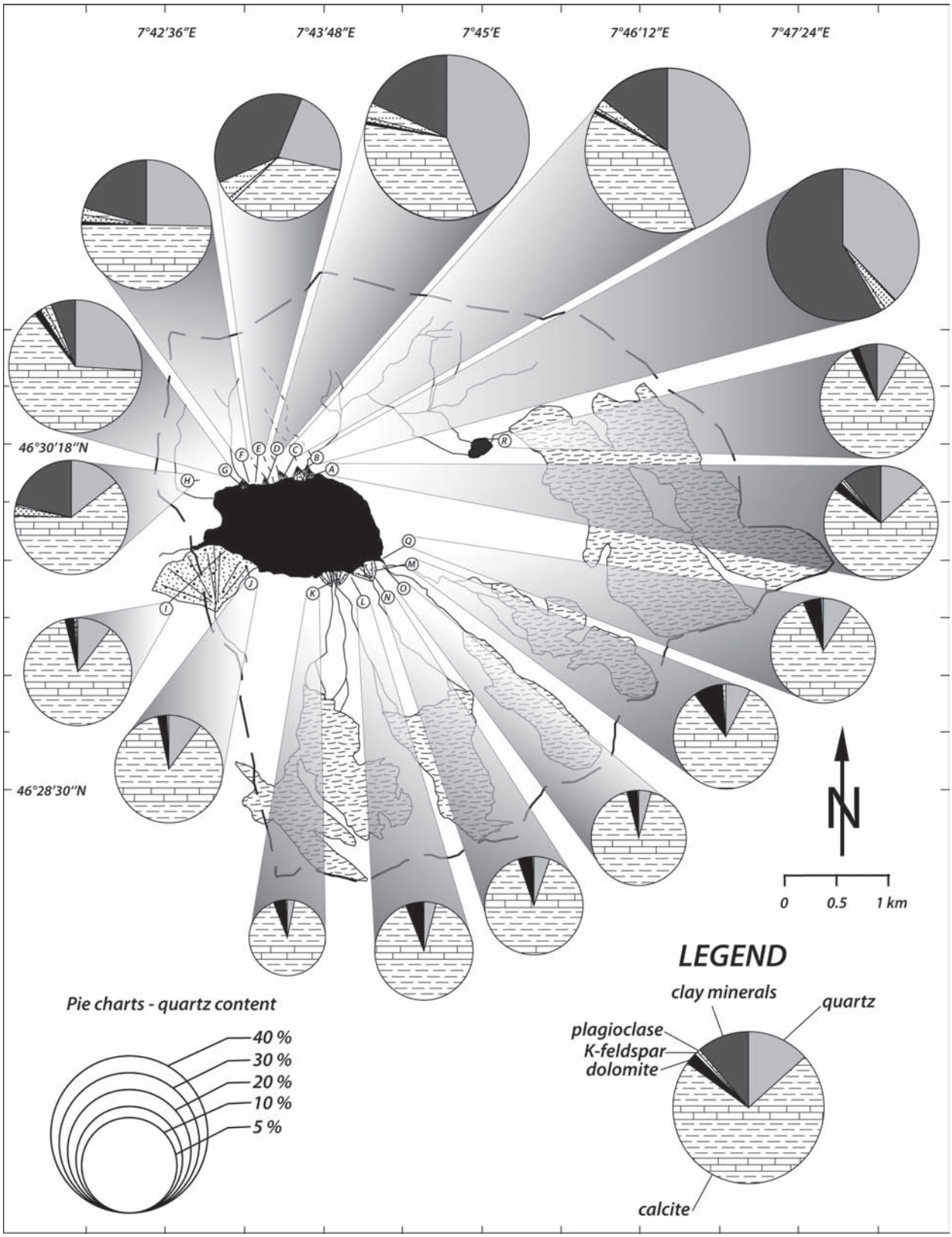

Figure 6: Mineralogy of the delta sediments around the shoreline of Lake Oeschinen. The diameters of the pie charts represent the quartz content of the sediments. Note the contrasts between the rivers from the north (sample locations C-H) and the glacial rivers from the south (sample locations K-Q). Location B represents soil cover.

by proportions of calcite (~70 %), quartz (~13 %), clay minerals (~11 %) and dolomite (~2.5 %). Both K-feldspar and plagioclase had proportions < 1%. In contrast, particles deposited in the proglacial lake (sample location R) comprised more calcite (~84 %), and less quartz (~8 %) and clay minerals (~6%).

Soils - Soil cover in the northern catchment was characterized by proportions of clay minerals (~59 %), quartz (~38 %). Plagioclase and K-feldspar had proportions of 2.6 % and 0.8 %, respectively.

4.1.2. Mineralogical and elemental signals from the catchment

As seen in the previous section (4.1.1), the mineralogy of the creek deltas mirrored local differences in the catchment geology. The source areas of sediment particles could therefore be identified using diagnostic mineralogical and elemental ratios (Figure 7). Contrasts were best expressed by the mineralogical ratios cal/qz, cal/ill and cal/chl. Alternatively, the elemental ratios Ca/Si and Ca/Al yielded the same information because Si and Al occur in the lattice of quartz, illite and chlorite but not in calcite. The Flysch signals considerably differed from the glacial signals: at the southern shoreline, high calcite/clay mineral ratios reflected the absence of chlorite and illite (Figure 7). The cal/qz ratio at the glacial creek deltas was considerably higher (~15.9) than the Flysch signal (~1.3). A mixed Flysch and glacial signal was detected at the Berglibach delta (calcite/quartz ~5.4, Ca/Si ~3.6). However, the glacial signal from the Blüemlisalp glacier appeared to be superimposed on the Flysch signal.

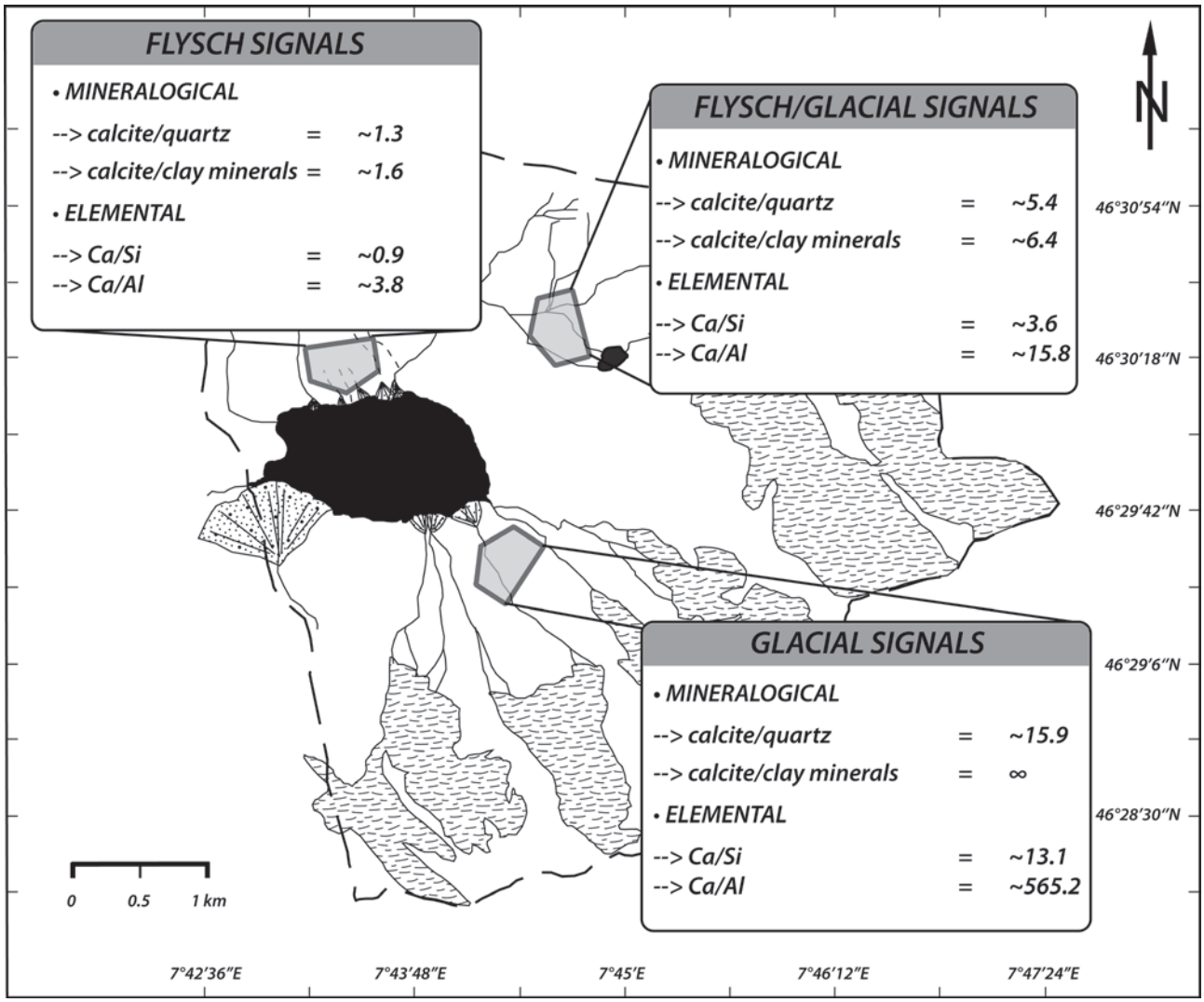

Figure 7: Mineralogical and elemental signals from the catchment. Note that the Flysch, mixed Flysch/glacial, and glacial signal were in contrast to each other. Diagnostic mineralogical and elemental ratios are indicated.

4.2. Sediment traps

4.2.1. Particle flux

During the entire observation period, maximum particle flux was always found in the lowest sediment trap deployed at 4 m above the lake bottom. Figure 9 shows both seasonal variations in particle flux (dotted areas) and the mean grain size of particles trapped at 4 (A), 15 (B), 30 (C), and 45 m (D) above the lake bottom (dashed line). Additional parameters such as median, sorting, skewness and the individual proportions of clay, silt and sand are given in Appendix A, Table A2).

In early summer (30 May to 12 July 2007), sedimentation rates exceed 2 mg dry sediment cm^{-2} day^{-1} (Figure 9, A). Around ~45 % of all particles were trapped near the lake ground. The sediments were characterized by a mean grain size ~8 µm with 1 % sand. At smaller depths, particles appeared to be finer-grained around ~4.5 µm (Figure 9, B, C and D).

During the second sampling interval (12 July to 20 September 2007), sedimentation rates slightly dropped below 1.9 mg dry sediment cm^{-2} day^{-1} in the lowest sediment trap. Particles were characterized by both a higher mean grain size of 11 µm and a higher proportion of sand (~3 %) than during spring snowmelt. At 15, 30 and 45 m above lake ground, similar seasonal patterns were found; however, amplitudes of particle flux were dampened and did not exceed 1.1 mg dry sediment cm^{-2} day^{-1} . Mean grain size distributions did not exceed 5 µm in the upper traps.

A major decrease in particle flux was observed in autumn (20 September to 11 November 2007). In all traps, particle flux dropped below 0.2 mg dry sediment cm^{-2} day^{-1}. The proportion of particles in the clay fraction doubled from 17 % in high summer to 34 % in autumn (means for the trap at 4 m above lake ground).

From 11 November 2007 until 25 June 2008 particle flux averaged 1.5 mg dry sediment cm^{-2} day^{-1} ; mean grain size was 14 µm. Importantly, both winter and spring snowmelt sedimentation processes were represented by this sampling interval. Sediment flux and grain size distributions could therefore not be traced separately. Moreover, due to ice cover, the sediment trap at 45 m above lake ground was not deployed; data are not available for this sampling interval.

4.2.2. Mineralogy of trapped particles

Seasonal differences were found in the mineralogy of sediment particles that are trapped 4 m above the lake ground. Figure 8 shows a XRD diffractogram with qualitative seasonal differences observed

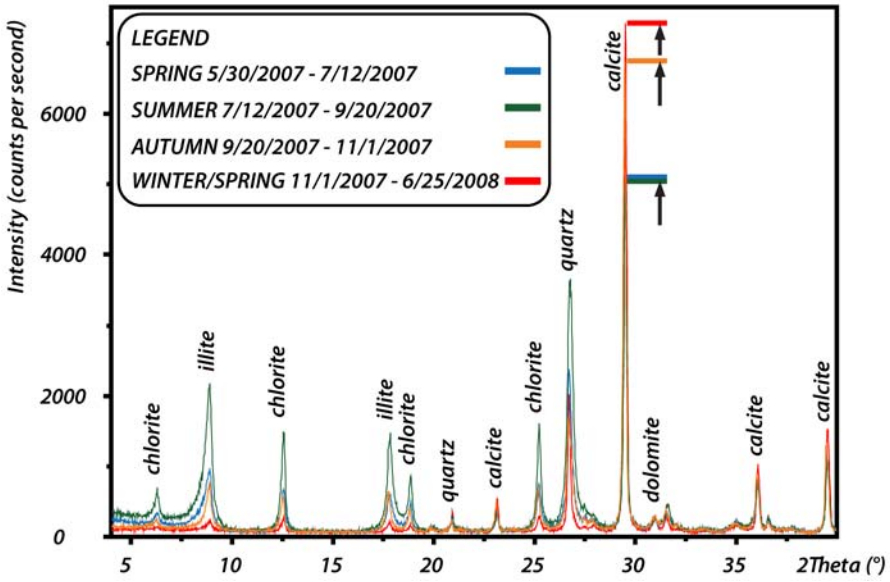

Figure 8: XRD diffractogram showing qualitative mineralogical compositions of sediment particles trapped during the observation period May 2007 – June 2008. Note that the peak intensities of the clay minerals (illite and chlorite) and quartz versus calcite differed considerably between summer (green curve) and winter (red curve).

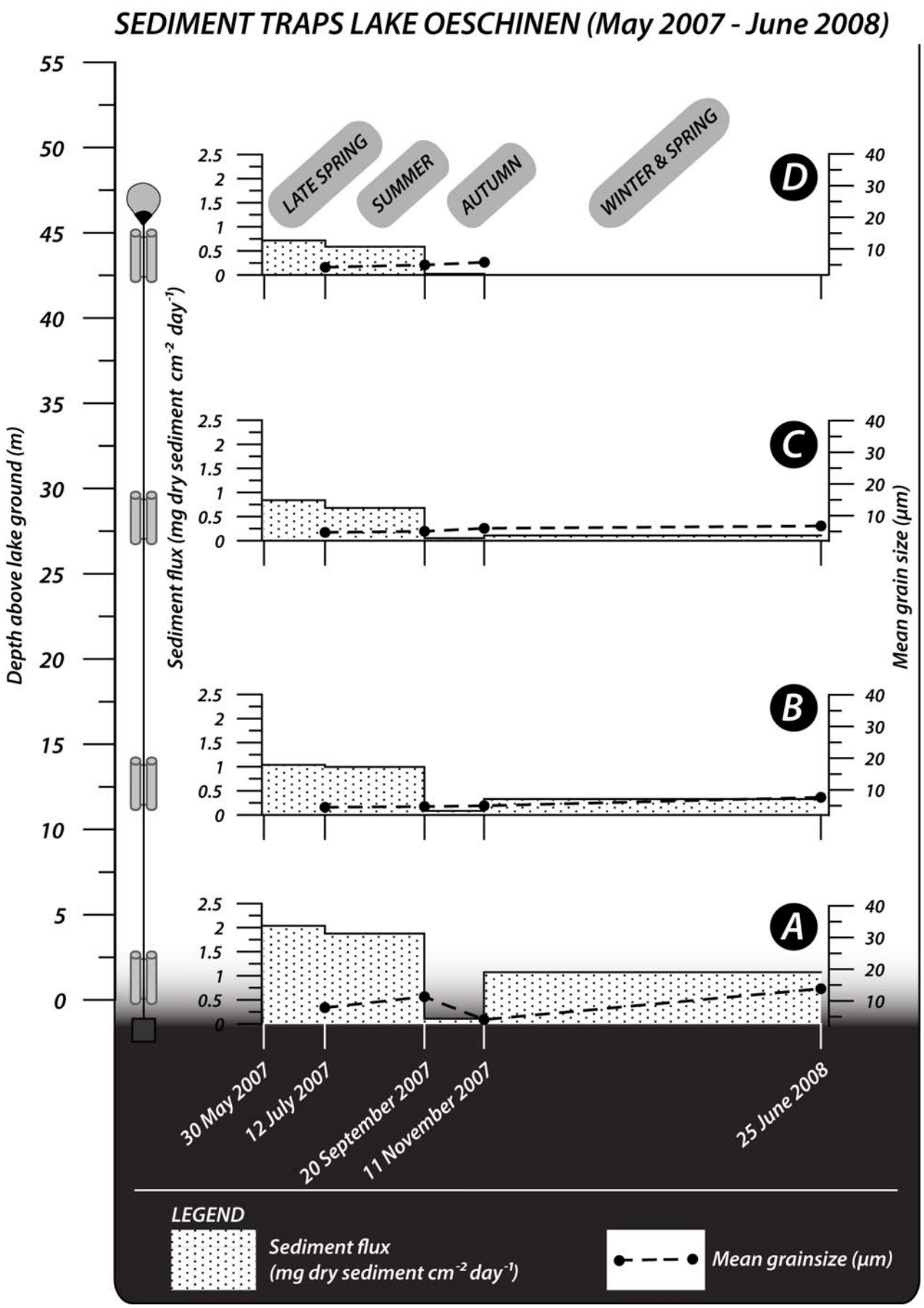

Figure 9: Sediment trap data from May 2007 to June 2008. Particles flux is expressed as mg dry sediment cm^{-2} day^{-1} *, (left axis, dotted areas) and mean grain size (right axis, dashed lines) are shown for the depths 4 m (A), 15 m (B), 30 m (C), 45 m (D) above lake ground.*

for illite (at 8.9° 2θ), chlorite (at 12.6° 2θ), quartz (at 26.7° 2θ) and calcite (at 29.5° 2θ). During the progression of summer (green curve), proportions of both quartz and clay minerals (illite and chlorite) appeared to be higher than during spring snowmelt (blue curve). Particles trapped in autumn (orange curve) and during winter (red curve) were characterized by relatively high proportions of calcite.

4.3. Interpretation of interannual sedimentation processes

High sedimentation rates in spring were caused by snowmelt runoff in the catchment. Bedrock material was mobilized and particles were transported by the creeks to the lake. Field observations (26 May 2010, dry weather) showed that the suspension load of the creeks from the north (Lägerbach and Heubergbach) was high during snowmelt. In contrast, the creek water from the Blüemlisalp glacier was clear; no particles were transported.

In high summer, around 45% of the sediments were trapped near lake ground. Hence, underflows appeared to be the dominant sediment transport processes. Overflows and interflows seemed to be less important. However, snow and ice melt runoff during summer may have increased the density of the creek water. Consequently, the lake water density was higher than creek water density and sediment plumes entered the lake as overflows ($\rho_{inflow} < \rho_{epilimnion}$) or at an intermediate depth as interflows ($\rho_{inflow} > \rho_{epilimnion}$ and $\rho_{inflow} < \rho_{hypolimnion}$).

During late summer, a higher proportion of sand may have resulted from an increase in the creek flow velocity. The effect of the snow melt was probably intensified by rainstorms that remarkably altered creek discharge and the potential for mechanical erosion of bedrock. Due to negative surface charge, clay particles collided and adhered to one another and were deposited in summer. Whereas the influence of snowmelt was continually decreasing during the progression of summer, rainstorms and glacial melt became the main factors controlling sediment supply to the lake.

Low sedimentation rates in autumn were probably the result of weak rainfall intensities, precipitation already in the form of snow and reduced glacial melting. Most creeks originating from the northern catchment were inactive during this season. Thus, sediment input to the lake was generally low. In all sediment traps, mean grain size distributions were in the range of 4 to 6 µm. Clay particles, which had remained in the water column due to thermal stratification in summer, were slowly settling.

Although data are missing for the winter season, it can be assumed that only clay-size particles were deposited because all creeks were frozen and ice cover inhibited additional sediment supply to the lake. According to Stokes law, a clay particle of 2 µm diameter has a settling velocity of ~20 cm/day. Thus, it takes several months (~275 days for 55 m water depth) until clay particles have settled to the lake bottom. These slow settling velocities make it clear that particles in the clay fraction were only deposited in winter, but originally entered the lake in summer.

4.4. Hypothesis for varve formation

Preliminary findings from section 4.2 lead to the hypothesis that individual varves comprise different laminae deposited in spring (1), summer (2) and winter (3). Particle flux, grain size distributions (Figure 9) and mineralogy (Figure 8) differed considerably during an interannual cycle of sedimentation. Figure 10 illustrates hypothetical properties of an individual varve.

During spring snowmelt, a layer containing sand is deposited. However, there is no diagnostic source area for these particles because snow cover is melting in the entire catchment.

In summer, rainstorms provide high energy for ero-

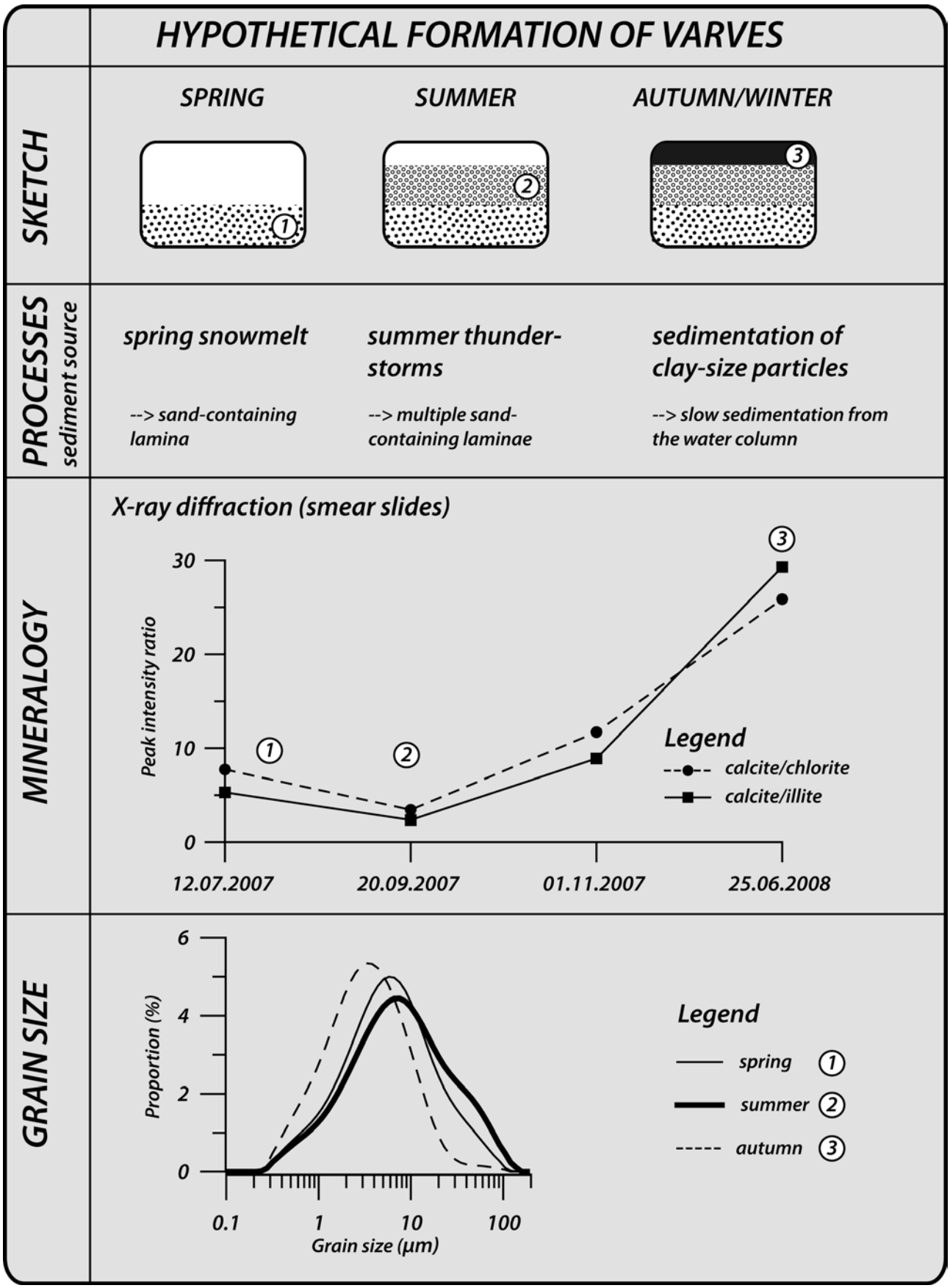

Figure 10: Hypothetical varve formation. Data from the sediment trap analyses (particle flux, XRD, and grain size) are summarized for the different seasons. Top: Schematic sketch showing the hypothetical varve formation with the seasonal signals spring (1), summer (2), and autumn/winter (3). Middle: X-ray diffraction peak intensity ratios cal/chl and cal/ill. The ratios are diagnostic for the season summer (2) and winter (3). Bottom: grain size distributions for the season spring (thin line), summer (thick line) and autumn (dashed line).

sion and transport of coarser particles; the proportion of sand is higher than in spring. Clay minerals (illite and chlorite) are easily eroded from the Flysch units. Consequently, summer layers have lower cal/ill and cal/chl ratios than spring and winter layers. Alternatively, the same assumptions are valid for the elemental ratios Ca/Al and Ca/Si.

During winter, slow sedimentation of calcite particles (clay fraction) is the dominant sedimentation process. A calcareous layer is deposited; cal/ill and cal/chl ratios are higher than in summer.

In conclusion, an individual varve comprises one spring, multiple summer, and one winter lamina. Using XRF scans for sediment analysis, summer layers very likely show high Al and Si concentrations. Ca peaks, in contrast, should represent winter layers. Furthermore, the proportion of sand within a varve is possibly a proxy for the intensity and the number of summer rainstorms.

4.5. Sediment record – mastercore

Four piston and one freeze core were recovered from Lake Oeschinen 15 and 16 June 2007 (Table 3, Figure 4). For this study, the freeze core (Oeschi 07-3) was chosen to be the mastercore. The coring site of the mastercore is located between the deltas Berglibach and the glacial creek deltas "Bäche in den Fründen" (see Figure 4).

4.5.1. Core description and sedimentary facies

The core has a total length of 150 cm and width of ~15 cm. In this study, the top 50 cm of the core were analyzed. Sediment analysis revealed that two sedimentary facies A and B were present in the mastercore that represent annually laminated and event layers, respectiveley (Figure 11).

- ***FACIES A – Varves***

Sedimentary facies A was characterized by rhythmically laminated sediments that alternately comprised sandy and clay-rich laminae. All photographs shown in this section were taken from thin sections of the mastercore. Colors may therefore differ from photographs of the frozen sediment core.

The contacts between sandy and clay-rich laminae appeared to be continuous. Therefore, a couplet of two laminae (a sandy and an overlying clay-rich lamina) represented a fining upward sequence. In contrast, the contacts between clay-rich and overlying sandy laminae were sharp. Qualitative elemental concentrations, obtained from the micro XRF scans, showed that sandy laminae comprised relatively high concentrations of the elements Fe, K and Si (Figure 12, green = Fe, blue = Ca, and yellow = K). In the finer-grained laminae, relatively high concentrations of Ca were measured. Peaks in the Ca/Si elemental ratio only appeared in clay-rich laminae. All calcite (89 %), quartz (8 %), dolomite (2 %), clay minerals (1%) and feldspars (<1 %) were found in facies A. However, this mineralogical composition only holds only true for the sequence 47.5 – 50 cm sediment depth and may differ in other varved sequences.

Facies A can be sub-divided into 3 distinctive varve types (Figure 13): ***type I*** was characterized by a thin

Table 3. Coring locations, length of the sediments cores, water depths and coordinates.

Core	*Length (cm)*	*Water depth (m)*	*Coordinates*
Oeschi 07-1	*115*	*51.1*	*N 46°30'040" E07°43'435(4)"*
Oeschi 07-2	*220*	*51.1*	*N 46°30'040" E07°43'435(4)"*
Oeschi 07 -3 (freeze core)	*145*	*51.1*	*N 46°30'040" E07°43'435(4)"*
Oeschi 07-4	*114*	*51*	*N 46°30'039" E 07°43'439"*
Oeschi 07-5	*210*	*51*	*N 46°30'039" E 07°43'439"*

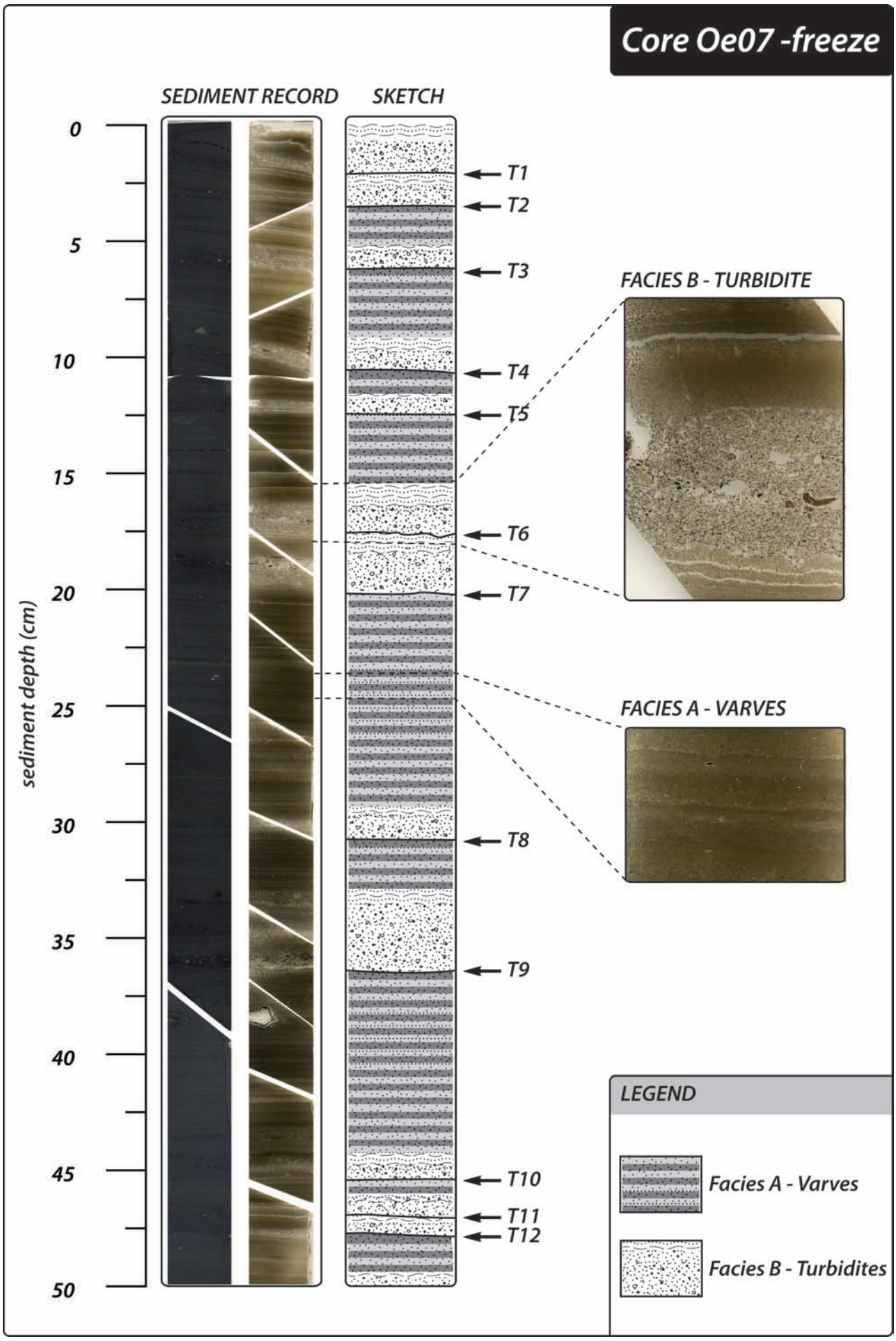

Figure 11: Composite photographs of the freeze core Oeschi 07-3 (left) and a schematic sketch (right).

(1 – 1.5 mm) fining upward sequence. This type was mainly found at the very bottom of the analyzed section (47.5-50 cm sediment depth, Figure 12). ***Type II*** was thicker than type I (>3 mm) and comprised coarser particles. In contrast, varves identified as ***type III*** comprised multiple micro laminations whereas each was representing a fining upward sequence. Contacts between individual micro laminations appeared to be either sharp or wavy (= erosive). A clear identification of varve type III was difficult because individual micro laminations may be mistaken for a varve of type I. However, as seen with type I and II, an annual cycle of sedimentation was only completed with a very fine-grained top. Thus, only the clay-rich top of a varve with its diagnostic Ca/Si ratio denoted the completion of an annual sedimentation cycle. Importantly, this feature was essential for a correct identification of all varve types.

Facies A is interpreted as varves that individually comprise a summer (sandy, low Ca/Si ratio) and a winter lamina (clay-rich, high Ca/Si ratio). Micro laminations found in summer laminae (varve type III) are very likely the result of individual summer rainstorms that provide energy for erosion and transport of coarse, sandy particles. This interpretation is supported by the sediment trap data (see Figure 8) that revealed that clay minerals (no Ca in the lattice, low Ca/Si ratio) were predominantly deposited in summer. Particles trapped during winter, in contrast, contained higher proportions of calcite. Due to complex micro laminations in summer laminae (varve type III), Ca/Si peaks are the only diagnostic feature that can be used for the identification

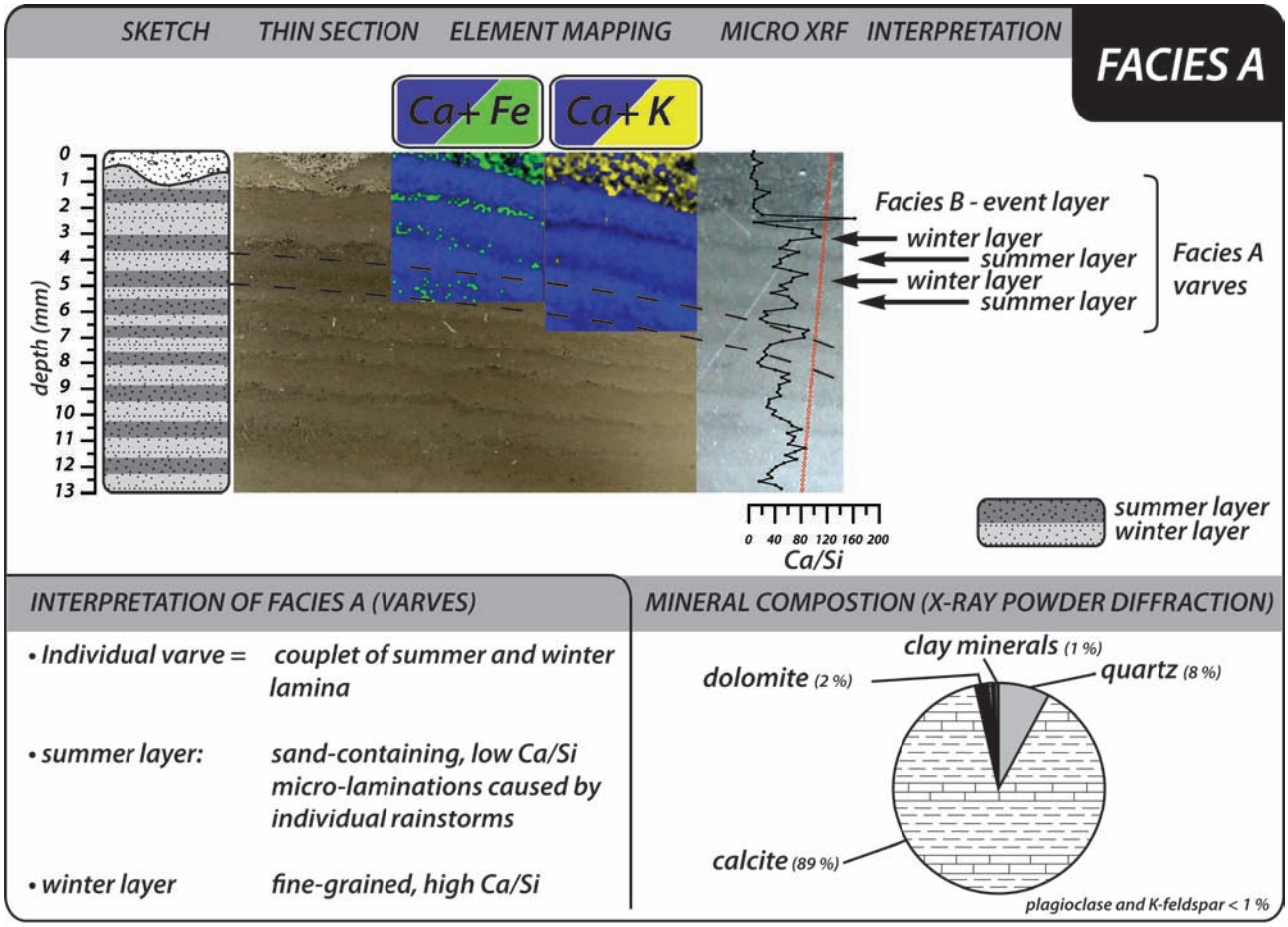

Figure 12: Geochemical and mineralogical characteristics of facies A. Top from left to right: Schematic sketch of the varved sequence from 47.5 -50 cm sediment depth, photograph of the thin section, X-ray fluorescence elemental maps showing qualitative elemental concentrations for the elements Ca (blue), Fe (green) and K (yellow). Bottom from left to right: Interpretation of the sedimentary facies, quantitative mineralogical composition of the varved sequence from 47.5 – 50 cm sediment depth. Note that mineralogical compositions of other varved sequences may differ.

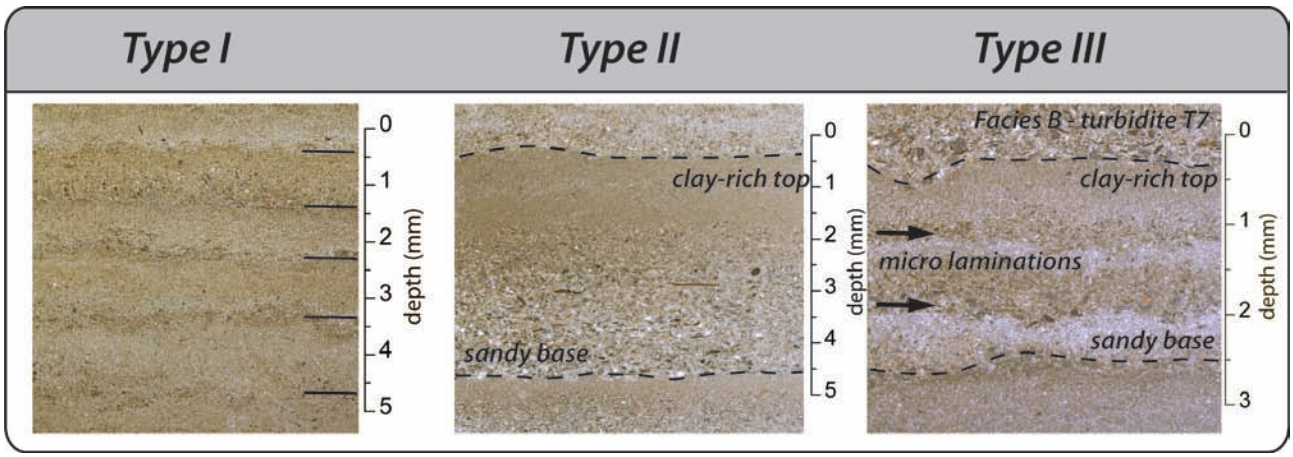

Figure 13: Photographs of 3 different varve types found in the sediment record of Lake Oeschinen.

of varves.

- ***FACIES B – graded layers (turbidites)***

Facies B represents graded layers that are deposited within a short time period (hours to days) with extremely high sedimentation rates. Event layers had a darker color than facies A and have a thickness > 10 mm. The contacts at the bottom were either sharp or wavy (Figure 14, left and right, respectively). Sediment particles at the base of an event layer appeared to be in the sand fraction. In general, event layers were characterized by fining upward sequences. However, internal laminations, representing individual fining-upward sequences, were distinctive features of event layers. Organic macro fossils (e.g. fir needles), that are found in most event layers (e.g. T7 and T9, Figure 11), appeared to have a preferred orientation. The top of event layers were very fine-grained.

Mineralogical analysis revealed that the turbidites T6 and T7 (Figure 11) mainly contained calcite (~60 %, average of the T6 and T7) followed by quartz (~30 %) and clay minerals (~7%). Proportions of dolomite, K-feldspar and plagioclase did not exceed 2 % (Figure 15). Ca/Si ratios showed lower ratios than in facies A. Importantly, in the clay-rich top of an event layer a Ca/Si peak was found.

Facies B is interpreted as turbidite deposits either caused by flood events in the catchment area or delta collapse. In particular during summer rainstorms, coarse particles are eroded from the Flysch units (northern catchment) and transported to the lake. This interpretation is supported by the mineralogical composition of the turbidites T6 and T7: high proportions of quartz and clay minerals are diagnostic for the Tertiary Flysch units as a source area of particles.

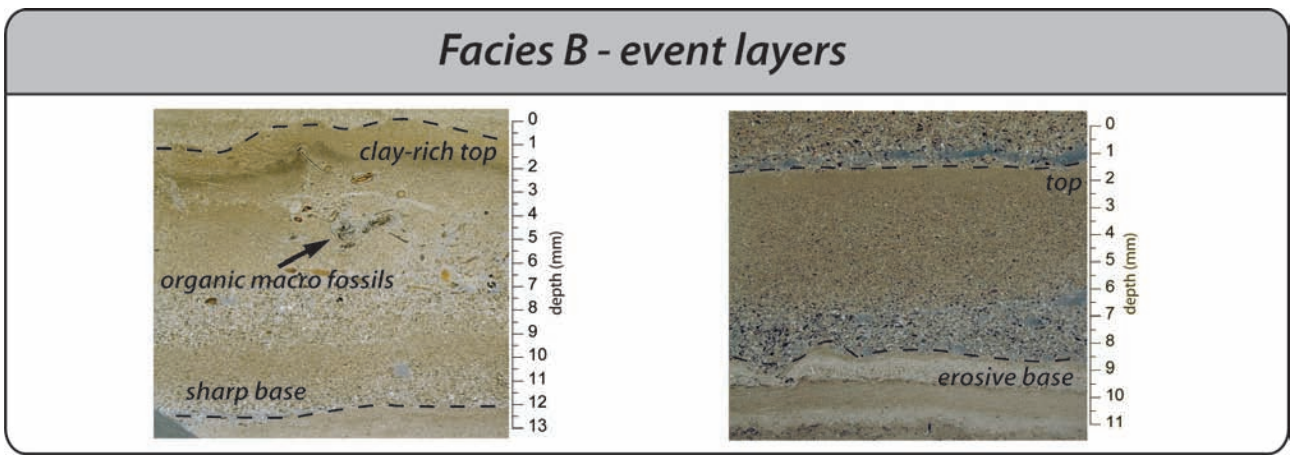

Figure 14: Photographs of the turbidites T10 (left, 45 cm sediment depth) and T12 (right, 47.5 cm sediment depth)

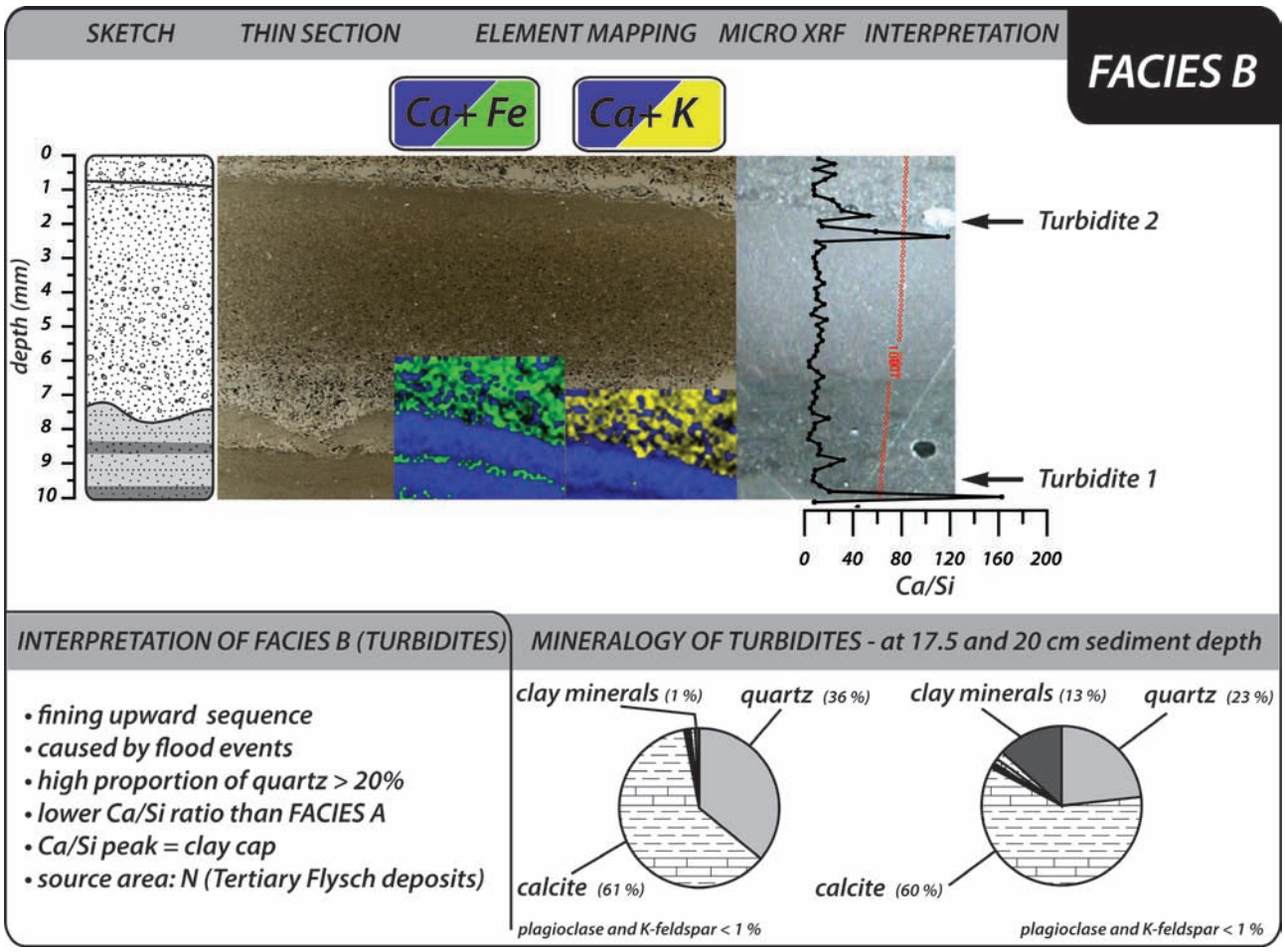

Figure 15: Geochemical and mineralogical characteristics of facies B. Top from left to right: Schematic sketch of event layer T12 at 47.5 cm sediment depth, photograph of the thin section, X-ray fluorescence elemental maps showing qualitative elemental concentrations for the elements Ca (blue), Fe (green) and K (yellow). Bottom from left to right: Interpretation of the sedimentary facies, quantitative mineralogical composition of the turbidites T6 and T7 at 15-20 cm sediment depth.

In conclusion, clay caps at the top of turbidites (Facies B) and winter layers (Facies A) do not differ in their geochemical compositions. Hence, when using XRF data for identification of individual varves, Ca/Si peaks at the top of event layers and the winter layer must not be mixed up.

4.5.2. Sediment chronology

4.5.2.1. ^{210}Pb and ^{137}Cs

Image analysis of the thin sections revealed that 12 turbidites occurred in the top 50 cm of the master-core. All event layers were removed from the ^{210}Pb data set. Total ^{210}Pb activity reached equilibrium with ^{226}Ra at ~40 cm total sediment depth (Figure 16, left). Supported ^{210}Pb activity, estimated from ^{226}Ra activity, showed constant background values of ~40 Bq kg^{-1}. Unsupported ^{210}Pb activity exponentially decreased from the top to the bottom of the core (Figure 16, middle). ^{137}Cs activities first appeared at 35 cm total sediment depth. The radiocaesium peak, comprising the AD 1963 chronomarker horizon, was found at 28 cm. At ~13 cm, a minor ^{137}Cs peak probably represented the AD 1986 reactor fire in Chernobyl (Figure 16, right).

The CIC model yielded multiple age inversions and errors >100 yr and was therefore rejected. Figure 17 shows the CRS model (line) that was consistent with the AD 1963 radiocaesium peak (black circle, ~28 cm total sediment depth); the age difference was only -2 yr. Consequently, the CRS model could be constrained by the 1963 radiocaesium peak (dashed

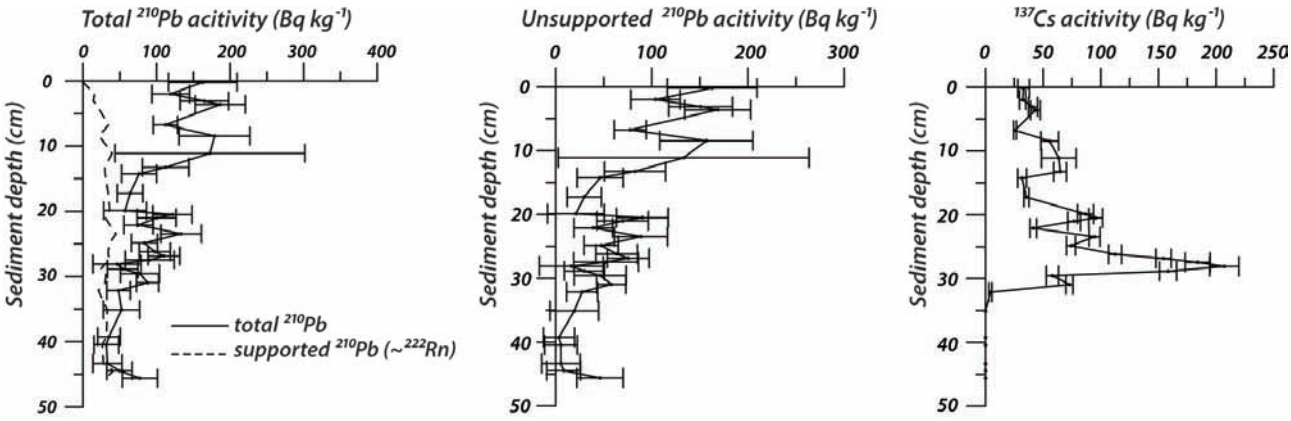

Figure 16: ^{210}Pb and ^{137}Cs activities in the mastercore - A) total and supported ^{210}Pb, B) unsupported ^{210}Pb, C) ^{137}Cs concentrations versus depths.

line = composite CRS model); the age-depth model was forced through an independent time marker. As a result, a time shift of minus 2 years was observed before AD 1963 between the CRS and the constrained CRS model. Furthermore, the numeric age for the start of the ^{137}Cs atmospheric fallout dated back to AD 1954. This date was in good agreement with literature data that reported the start of atmospheric nuclear bomb testing in AD 1952 (Appleby, 2001). The age-depth model was also verfied by the AD 1986 ^{137}Cs peak (black circle, ~13 cm total sediment depth) and by the AD 1987 historical flood event (black triangle, ~12 cm total sediment depth). The CRS model was therefore validated by four independent time markers and the final age model was developed by constraining the CRS model to the AD 1963 ^{137}Cs peak.

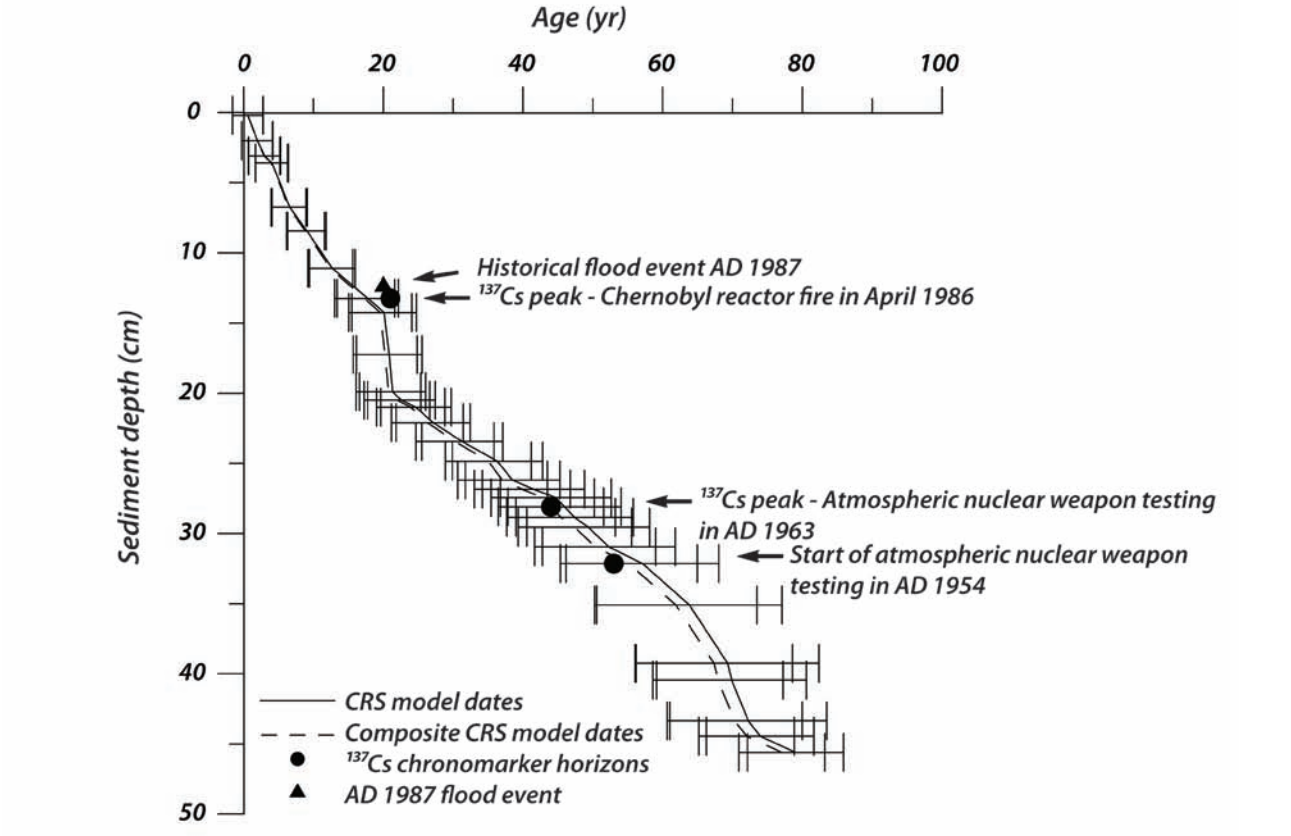

Figure 17: Comparison of the CRS (line) and ^{137}Cs-AD 1963-constrained CRS (dashed line) age-depth models. The ^{137}Cs chronomarker horizons (AD 1954 start of nuclear weapon testing at 32.1 cm, AD 1963 peak at 28.1 cm, AD 1986 Chernobyl reactor fire peak at 13.2 cm total sediment depth) are indicated with black circles and the AD 1987 historical flood event (12.4 cm total sediment depth) with a black trianlge.

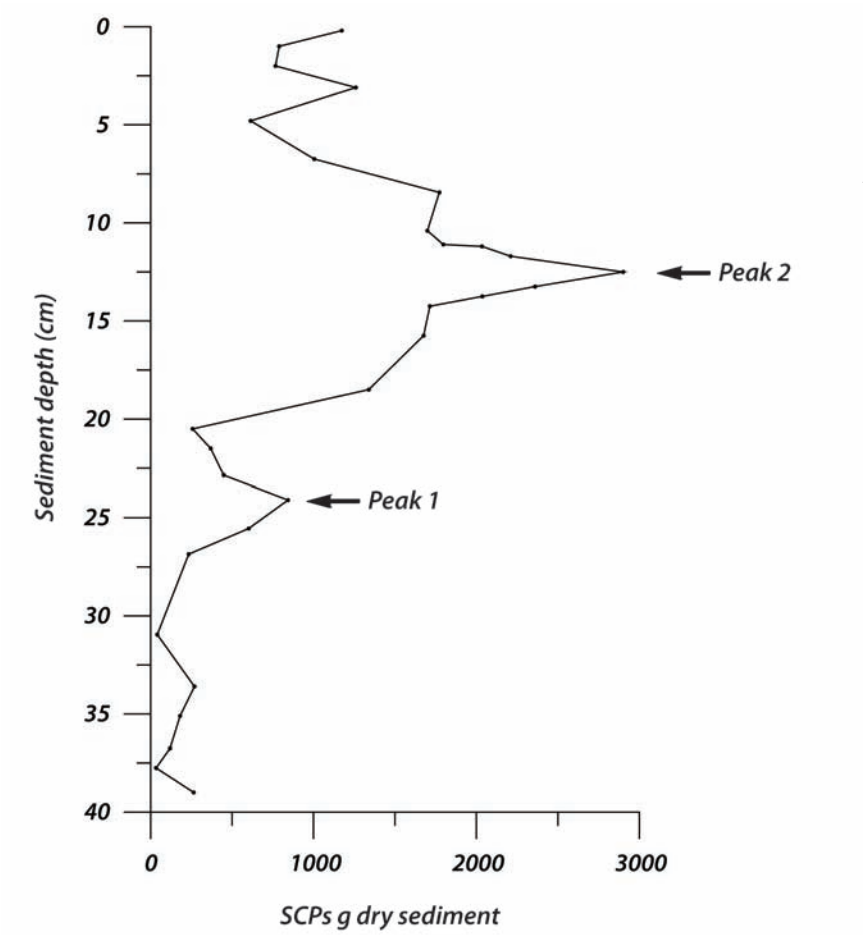

Figure 18: SCP profile of the sediment core Oeschi 07-3. SCP concentrations are expressed as number of SCPs per g dry sediment. Two peaks were found at 24.1 cm (peak 1) and 12.5 cm (peak 2) total sediment depth.

4.5.2.2. Spheroidal carbonaceous particle counts

Spheroidal carbonaceous particles were found in the entire sediment sequence analyzed (top 40 cm of the mastercore). The samples were characterized by the occurrence of numerous charcoal particles that were found throughout the entire sediment sequence. In particular, the distinction between small SCPs and charcoal particles was difficult. In the bottom of the SCP profile, the concentrations averaged 160 SCPs per g dry sediment (Figure 18). Two peaks were observed at 24 and 12.5 cm total sediment depth. The soot particle concentrations of the lower and upper peak averaged 850 and 2900 SCPs per g dry sediment, respectively. According to the composite CRS model, the minor peak (24 cm total sediment depth) dated back to AD 1972 with a standard error of 6 yr. Numerical ages for the upper peak revealed an age of 17 yr (AD 1990) with a standard error of 4 yr.

4.5.2.3. Varve counts

The process study (section 4.4) and the characterization of lithotypes (section 4.5.1) revealed that the elemental ratio Ca/Si or Ca/Al enabled the identification of sedimentary facies A (varves) and B (turbidites).

On the basis of the thin sections and XRF data, varves and event layers of the upper-most ~50 cm of the mastercore were classified. Figure 19 shows the resin impregnated sediment blocks 1 to 4 and the Ca/Si ratios. Varves and turbidites were numbered from the top to the bottom of the mastercore.

Varves in the upper-most block 1 (Figure 19, left), however, could not be classified because the layers were inclined. The XRF scanning detector had a width of 12 mm and layers must therefore be perpendicular to the scanning direction. Data points of block 1 therefore represent mixed geochemical signals. Diagnostic Ca/Si ratios of winter layers could not clearly be identified.

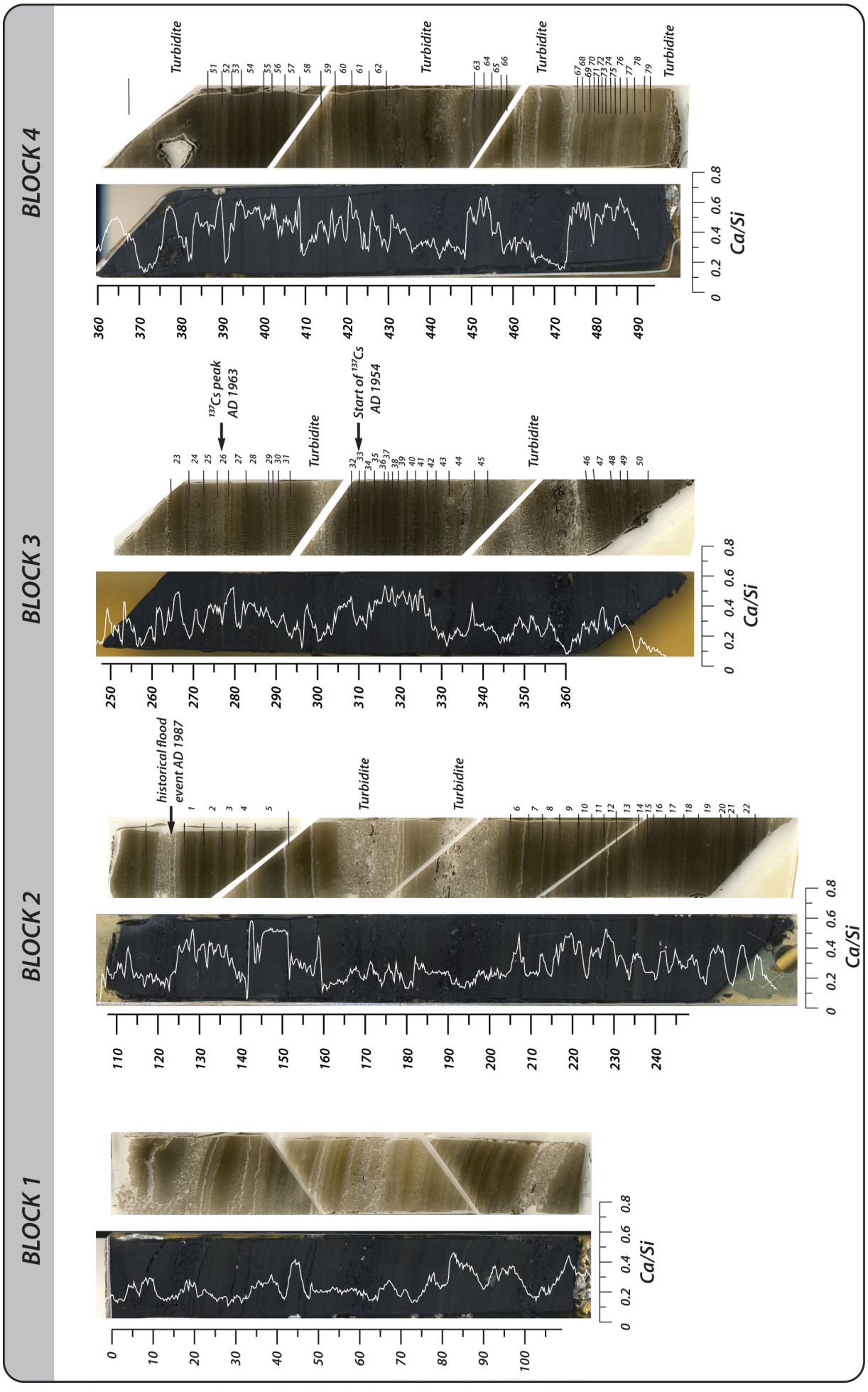

Figure 19: Varve counts of the top 50 cm of the mastercore. Resin impregnated sediment blocks 1 to 4 with Ca/Si ratios. Varves and turbidites are marked with lines. Varve thickness was measured with the software WinGeol lamination tool.

The varve record starts below the historical flood event in AD 1987. Until the bottom of block 4, 80 varves were identified. Average varve thickness was 3 mm with a standard deviation of 1.6 mm. The oldest varve in this record dates back to AD 1907.

4.6. Comparison of varve thickness with instrumental data

4.6.1. Entire varve record AD 1907 - 1986

Varve thickness was compared with cumulative summer precipitation from the meteorological station in Kandersteg and Adelboden (Figure 20) and mean summer air temperatures from Château d'Oex. Due to dating uncertainties of the varve chronology, the time series were filtered using a 3 yr running mean. Table 4 (top) shows the correlation coefficients with cumulative summer precipitation (pp) MJJA and MJJAS for the time span AD 1907 – 1986. Correlation analysis revealed significant correlations at the 95 % confidence level (shown in bold) with both data from Kandersteg and Adelboden. However, the varve-climate relationships appeared to be stronger with data from Kandersteg. Furthermore, the cumulative precipitation (MJJA) explained more variability ($r^2 = 0.12$) in varve thickness than pp MJJAS ($r^2 = 0.09$). With mean summer temperatures (MJJAS), however, no significant correlations were found ($r = -0.1$, not significant at $p < 0.05$, $n = 80$).

4.6.2. Varve record AD 1920 - 1986

As shown in Figure 20, varve thickness and pp MJJA appeared to be weakly negatively correlated during the period AD 1907 - 1919 (-0.19, not significant at $p < 0.05$, $n = 13$). Thus, for the period AD 1920 – 1986, varve-precipitation relationships appeared to be stronger if the first 13 yr of the time series (AD 1907 – 1919) were excluded from the correlation analysis.

Table 4 (bottom) shows the correlation coefficients r between varve thickness and pp MJJA and pp MJJAS for the period AD 1920 – 1986. In general, the same

Table 4: Top: Correlation coefficients r between varve thickness and cumulative summer precipitation MJJA and MJJAS calculated with instrumental meteorological data from Kandersteg and Adelboden for the entire observation period AD 1907 – 1986. Bottom: Correlations coefficients calculated for the time period AD 1920 - 1986. Due to dating uncertainties, time series was filtered using a 3 yr running mean. Correlation coefficients r shown in bold are significant at p < 0.05.

AD 1907 - 1986 (n=80)	*pp MJJA (r)*	*pp MJJAS (r)*
Data Kandersteg		
non-filtered	***0.34***	***0.3***
3 yr filtered	***0.49***	*0.48*
Data Adelboden		
non-filtered	***0.29***	***0.26***
3 yr filtered	*0.37*	*0.4*

AD 1920 - 1986 (n=67)	*pp MJJA (r)*	*pp MJJAS (r)*
Data Kandersteg		
non-filtered	***0.43***	***0.36***
3 yr filtered	***0.64***	***0.57***
Data Adelboden		
non-filtered	***0.29***	***0.25***
3 yr filtered	*0.35*	*0.38*

varve-climate relationships were found as with data from the entire observation period AD 1907 - 1986. However, correlations were stronger. With non-filtered and 3 yr filtered time series pp MJJA, correlations of r = 0.43 (significant at p <0.05) and r = 0.64 (significant at p <0.05) were found, respectively.

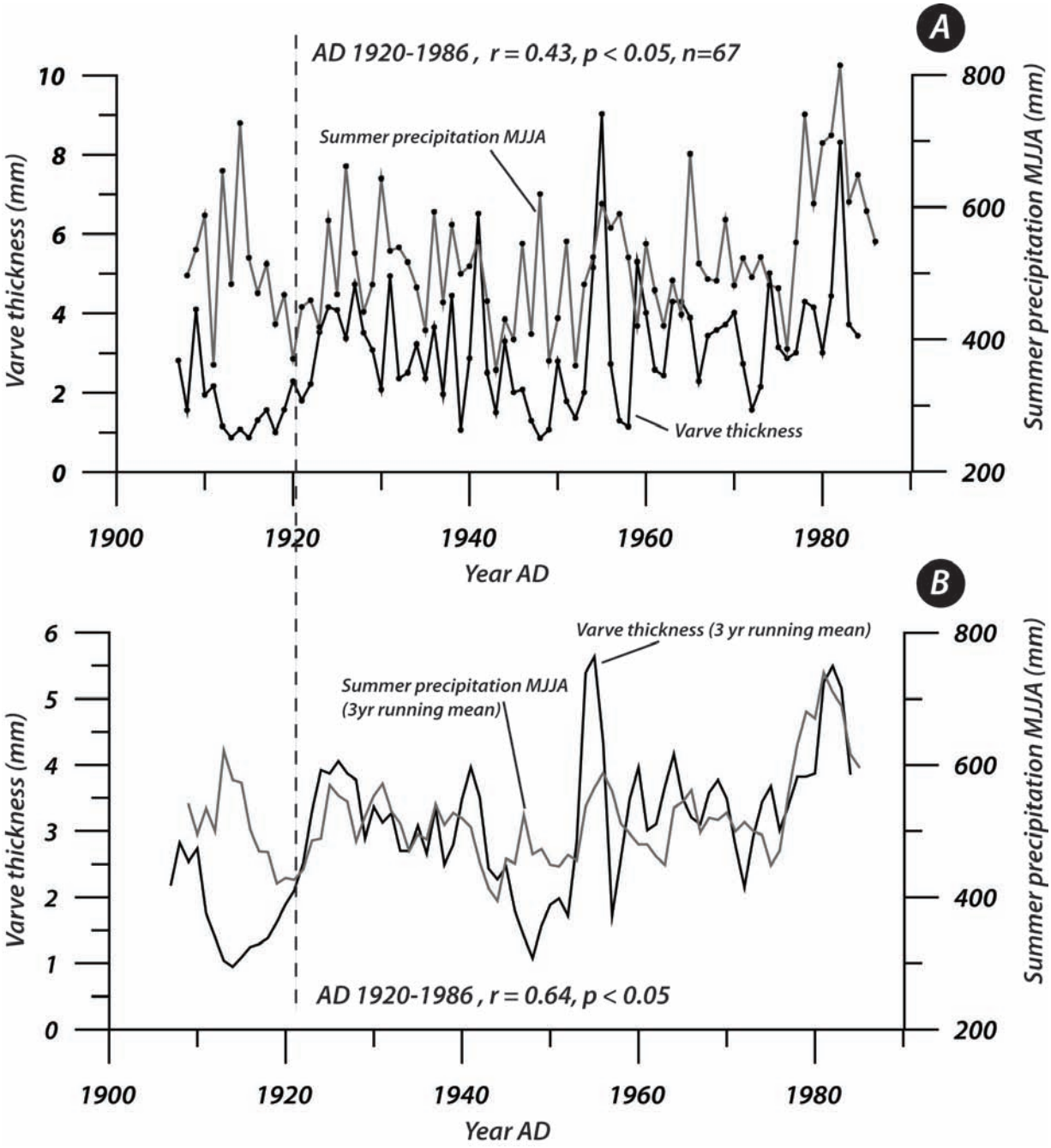

Figure 20: Comparison of the varve thickness (AD 1907 -1986) with cumulative summer precipitation MJJA measured at the meteorological station in Kandersteg. Note that between AD 1907 – 1919, varve thickness and cumulative summer precipitation MJJA appeared to be negatively correlated. Top: Non-filtered time series: r = 0.43 at p <0.001, for the period AD 1920 - 1986. Bottom: 3yr filtered (3 yr running mean) time series: r = 0.64, p<0.01, for the period AD 1920 – 1986.

5. Discussion

5.1. Chronology

As the chronology of the mastercore was the basis of all comparisons of physical proxy data with instrumental data, dating results are discussed in detail in the following paragraphs. The SCP profile, however, is discussed separately because the results appeared to be inconclusive.

The SCP profile of Lake Oeschinen did not mirror the typical European patterns described by Rose (2001): a rapid increase in the SCP fallout was found during the mid 1940s to 1950s (means for Switzerland, Lotter et al. unpublished). Maximum SCP fallout was assumed to peak during the late AD 1970s. In contrast, highest SCP concentrations in the sediments of Lake Oeschinen appeared in the mid AD 1980s (Figure 21, at 12.5 cm sediment depth). For a correct reconstuction of the past SCP fallout, however, the SCP concentrations needed to be expressed a SCP flux (SCP $cm^{-2}\,yr^{-1}$). Assuming a constant sedimentation rate now for discussing the SCP profile, possible reasons for the observed SCP pattern include:

- ***Secondary source of SCPs***: During the 1980s and 1990s, construction machinery was used for the construction of roads in the study area (D. Wandfluh, owner of Hotel Oeschinen, personal communication). Thus, the primary SCP flux, representing the overall oil consumption of Switzerland including the late AD 1970s peak was probably superimposed by a secondary SCP source. The remote location of the study site could possibly have intensified this effect.

- ***Sample preparation***: Sample homogenization, when filling sample aliquots in Petri dishes, is a very sensitive procedure. It was not proven that the sample aliquot really represented the true SCP concentration of the entire sample.

- ***SCP counts using a light microscope***: A magnification of 50 x was probably not sufficient for the identification of SCPs. The size of fly-ash particles is highly variable (1-50 µm, Clark, unpublished) and decreases with an increasing distance from the source (Rose, 2001). As a result, SCPs found in sediments of remote high-Alpine Swiss lakes are relatively small in size unless there is a secondary source of SCPs (see previous section). Consequently, a higher magnification would be required for scanning the sample and identification of SCPs that are not derived from a secondary source.

- ***Human factor***: Although objective criteria exist for the distinction of diverse fly-ash particles, the identification of an SCP is often subjective and counts provided by different persons can vary considerably. SCP profiles created by inexperienced counters must only be used as qualitative measure for SCP concentrations.

Alternatively, automated optical methods enable a reproducible quantification of fly-ash particles such as SCPs. However, only a few studies have been conducted using quantitative particle analyses through image-processing techniques (e.g. Thevenon and Anselmetti, 2007; Thevenon et al., 2009). Analyzing a known grain size fraction (sieving of the sample) with objective criteria (e.g. thresholds for the grey value and sphericity) likely yield more reliably SCP profiles.

Moreover, the validity of the SCP peak as an independent chronomarker horizon is questionable: in the non-varved sediments of the high-alpine lake Hagelseewli (46° 40'N, 08°02'E, 2339 m a.s.l.), the SCP peak was assumed to date back to 1977 ± 4 yr (Lotter et al., 2002). In contrast, Kamenik et al. (2009) stated that the maximum SCP fallout in the Engadine valley occurred in AD 1970. In the same study

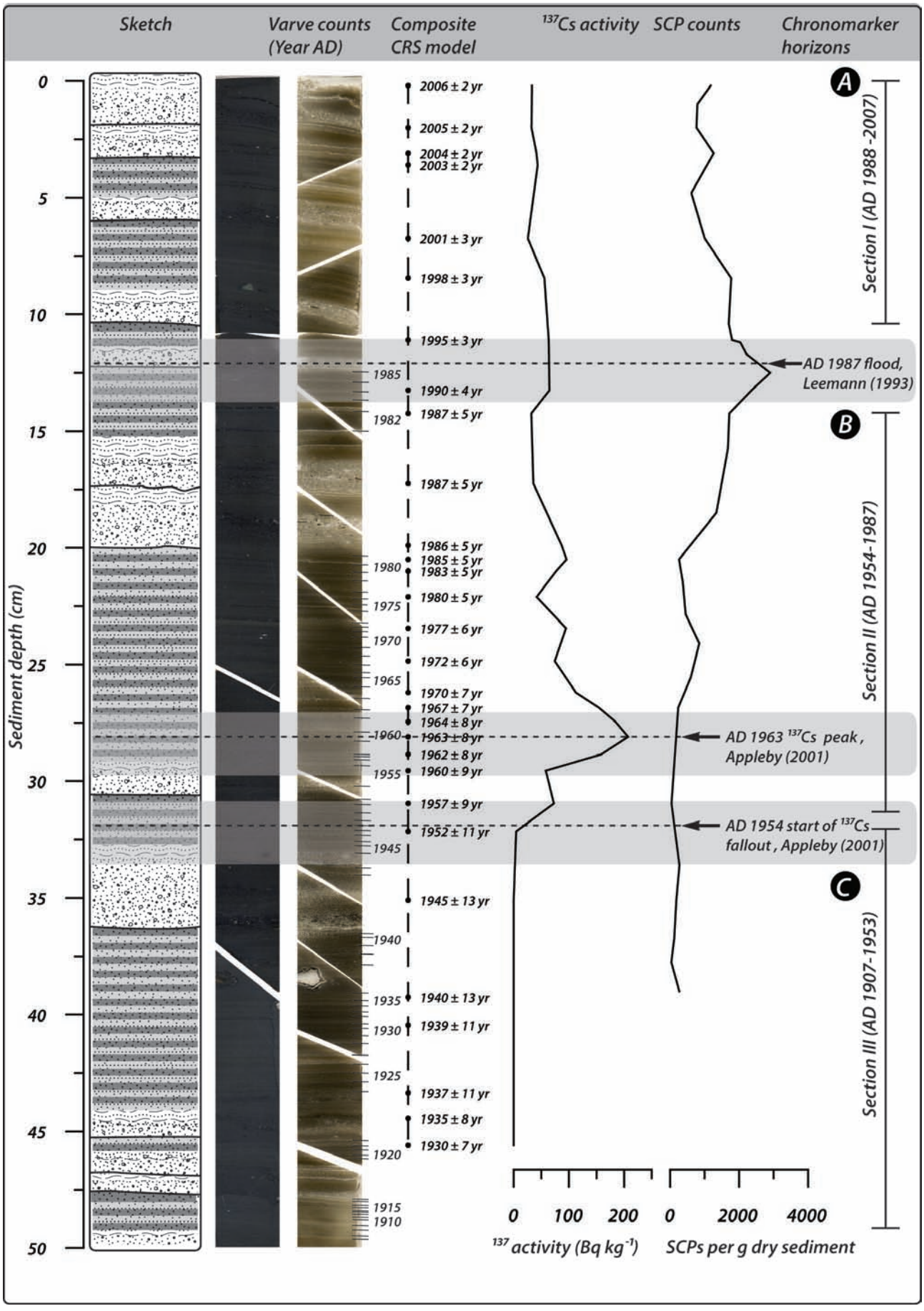

Figure 21: Chronology of the mastercore Oeschi 07-3. The varve chronology is compared with the composite CRS model, radiocaesium activities and SCP counts.

area (Lej da la Tscheppa, 46°27' N, 9°45' E, 2616 m a.s.l.), the SCP peak was proposed for AD 1973 (von Gunten et al., 2008). Suggestions for the SCP peak in the Swiss Alps apparently comprise a time span of more than 10 yr. Thus, the SCP peak is not a precise chronomarker horizon and cannot be used for accurately constraining age-depth models. However, SCP profiles are very valuable for the reconstruction of anthropogenic pollution history such as mining activities (e.g. von Gunten et al., 2009b).

The final varve chronology (Figure 21) was based on varve counts, the composite CRS model and chronomarker horizons for validation. Both the varve counts and the composite CRS age-depth model provided relatively consistent results. In general, ages provided by the varve counts appeared to be systematically older than the ^{210}Pb ages, however, still within the error range of the numerical ages.

The robustness of the final chronology was not constant through time, but had to be divided into three sections I (AD 1988 – 2007), II (AD 1954 – 1987), and III (pre AD 1954).

- For the youngest section (AD 1988 – 2007), no varve chronology could be established (Figure 21, A). Due to inclined orientation of layers, diagnostic winter laminae could not be detected with XRF data.

- The most robust chronology was available for the period AD 1954 – 1987 (Figure 21, B). The varve chronology was validated by four independent chronomarker horizons (AD 1954 start of ^{137}Cs fallout, the AD 1963 ^{137}Cs peak, the AD 1986 Chernobyl peak and the historical AD 1987 flood event).

- Before AD 1954, the varve chronology could only be validated by the composite CRS model (Figure 21, C). Unfortunately, dating errors of the composite CRS model varied between 8 and 13 yr. The last data point is located at 45.6 cm sediment depth.

In conclusion, only the validation of a varve chronology with multiple independent time markers reveals if a chronology is robust. For the mastercore of this study, the chronology was very robust for the middle part of the core (AD 1954 – AD 1987). For the upper-most part (AD 1988-2007), a varve chronology could not be established due to imprecise XRF data. The varve chronology of the bottom part (AD 1907 – 1954) was consistent with the ^{210}Pb age-depth model. However, due to larger dating errors, the chronology was less robust than the middle section of the core.

5.2. Sediment composition and proxy interpretation

Annual layers deposited in the proglacial Lake Oeschinen appeared to be clastic varves as first described by De Geer (1912). In general, our results were in agreement with preliminary findings from Leemann (1993).

However, in contrast to Leemann's (1993) findings, it was shown that seasonally trapped particles differed in their mineralogical composition. All summer, winter laminae and event layers (turbidites) were characterized by diagnostic mineralogical compositions. High-resolution XRF data provided valuable geochemical information that enabled the identification of sedimentary facies. However, the quality of the data points had to be critically evaluated. The geochemical composition of declined laminae, for instance, could not be exactly determined because the XRF scanning detector was 12 mm in width. Laminae therefore have to be perpendicular to the scanning direction. XRF data from declined laminae could therefore not be used for identification of diagnostic winter layers. Furthermore, for the preparation of the resin-impregnated sediment blocks, aluminium trays were used that are only a few millimeters wider than the XRF scanning detec-

tor. Thus, Al counts may possibly have resulted from the aluminium tray. Therefore, the data could not be used for the calculation of elemental ratios. Using a micro XRF device instead, a higher resolution up to 50 µm could be achieved. Due to the vacuum conditions during the measurement, data would probably be more accurate than data obtained from the AVAATECH X-Ray Fluorescence Core Scanner.

In this study, the use of geochemical proxies derived from high-resolution XRF scans was only useful due to contrasts in the catchment geology. The Ca/Si ratio appeared to be a proxy for both the source area of particles and the erosional processes in the catchment: low Ca/Si ratios indicated that particles originated from the non-glaciated, northern catchment (Tertiary Flysch deposits). Spring snowmelt and summer precipitation are the main factors that cause sediment transport from this area. This signal was found in both summer laminae and in event layers. Winter laminae, in contrast, comprised very fine-grained calcite particles (high Ca/Si ratios) that were probably eroded from the bedrock by the glaciers and released due to ice melt during summer. Because particles were very fine (clay fraction), particles were only deposited with a time lag in winter. Furthermore, turbidites mainly comprised particles from the northern catchment (low Ca/Si ratios). The frequent occurrence of turbidites (12 during AD 1907-2007) showed that the small catchment of Lake Oeschinen is very sensitive to rainstorms and flood events.

5.3. Working hypothesis – Climate controls on varve formation

To test the working hypothesis that varve thickness was primarily controlled by summer precipitation, varve thickness was compared with mean summer temperatures and cumulative summer precipitation. The results showed that varve thickness was only partially controlled by summer precipitation MJJA ($r = 0.43$, $p < 0.05$, means for AD 1920 – 1986). Surprisingly, for the period AD 1907-1920, varve thickness appeared to be weakly negatively correlated with summer precipitation ($r= -0.19$, not significant at $p < 0.05$). Varves formed during this period were anomalously thin with an average thickness of 1.7 mm (Figure 21, 47.5 – 50 cm sediment depth).

Reduced sediment supply during AD 1907-1920 was probably the result of low summer temperatures. Pfister et al. (1999) reported that during the period AD 1906 – 1925, summer months were anomalously cold. Briffa et al. (1998) analyzed temperature-sensitive tree-ring density chronologies of northern boreal forests over the past 600 years and found that volcanic eruptions had large effects on summer temperatures. All the volcanic eruptions in AD 1902 (Santa Maria, Guatemala, 14.8N 91.6W), AD 1907 (Ksudach, Kamchatka, 51.8N 157.5E) and 1912 (Novarupta, Alaska, 58.3N 155.2W) were interpreted as very climate-sensitive volcanic eruptions that caused cold summer temperatures on the northern hemisphere. Furthermore, there was a synchroneity of these volcanic events with a solar minimum of the Gleissberg periodicity around AD 1910 (McCracken et al., 2001). Hence, cold summer temperatures during the period AD 1906 – 1925 were possibly caused by both volcanic and solar forcing factors.

In response to this cold anomaly, 75 % of the Swiss glaciers were readvancing around 1920 (Patzelt, 1985). The Blüemlisalp glacier re-advanced during the period AD 1914 -1926 with a time lag of ~8 yr (data from Glaciological reports (1881-2009)). Snowmelt as well as the intensity of convective summer rainstorms was very likely reduced. This short term climate change has probably resulted in a reduction of both mobilization and transport of sediment particles. Similar observations were reported by Ohlendorf et al., (1997) who studied Lake Silvaplana in the Engadine valley. In the 127 yr long record (AD 1864 – 1990), minimum mass accumulation rates occurred between AD 1909 and 1916. The synchrone-

ity of anomalously low sedimentation rates in Lake Silvaplana and Lake Oeschinen from AD 1909 - 1916 indicated that the same climatic signal was probably preserved in the varved sediments. In addition, this finding demonstrated that the varve chronology presented in this Thesis was robust for the entire period AD 1907- 1986.

In conclusion, cumulative summer precipitation was the major climate factor that influenced the thickness of modern varves in Lake Oeschinen. The working hypothesis was therefore verified. However, other factors influencing sediment transport mechanisms have to be considered. Spring snow melt, for instance, is an important process that causes major sediment input to the lake. Factors that possibly determine sediment supply during spring snowmelt include not only precipitation but also properties of the snow cover, temperature and sediment availability. Furthermore, an individual sediment core, such as the mastercore analyzed in this study, only represents a specific location in a lake.

Also in Lake Oeschinen, thickness of individual varves and event layers varied remarkably at different coring locations (see Leemann, 1993).

In general, the question arose whether complex processes in natural systems such as varve forma-

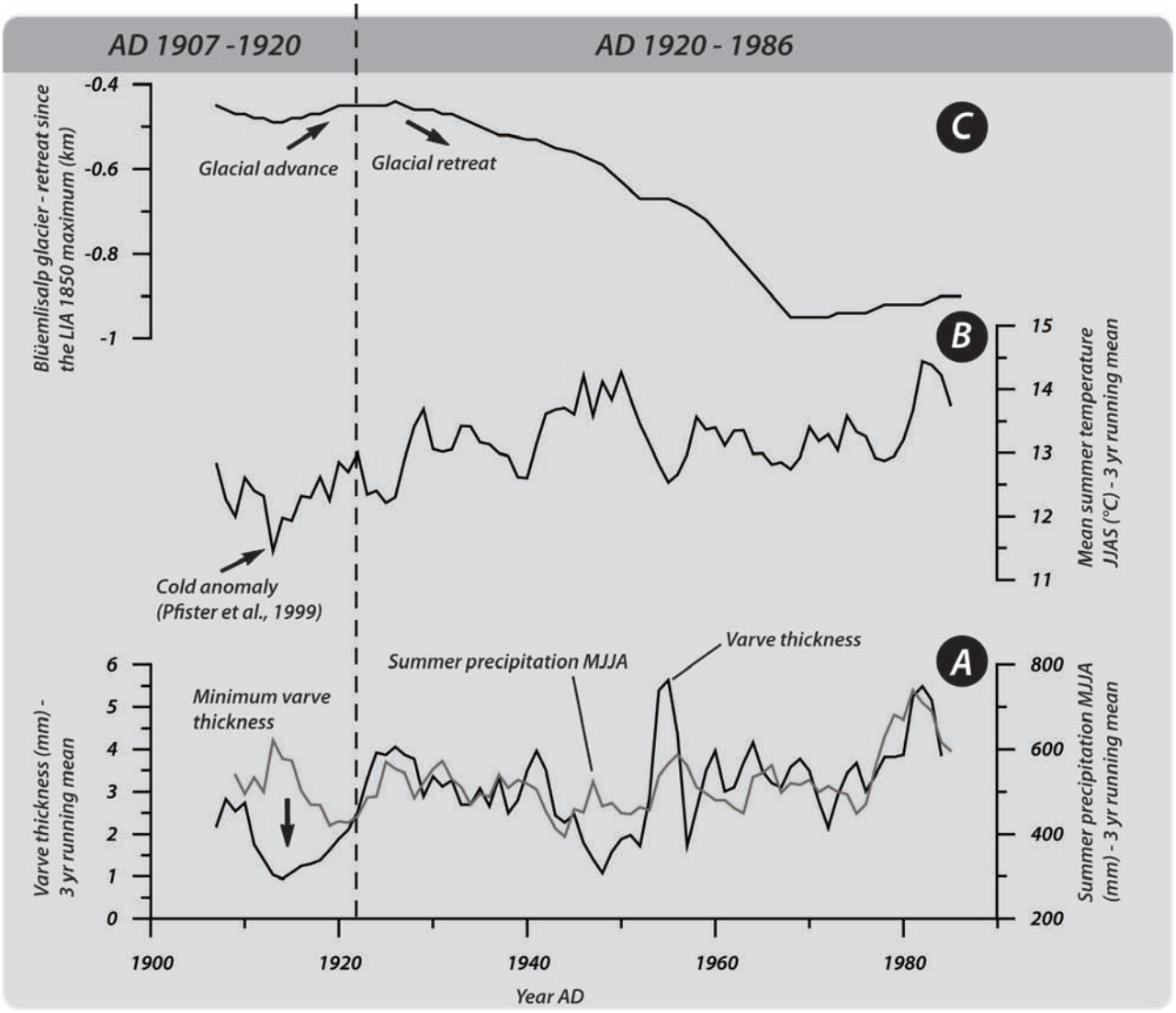

Figure 22: Compilation of parameters that likely influenced varve formation in Lake Oeschinen from AD 1907-1986. A) Varve thickness compared with cumulative summer pp MJJA from Château d'Oex, B) Mean summer temperatures JJAS C) Length of the Blüemlisalp glacier relative to the LIA AD 1850 high stand. Note that during AD 1907 – 1920, anomalously cold summer temperatures occurred that resulted in an advance of the Blüemlisalp glacier.

tion could be expressed by simple linear climate-varve relationships. Hodder et al. (2007) therefore proposed a more careful consideration of the validity of linear statistical model (LSM) approaches. The translation of different climatic signals into varves is very complex and both deterministic and stochastic components are involved. Using a multivariate approach (e.g. principal component regression) may help to achieve a more realistic estimate of the factors that control varve formation in Lake Oeschinen.

The results also demonstrated that the relationship between summer precipitation and varve thickness was not stable during the entire time period analyzed. It is generally assumed that different climatic regimes may lead to changing state conditions in natural systems (Blass et al., 2007b). Lenton et al. (2008) stated that critical thresholds, also referred to as tipping elements, could alter the state or the development of a natural system. In our case, the formation of the proglacial lake in the early AD 1950s probably has to be considered as a tipping element in the system. Particles eroded from the Blüemlisalp glacier were deposited in this proglacial lake that has acted as a new sink for sediments; particles were no longer deposited in Lake Oeschinen.

5.4. Comparison with Leemann (1993) and other studies

The findings proposed in the previous section (5.3) were in contrast to the findings of Leemann (1993). For the period AD 1962 - 1982, Leemann (1993) found a positive correlation (r= 0.45 n = 21, p not reported) between varve thickness and mean summer air temperatures (JJAS). Therefore, Leemann (1993) reported that the sedimentary record of Lake Oeschinen carried a mixed meteorological signal that was primarily controlled by mean summer temperatures. Summer precipitation, in contrast to our finding, was assumed to be only a second order factor superimposed by the temperature signal.

Table 5: Comparison of correlation coefficients r from Leemann (1993) and this study, correlation coefficients in bold are significant at p < 0.05.

AD 1962 – 1982 (n =21)	*mean summer temperature (JJAS) - Adelboden*
Leemann (1993)	***0.45***
This study	*0.39*

For a direct comparison with Leemann's (1993) results, varve thickness determined in this study was compared with mean summer air temperatures (JJAS) from Adelboden (AD 1962 – 1982). Correlation coefficients are shown in Table 5. By applying a t-test, Leemanns (1993) correlation (r = 0.45) appeared to be significant at $p < 0.05$. In contrast, comparisons with our varve thickness time series yielded a weaker correlation (r = 0.39, not significant at $p < 0.05$).

Leemann's (1993) varve-temperature relationship, however, only explained 20 % of the variance (r^2 = 0.2) in varve thickness during the very short time span of only 20 yr. High frequency climate signals (e.g. summer precipitation), however, are superimposed by lower frequency signals such as glacial variations. Thus, decadal to centennial climate signals cannot be identified with very short time series and longer records are required. In contrast, our precipitation-varve relationship for a 66 yr long record (AD 1920-1986) explained 40 % of the variance in varve thickness.

Leemann (1993) found that sediment particles only entered Lake Oeschinen in summer. Interestingly, varve thickness was only compared with mean annual and winter precipitation, but not with cumulative summer precipitation. These comparisons were not reasonable taking into account Leemann's (1993) own interpretations of the interannual sedimentation patterns. Furthermore, it remains unknown why Leemann (1993) did not use precipitation data

from the meteorological station in Kandersteg that are more representative for the catchment of Lake Oeschinen.

The weakest point in Leemann's (1993) argument, however, was his study design. Because there was no meteorological or hydrometric station located at Lake Oeschinen, Leemann (1993) studied the relationship between climate variables and suspension load of river Lonza that drains the Lötschen valley (11 km southeast of Lake Oeschinen). Mean summer temperatures, river discharge and particle load were linked with each other. Leemann (1993) found that summer temperatures (AMJJASO) and suspension loads were positively correlated ($r = 0.56$, p is not reported). Leemann (1993) assumed that the same principle held true for the sediment supply to Lake Oeschinen.

However, the catchment of Lake Oeschinen and the river Lonza differ remarkably. For example, the catchment area of Lake Oeschinen is only one third of the catchment area of the Lonza river (means for the hydrometric station Blatten). Importantly, small catchment areas are more sensitive to intensive heavy precipitation events and discharge than larger catchment areas (Spreafico and Weingartner, 2005). In the Kander valley, both cumulative summer precipitation and mean annual precipitation are higher than in the Lötschen valley (means for AD 1974 -1998, data from Meteo Schweiz). Furthermore, geological settings differ remarkably between our study site and the Lötschen valley. Tertiary Flysch units, which are easily eroded by precipitation, are not found in the crystalline Lötschen valley. The processes causing erosion and transport of sediment particles (e.g. glacial abrasion), in the two catchments are therefore not comparable. Hence, the summer temperature driven varve-climate relationship of Leemann (1993) was rejected. Instead, a multivariate approach with multiple climate variables (e.g. summer precipitation, summer temperatures and factors influencing snowmelt) should be conducted with the varve thickness data provided in this Thesis.

Our varve-climate relationship presented for Lake Oeschinen was compared with other studies that investigated proglacial lakes in the Swiss Alps. For the glaciolacustrine sediments in Steinsee (Sustenpass, 46°43'N, 08°26'E, 1930 m a.s.l.), Blass et al. (2003) found that varve thickness was partially controlled by mean annual summer precipitation ($r^2 = 0.35$, $n = 35$, p is not reported, data from the meteorological station at Grimsel). In this specific system, sediment flux to the lake was assumed to be regulated by sediment availability combined with increasing instability of the subglacial and proglacial drainage network. In contrast, in the proglacial Lake Silvaplana, MAR appeared to be mainly controlled by mean summer temperatures, followed by summer precipitation and the number of days with snow per year (Ohlendorf et al., 1997).

In conclusion, the findings of this study and its comparison with other studies showed that processes causing erosion and transport of sedimentary particles are very complex and site-specific, and cannot be fully explained by simple linear regression models. For understanding how climate signals are transferred to varves, a careful consideration of all temporally and spatially connected processes is required.

6. Conclusions and Outlook

6.1. Conclusions

The main objective of this Thesis was to test the working hypothesis that varve thickness in Lake Oeschinen is primarily controlled by summer precipitation. To gain knowledge about varve formation in Lake Oeschinen, a process study was conducted to investigate interannual patterns of sedimentation and to trace the source of sediment particles. We used high-resolution XRF data from the top 50 cm of a sediment core for the identification of varves and event layers. Next, varve thicknesses of an 80 yr long record (AD 1907-1986) was compared with meteorological parameters to detect the main climate factors that control sediment supply to Lake Oeschinen.
On the basis of the results from this study, the following major conclusions can be drawn:

- Contrasts in the catchment geology and associated climate-sensitive erosional and sedimentation processes were the major factors that determined varve formation in Lake Oeschinen. Delta fan mineralogy and sediment trap data showed that the source of sedimentary particles could be traced using diagnostic mineralogical and elemental ratios. The Ca/Si ratios, derived from high-resolution XRF scans, were a powerful proxy for identification of sedimentary facies. Ca/Si peaks (winter layers) denoted the boundaries between individual varves and were therefore crucial for counting varves.

- The creation of a robust chronology was the basis for all comparisons of physical proxy data with instrumental meteorological data. The initial sampling strategy determined the quality of the ^{210}Pb models that were used for validation of the varve counts. Independent chronomarker horizons (e.g. AD 1963 ^{137}Cs peak and historical flood events) were important for the validation of ^{210}Pb models and varve chronologies.

- Varve thickness in Lake Oeschinen was primarily controlled by cumulative summer precipitation (MJJAS) ($r=0.64$ at $p< 0.05$, means for AD 1920-1986); the working hypothesis was verified. However, only 40% of the variance was explained by summer precipitation (MJJAS). This result suggested that other low and high frequency climate signals were also preserved in the varves.

- For understanding natural climate archives such as varved sedimentary records, a careful study design is essential. Like in all empirical natural sciences, complex processes can only be understood by the formulation hypotheses that are tested with experiments and observations. At the beginning of our study, field observations indicated that sediment supply was mainly related to summer precipitation. Taking into account this observation, the climatic and the geological setting of the study area, the hypothesis was formulated that varve thickness was primarily controlled by summer precipitation. Our study was split into three consecutive steps (process study (1), analysis of the mastercore (2) and statistical analyses (3)) and the strategy of each step was based on the previous findings. An iterative approach had the great advantage that only analytical methods were chosen that were meaningful for the overall aims of the study. Testing multiple hypotheses to verify a theory, however, was very time consuming and a challenge because ideas often had to be rejected. Nevertheless, this approach is fundamental for paleolimnological studies and also the development of future study designs.

6.2. Outlook

The varve thickness time series provided by this Thesis is an ideal basis for further statistical analyses. A multivariate approach (e.g. principal component regression analysis) would help to achieve a more realistic estimate of the factors that control varve formation in Lake Oeschinen. For instance, mean summer temperatures and properties of the snow cover have the potential to explain more of the variability in varve thickness apart from cumulative summer precipitation. Both non-climatic (e.g. the formation of the proglacial lake in the AD 1950s) and climatic trends could be separated by band-pass filtering (e.g. 100 yr loess filter) the varve thickness time series (e.g. Blass et al., 2007a; Trachsel et al., 2010). Low frequency and high frequency climatic components could be detected in this way.

Furthermore, the hypothesis could be tested that the mass flux from the Flysch units was positively correlated with cumulative summer precipitation. The proportion of Flysch particles in the individual summer laminae may potentially be estimated with mixing ratios between particles from the northern and southern catchment. Both source areas carry different mineralogical and elemental fingerprints of the bedrock geology. Different strategies would allow this hypothesis to be tested: (1) the freeze core could be sampled varve by varve and the samples analyzed for their mineralogical compositions (XRD smear slides). Correlation and regression analysis may yield information about the relationship between a time series with diagnostic XRD peak intensity ratios (e.g. cal/ill) and cumulative summer precipitation (see Trachsel et al., 2008). (2) Alternatively, novel approaches with ultra high-resolution XRF scans and elemental mapping may be investigated. In the individual summer laminae, the counts of diagnostic elements (e.g. Al or K for clay minerals that are only found in the Tertiary Flysch units) could be integrated over their areas. Thus, Al or K counts per individual summer laminae may provide a proxy for the mass flux from the Flysch units. Moreover, correlation and regression analysis may provide information about the potential use of qualitative elemental counts for quantitative climate reconstructions.

The occurrence of 12 turbidites in the analyzed period (AD 1907 – 2007) showed that the catchment area of Lake Oeschinen is very sensitive to flood events. The sedimentary record of Lake Oeschinen therefore has great potential for the reconstruction of the frequency and intensities of flood events in the Bernese Alps throughout the mid to late Holocene. The ages of the recent event layers, however, need to be compared with the dates of extreme rainstorm events that occurred in the catchment area during the period AD 1907 - 2007. The interannual timing of such an event probably plays an important role in understanding the factors that trigger the mobilization of large amounts of sediment particles. Importantly, interannual lake level fluctuations average ~12 m. During spring and early summer, the shoreline and the delta fans are air-exposed and the sediments may be more easily eroded and transported by the creeks than during the lake level high stand in September. Rainstorms that occured in early summer could therefore have a stronger effect on mobilization of sediment particles around the shoreline than rainstorms in late summer or autumn. Detailed comparisons of the ages of event layers with extreme rainstorms events may also help to identify thresholds (e.g. rainfall intensities, mm/day) that cause these turbidites.

Acknowledgements

Special thanks are dedicated to my supervisor Martin Grosjean: Thank you for your support and trust. I was given a lot of freedom for this Master's Thesis as well as while working as an assistant in the research group. It was a great opportunity to learn about different analytical lab methods. I also thank my advisor Mathias Trachsel for his support in the lab and during fieldwork at Lake Oeschinen.

I am very thankful to everybody who contributed to this Thesis: Urs Eggenberger and his team (Department of Geology, University of Bern) for the help with the XRD analyses, Jürg Beer and Marian Fujak (EAWAG Dübendorf) for their analyses of ^{210}Pb samples, Daniel Ariztegui (Department of Geology, University of Geneva) for the elemental mapping, and Gerald Haug and his team (Department of Geology, ETH Zurich) for the XRF scans.

I am deeply grateful to all "Paleolimnos" at University of Bern for their support in the lab and fruitful discussions. Thank you: Rixt de Jong, Julie Elbert, Daniela Fischer, Martin Grosjean, Samuel Hagnauer, Christian Kamenik, Isabelle Larocque, Louise Newman, Krystyna Saunders, Monique Stewart, Mathias Trachsel and Richard Wartenburger. I had a really great time with you during the last two years. Coffee breaks were always fun and I enjoyed spending lunchtime with you.

Special thanks are dedicated my roommates Richard Wartenburger, Samuel Hagnauer and Rie Nemoto. We had a lot of fun, not only in the office but also swimming in the Aare river.

Finally, I would like to thank my parents Gabi & Bert, my sister Jessica, my grand parents Oma & Opa, and all of my friends who always supported me during my studies: Merci vilmol für euri Unterstützig! Ihr sind die Beschte!

References

APPLEBY, P.G., 2001, Chronostratigraphic techniques in recent sediments. In: Last, W.M., Smol, J.P. (eds), Tracking Environmental Change Using Lake Sediments. Volume 1: Basin Analysis, Coring, and Chronological Techniques: Dordrecht, Kluwer Academic Publishers, p. 171-201.

ARNAUD, F., LIGNIER, V., REVEL, M., DESMET, M., BECK, C., POURCHET, M., CHARLET, F., TRENTESAUX, A., AND TRIBOVILLARD, N., 2002, Flood and earthquake disturbance of ^{210}Pb geochronology (Lake Anterne, NW Alps): Terra Nova, v. 14, p. 225-232.

BECKHOFF, B., KANNGIESSER, B., LANGHOFF, N., WEDELL, R., AND WOLFF, H., 2006, Handbook of practical X-ray fluorescence analysis: Berlin, Springer, p. 863.

BINFORD, M., 1990, Calculation and uncertainty analysis of ^{210}Pb dates for PIRLA project lake sediment cores: Journal of Paleolimnology, v. 3, p. 253-267.

BIRKS, H., 1998, D.G. Frey and E.S. Deevey Review 1: Numerical tools in palaeolimnology – Progress, potentialities, and problems: Journal of Paleolimnology, v. 20, p. 307-332.

BLASS, A., ANSELMETTI, F., AND ARIZTEGUI, D., 2003, 60 years of glaciolacustrine sedimentation in Steinsee (Sustenpass, Switzerland) compared with historic events and instrumental meteorological data: Eclogae Geologicae Helvetiae, v. 96, p. 59.

BLASS, A., ANSELMETTI, F., GROSJEAN, M., AND STURM, M., 2005, The last 1300 years of environmental history recorded in the sediments of Lake Sils (Engadine, Switzerland): Eclogae Geologicae Helvetiae, v. 98, p. 319-332.

BLASS, A., BIGLER, C., GROSJEAN, M., AND STURM, M., 2007a, Decadal-scale autumn temperature reconstruction back to AD 1580 inferred from the varved sediments of Lake Silvaplana (southeastern Swiss Alps): Quaternary Research, v. 68, p. 184-195.

BLASS, A., GROSJEAN, M., TROXLER, A., AND STURM, M., 2007b, How stable are twentieth-century calibration models? A high-resolution summer temperature reconstruction for the eastern Swiss Alps back to AD 1580 derived from proglacial varved sediments: The Holocene, v. 17, p. 51.

BRADLEY, R., 2000, Past global changes and their significance for the future: Quaternary Science Reviews, v. 19, p. 391-402.

BRIFFA, K., JONES, P., SCHWEINGRUBER, F., AND OSBORN, T., 1998, Influence of volcanic eruptions on Northern Hemisphere summer temperature over the past 600 years: Nature, v. 393, p. 451.

CASTY, C., WANNER, H., LUTERBACHER, J., ESPER, J., AND BÖHM, R., 2005, Temperature and precipitation variability in the European Alps since 1500: International Journal of Climatology, v. 25, p. 1855-1880.

DAWDY, D., AND MATALAS, N., 1964, Statistical and probability analysis of hydrologic data, part III: Analysis of variance, covariance and time series: Handbook of Applied Hydrology: A Compendium of Water-Resources Technology, p. 8.68–8.90.

DE GEER, G., 1912, Greochronologie der letzten 12000 Jahre: Geologische Rundschau, v. 3, p. 457-471.

DENKER, R., OOSTEN-NIENHUIS, N., AND MEIER, R., 2008, Sample preparation for X-ray analysis - the critical first steps: Global Cement Magazine, p. 17-18.

GIERLOWSKI-KORDESCH, E., AND KELTS, K., 2000, Lake basins through space and time, American Association of Petroleum Geologists, p. 648.

Glaciological reports (1881-2009). "The Swiss Glaciers", Yearbooks of the Cryospheric Commission of the Swiss Academy of Sciences (SCNAT) published since 1964 by the Labratory of Hydraulics, Hydrology and Glaciology (VAW) of ETH Zürich. No. 1-126, (http://glaciology.ethz.ch/swiss-glaciers/).

GRIFFIN, J.J., AND GOLDBERG, E.D., 1981, Sphericity as a characteristic of solids from fossil fuel burning in a Lake Michigan sediment: Geochimica Et Cosmochimica Acta, v. 45, p. 763-769.

HÅKANSON, L., AND JANSSON, M., 1983, Principles of lake sedimentology, Berlin, Springer, p. 315.

HILLIER, S., 2000, Accurate quantitative analysis of clay and other minerals in sandstones by XRD: comparison of a Rietveld and a reference intensity ratio (RIR) method and the importance of sample preparation: Clay Minerals, v. 35, p. 291-302.

HODDER, K.R., GILBERT, R., AND DESLOGES, J.R., 2007, Glaciolacustrine varved sediment as an alpine hydroclimatic proxy: Journal of Paleolimnology, v. 38, p. 365-394.

IPCC, 2007, Climate Change 2007: The physical science basis: Contribution of Working Group I to the Fourth Assessment Report of the Intergovernmental Panel on Climate Change, Cambridge University Press.

KAMENIK, C., VAN DER KNAAP, W., VAN LEEUWEN, J., AND GOSLAR, T., 2009, Pollen/climate calibration based on a near-annual peat sequence from the Swiss Alps: Journal of Quaternary Science, v. 24, p. 529-546.

KOTTEK, M., GRIESER, J., BECK, C., RUDOLF, B., AND RUBEL, F., 2006, World map of the Koppen-Geiger climate classification updated: Meteorologische Zeitschrift, v. 15, p. 259-263.

KULBE, T., AND NIEDERREITER, R., 2003, Freeze coring of soft surface sediments at a water depth of several hundred meters: Journal of Paleolimnology, v. 29, p. 257-263.

LAROCQUE, I., GROSJEAN, M., HEIRI, O., BIGLER, C., AND BLASS, A., 2009, Comparison between chironomid-inferred July temperatures and meteorological data AD 1850-2001 from varved Lake Silvaplana, Switzerland: Journal of Paleolimnology, v. 41, p. 329-342.

LAST, W.M., 2001, Textural Analysis of Lake Sediments, In: Last, W.M., Smol, J.P. (eds), Tracking Environmental Change Using Lake Sediments. Volume 2: Physical and Geochemical Methods: Dordrecht, Kluwer Academic Publishers, p. 41-81.

LEEMANN, A., 1993, Rhythmite in alpinen Vorgletscherseen: Warvenstratigraphie und Aufzeichnung von Klimaveränderungen. PhD thesis: Zurich, ETH Zurich, p. 129.

LENTON, T.M., HELD, H., KRIEGLER, E., HALL, J.W., LUCHT, W., RAHMSTORF, S., AND SCHELLNHUBER, H.J., 2008, Tipping elements in the Earth's climate system: Proceedings of the National Academy of Sciences of the United States of America, v. 105, p. 1786-1793.

LOIZEAU, J., ARBOUILLE, D., SANTIAGO, S., AND VERNET, J., 1994, Evaluation of a wide range laser diffraction grain size analyser for use with sediments: Sedimentology, v. 41, p. 353-361.

LOTTER, A., STURM, M., TERANES, J., AND WEHRLI, B., 1997, Varve formation since 1885 and high-resolution varve analyses in hypertrophic Baldeggersee (Switzerland): Aquatic Sciences-Research Across Boundaries, v. 59, p. 304-325.

LOTTER, A., AND LEMCKE, G., 1999, Methods for preparing and counting biochemical varves: Boreas, v. 28, p. 243-252.

LOTTER, A.F., APPLEBY, P.G., BINDLER, R., DEARING, J.A., GRYTNES, J.A., HOFMANN, W., KAMENIK, C., LAMI, A., LIVINGSTONE, D.M., OHLENDORF, C., ROSE, N., AND STURM, M., 2002, The sediment record of the past 200 years in a Swiss high-alpine lake: Hagelseewli (2339 ma.s.l.): Journal of Paleolimnology, v. 28, p. 111-127.

MANN, M., PARK, J., AND BRADLEY, R., 1995, Global interdecadal and century-scale climate oscillations during the past five centuries: Nature, v. 378, p. 266-270.

MANUTCHEHR-DANAI, M., 2009, Dictionary of gems and gemology: Berlin, Springer, p. 1034.

MCCRACKEN, K., DRESCHHOFF, G., SMART, D., AND SHEA, M., 2001, The Gleissberg periodicity in large fluence solar proton events, Volume 2001, p. 3205.

MENOUNOS, B., CLAGUE, J., GILBERT, R., AND SLAYMAKER, O., 2005, Environmental reconstruction from a varve network in the southern Coast Mountains, British Columbia, Canada: The Holocene, v. 15, p. 1163.

MEYER, M.C., FABER, R., AND SPOTL, C., 2006, The WinGeol Lamination Tool: new software for rapid, semi-automated analysis of laminated climate archives: Holocene, v. 16, p. 753-761.

MOORE, J., HUGHEN, K., MILLER, G., AND OVERPECK, J., 2001, Little Ice Age recorded in summer temperature reconstruction from vared sediments of Donard Lake, Baffin Island, Canada: Journal of Paleolimnology, v. 25, p. 503-517.

NIKLAUS, M., 1967, Geomorphologische und limnologische Untersuchungen am Öschinensee. PhD thesis: Bern, Kümmerly und Frey, p. 116.

OHLENDORF, C., NIESSEN, F., AND WEISSERT, H., 1997, Glacial varve thickness and 127 years of instrumental climate data - A comparison: Climatic Change, v. 36, p. 391-411.

PATZELT, G., 1985, The period of glacier advances in the Alps, 1965 to 1980: Zeitschrift für Gletscherkunde und Glazialgeologie, v. 21, p. 403-407.

PFIFFNER, A., 2009, Geologie der Alpen: Bern, Haupt, p. 359.

PFISTER, C., LUTERBACHER, J., BRÄNDLI, D., WANNER, H., BRODBECK, B., AND NIELSON, P.-A., 1999, Wetternachhersage: 500 Jahre Klimavariationen und Naturkatastrophen (1496-1995): Bern, Verlag Paul Haupt, p. 304.

PICKRILL, R., AND IRWIN, J., 1983, Sedimentation in a deep glacier-fed lake - Lake Tekapo, New Zealand: Sedimentology, v. 30, p. 63-75.

RENBERG, I., AND WIK, M., 1985, Soot particle counting in recent lake sediments - An indirect dating method: Ecological Bulletins, p. 53-57.

ROSE, N., 2001, Fly-Ash Particles, In: Last, W.M., Smol, J.P. (eds), Tracking Environmental Change Using Lake Sediments. Volume 2: Physical and Geochemical Methods: Dordrecht, Kluwer Academic Publishers, p. 319-349.

SHANAHAN, T., OVERPECK, J., HUBENY, J., KING, J., HU, F., HUGHEN, K., MILLER, G., AND BLACK, J., 2008, Scanning micro-X-ray fluorescence elemental mapping: a new tool for the study of laminated sediment records: Geochemistry Geophysics Geosystems, v. 9, p. 1-14.

SMOL, J., 2002, Pollution of lakes and rivers - A paleoenvironmental perspective: London, Arnold, p. 280.

SPREAFICO, R., AND WEINGARTNER, R., 2005, Hydrologie der Schweiz - Ausgewählte Aspekte und Resultate: Bern, Bundesamt für Wasser und Geologie BWG, p. 137.

SUCHY, V., FREY, M., AND WOLF, M., 1997, Vitrinite reflectance and shear-induced graphitization in orogenic belts: A case study from the Kandersteg area, Helvetic Alps, Switzerland: International Journal of Coal Geology, v. 34, p. 1-20.

THEVENON, F., AND ANSELMETTI, F.S., 2007, Charcoal and fly-ash particles from Lake Lucerne sediments (Central Switzerland) characterized by image analysis: anthropologic, stratigraphic and environmental implications: Quaternary Science Reviews, v. 26, p. 2631-2643.

THEVENON, F., ANSELMETTI, F.S., BERNASCONI, S.M., AND SCHWIKOWSKI, M., 2009, Mineral dust and elemental black carbon records from an Alpine ice core (Colle Gnifetti glacier) over the last millennium: Journal of Geophysical Research-Atmospheres, v. 114, p. 1-11.

TINNER, W., KALTENRIEDER, P., SOOM, M., ZWAHLEN, P., SCHMIDHALTER, M., BOSCHETTI, A., AND SCHLUCHTER, C., 2005, The postglacial rockfall in the Kander valley (Switzerland): age and effects on palaeo-environments: Eclogae Geologicae Helvetiae, v. 98, p. 83-95.

TOMKINS, J., AND LAMOUREUX, S., 2005, Multiple hydroclimatic controls over recent sedimentation in proglacial Mirror Lake, southern Selwyn Mountains, Northwest ttories: Canadian Journal of Earth Sciences, v. 42, p. 1589-1599.

TRACHSEL, M., EGGENBERGER, U., GROSJEAN, M., BLASS, A., AND STURM, M., 2008, Mineralogy-based quantitative precipitation and temperature reconstructions from annually laminated lake sediments (Swiss Alps) since AD 1580: Geophysical Research Letters, v. 35.

TRACHSEL, M., GROSJEAN, M., LAROCQUE-TOBLER, I., SCHWIKOWSKI, M., BLASS, A., AND STURM, M., 2010, Quantitative summer temperature reconstruction derived from a combined biogenic Si and chironomid record from varved sediments of Lake Silvaplana (south-eastern Swiss Alps) back to AD 1177: Quaternary Science Reviews.

VON GUNTEN, L., GROSJEAN, M., BEER, J., GROB, P., MORALES, A., AND URRUTIA, R., 2009a, Age modeling of young non-varved lake sediments: methods and limits. Examples from two lakes in Central Chile: Journal of Paleolimnology, v. 42, p. 401-412.

VON GUNTEN, L., GROSJEAN, M., EGGENBERGER, U., GROB, P., URRUTIA, R., AND MORALES, A., 2009b, Pollution and eutrophication history AD 1800–2005 as recorded in sediments from five lakes in Central Chile: Global and Planetary Change, v. 68, p. 198-208.

VON GUNTEN, L., HEIRI, O., BIGLER, C., VAN LEEUWEN, J., CASTY, C., LOTTER, A., AND STURM, M., 2008, Seasonal temperatures for the past 400 years reconstructed from diatom and chironomid assemblages in a high-altitude lake (Lej da la Tscheppa, Switzerland): Journal of Paleolimnology, v. 39, p. 283-299.

WANNER, H., LUTERBACHER, J., CASTY, C., BÖHM, R., AND XOPLAKI, E., 2003, Variabilität von Temperatur und Niederschlag in den europäischen Alpen seit 1500: Welt der Alpen-Gebirge der Welt, Haupt, Bern, p. 61-76.

WELTJE, G.J., AND TJALLINGII, R., 2008, Calibration of XRF core scanners for quantitative geochemical logging of sediment cores: Theory and application: Earth and Planetary Science Letters, v. 274, p. 423-438.

WENK, H., AND BULAKH, A., 2004, Minerals: their constitution and origin: Cambridge, Cambridge University Press, p. 646.

WETZEL, R.G., 2001, Limnology : lake and river ecosystems: San Diego, Academic Press, p. 1006.

ZOLITSCHKA, B., MINGRAM, J., GAAST, S., JANSEN, J.H.F., AND NAUMANN, R., 2002, Sediment Logging Techniques, In: Last, W.M., Smol, J.P. (eds), Tracking Environmental Change Using Lake Sediments. Volume 1: Basin Analysis, Coring, and Chronological Techniques: Dordrecht, Kluwer Academic Publishers, p. 137-153.

Appendix A

Table A1: Raw sediment trap data of five sampling intervals within the observation period from 30 May 2007 - 17 October 2008.

sediment trap (ID)	depth [m above lake ground]	MAR (dry mass [g])				
		30 May 2007 - 12 July2007	20 September 2007	11 November 2007	25 June 2008	17 October 2008
A1	45	2.0	2.6	0.1	n.a	2.4
A2	45	1.9	2.6	0.1	n.a.	1.7
B1	30	2.4	3.1	0.1	1.8	2.5
B2	30	2.2	2.9	0.1	1.4	2.5
C1	15	2.9	4.4	0.2	5.0	2.9
C2	15	2.8	4.4	0.2	5.0	3.0
D1	4	5.0	15.659 (*)	0.3	15.9	10.5
D2	4	6.1	8.4	0.3	16.5	11.2

** sediment trap was probably lying on the lake ground, n.a = data not available*

Table A2: Grain size data of trapped particles

Sample Name	median	mean	mode	sorting	skewness	clay [%]*	silt [%]*	sand [%]*
D1_12.07.07 - Average	5.4	7.9	5.6	2.1	0.1	19.7	79.1	1.2
D1_20.09.07 - Average	6.8	11.3	6.6	2.4	1.0	16.8	80.0	3.3
D1_01.11.07 - Average	3.0	4.1	3.2	2.0	0.1	34.3	65.4	0.3
D1_25.06.08 - Average	9.3	13.8	9.6	2.2	0.1	12.4	84.1	3.5
C1_12.07.07 - Average	3.6	4.5	4.2	1.9	0.9	27.7	72.1	0.2
C_20.09.07 - Average	3.8	4.7	4.4	1.9	0.9	26.8	73.1	0.0
C1_01.11.07 - Average	3.7	5.0	4.4	2.1	0.9	29.2	70.2	0.6
C1_25.06.08 - Average	6.0	7.6	7.2	2.0	0.9	17.1	82.4	0.5
B1_12.07.07 - Average	3.8	4.7	4.5	1.9	0.9	26.9	73.0	0.1
B_20.09.07 - Average	3.9	5.1	4.7	2.0	0.9	26.3	73.7	0
B1_01.11.07 - Average	4.6	6.0	5.5	2.0	0.9	22.9	76.7	0.4
B1_25.06.08 - Average	5.1	6.7	5.7	2.0	0.9	19.8	79.6	0.5
A1_12.07.07 - Average	3.4	4.2	4.0	1.9	0.9	29.3	70.7	0
A_20.09.07 - Average	3.9	5.0	4.6	2.0	0.9	26.7	73.3	0
A1_01.11.07	4.2	5.8	4.7	2.1	0.9	25.5	72.8	1.7

** Clay = fraction <2 µm; silt = fraction from 2 - 63 µm; sand = fraction 63 - 2000 µm*

Table A3: Raw XRD data from the delta sediments in alphabetical order. See Figure 6.

A1				
Peak	measurement A	measurement B		mean proportions (%)
quartz 21	9.1	8.8		
quartz 27	9.75	9.66		
quartz 36	10.4	9.6	quartz	9.6
calcite	61.3	61.7	calcite	61.5
dolomite	1.75	1.25	dolomite	1.5
K-feldspar	0.73	0.97	K-Feldspar	0.9
plagioclase 22	0.1	0	plagioclase	0.3
plagioclase 28	0.59	0.45	other	26.3

A2				
Peak	measurement A	measurement B		mean proportions (%)
quartz 21	12.3	10.6		(%)
quartz 27	13.4	13.1		
quartz 36	14.3	13	quartz	13
calcite	72.5	69.2	calcite	71
dolomite	2.36	2.72	dolomite	3
K-feldspar	0.73	0.56	K-Feldspar	1
plagioclase 22	0.9	0	plagioclase	1
plagioclase 28	0.7	0.53	other	13

A3				
Peak	measurement A	measurement B		mean proportions (%)
quartz 21	17.5	18		
quartz 27	16.1	16.3		
quartz 36	21.6	16.7	quartz	18
calcite	80.9	84.4	calcite	83
dolomite	4.5	2.37	dolomite	3
K-feldspar	0.45	0.72	K-Feldspar	1
plagioclase 22	0.7	0	plagioclase	1
plagioclase 28	0.63	3.68	other	-5.6225

B1				
Peak	measurement A	measurement B		mean proportions (%)
quartz 21	32.6	34.3		
quartz 27	35.8	39		
quartz 36	43.3	44.5	quartz	38
calcite	0.19	0.13	calcite	0
dolomite	0.12	0.13	dolomite	0
K-feldspar	3.55	3.14	K-Feldspar	3
plagioclase 22	0	0	plagioclase	1
plagioclase 28	1.78	2.06	other	57

B2				
Peak	measurement A	measurement B		mean proportions (%)
quartz 21	36.4	32.6		
quartz 27	37.7	38.6		
quartz 36	41.4	40.9	quartz	38
calcite	0.18	0.04	calcite	0
dolomite	0.16	0.16	dolomite	0
K-feldspar	2.38	2.25	K-Feldspar	2
plagioclase 22	0	0	plagioclase	1
plagioclase 28	1.14	1.6	other	59

B3				
Peak	measurement A	measurement B		mean proportions (%)
quartz 21	35.6	35.7		
quartz 27	37.3	38.9		
quartz 36	37.3	39.1	quartz	37
calcite	0.06	0.04	calcite	0
dolomite	0.06	0.09	dolomite	0
K-feldspar	2.28	2.16	K-Feldspar	2
plagioclase 22	0	0	plagioclase	1
plagioclase 28	1.87	1.49	other	59

C1				
Peak	measurement A	measurement B		mean proportions (%)
quartz 21	38.5	41.7		
quartz 27	40	43.9		
quartz 36	43.9	44.6	quartz	42
calcite	41.9	40.2	calcite	41
dolomite	0.61	0.9	dolomite	1
K-feldspar	0.67	0.63	K-Feldspar	1
plagioclase 22	1.1	5	plagioclase	3
plagioclase 28	2.28	2.12	other	13

C2				
Peak	measurement A	measurement B		mean proportions (%)
quartz 21	41.9	42		
quartz 27	39.9	43.8		
quartz 36	41.1	43.8	quartz	42
calcite	35.9	34.2	calcite	35
dolomite	0.47	0.21	dolomite	0
K-feldspar	0.63	0.1	K-Feldspar	0
plagioclase 22	1.9	1.8	plagioclase	2
plagioclase 28	1.8	1.67	other	20

C3				
Peak	measurement A	measurement B		mean proportions (%)
quartz 21	49.7	48.1		
quartz 27	52.9	47.5		
quartz 36	47.5	51.2	quartz	49
calcite	38.8	36.8	calcite	38
dolomite	0.79	0.63	dolomite	1
K-feldspar	0.74	0.75	K-Feldspar	1
plagioclase 22	1.3	0.1	plagioclase	1
plagioclase 28	2.05	1.88	other	10

D1				
Peak	measurement A	measurement B		mean proportions (%)
quartz 21	43.1	46.7		
quartz 27	44	47.5		
quartz 36	46.1	51.7	quartz	47
calcite	40.3	42	calcite	41
dolomite	0.73	0.49	dolomite	1
K-feldspar	0.98	1.1	K-Feldspar	1
plagioclase 22	3.7	4	plagioclase	3
plagioclase 28	1.91	2.04	other	8

D2				
Peak	measurement A	measurement B		mean proportions (%)
quartz 21	38.5	41.4		
quartz 27	42.6	43.2		
quartz 36	38	40.6	quartz	41
calcite	39.6	41.9	calcite	41
dolomite	0.52	0.57	dolomite	1
K-feldspar	0.53	0.77	K-Feldspar	1
plagioclase 22	2.4	7.7	plagioclase	3
plagioclase 28	1.87	1.73	other	14

D3				
Peak	measurement A	measurement B		mean proportions (%)
quartz 21	41.9	46.6		
quartz 27	43.2	46.4		
quartz 36	42	45.5	quartz	44
calcite	38.5	0	calcite	19
dolomite	1.15	0	dolomite	1
K-feldspar	0.71	0.88	K-Feldspar	1
plagioclase 22	3.8	2.5	plagioclase	2
plagioclase 28	1.56	1.62	other	33

E1				
Peak	measurement A	measurement B		mean proportions (%)
quartz 21	22.3	19.5		
quartz 27	23.6	23.4		
quartz 36	24.5	22	quartz	23
calcite	34.8	31	calcite	33
dolomite	0	0	dolomite	0
K-feldspar	0.58	1.13	K-Feldspar	1
plagioclase 22	6.6	6.2	plagioclase	5
plagioclase 28	4.06	3.57	other	39

E2				
Peak	measurement A	measurement B		mean proportions (%)
quartz 21	21.7	19.5		
quartz 27	24.4	22.5		
quartz 36	22.3	21	quartz	22
calcite	44.5	38.9	calcite	42
dolomite	0.05	0.01	dolomite	0
K-feldspar	1.34	0.82	K-Feldspar	1
plagioclase 22	5.3	4.8	plagioclase	4
plagioclase 28	3.88	3.08	other	31

E3				
Peak	measurement A	measurement B		mean proportions (%)
quartz 21	19.8	18.4		
quartz 27	24	21.8		
quartz 36	23.9	22.7	quartz	22
calcite	28.4	29.4	calcite	29
dolomite	0.21	0.16	dolomite	0
K-feldspar	1.55	1.78	K-Feldspar	2
plagioclase 22	6.2	4	plagioclase	4
plagioclase 28	3.77	3.75	other	43

F1				
Peak	measurement A	measurement B		mean proportions (%)
quartz 21	24.7	24.9		
quartz 27	27.1	26.7		
quartz 36	29.1	30.2	quartz	27
calcite	50.8	49.6	calcite	50
dolomite	0.67	0.74	dolomite	1
K-feldspar	1.61	1.52	K-Feldspar	2
plagioclase 22	2.9	1.4	plagioclase	3
plagioclase 28	1.34	4.66	other	18

F2				
Peak	measurement A	measurement B		mean proportions (%)
quartz 21	23	24.1		
quartz 27	25.5	25.3		
quartz 36	26.2	25.9	quartz	25
calcite	49.7	50.4	calcite	50
dolomite	0.89	0.96	dolomite	1
K-feldspar	1.47	1.44	K-Feldspar	1
plagioclase 22	0.9	1.1	plagioclase	1
plagioclase 28	1.42	1.43	other	21

F3				
Peak	measurement A	measurement B		mean proportions (%)
quartz 21	25	21.7		
quartz 27	24.8	21.4		
quartz 36	26.1	24.3	quartz	24
calcite	52	45.7	calcite	49
dolomite	0.87	0.67	dolomite	1
K-feldspar	2.24	2.14	K-Feldspar	2
plagioclase 22	1.6	0.3	plagioclase	1
plagioclase 28	2.02	1.61	other	23

G1				
Peak	measurement A	measurement B		mean proportions (%)
quartz 21	28	25.3		
quartz 27	28.4	26.6		
quartz 36	29.9	26.1	quartz	27
calcite	66	62.8	calcite	64
dolomite	1.47	1.81	dolomite	2
K-feldspar	0.88	1.36	K-Feldspar	1
plagioclase 22	2.4	1.7	plagioclase	2
plagioclase 28	1.5	1.41	other	4

G2				
Peak	measurement A	measurement B		mean proportions (%)
quartz 21	23.6	25.4		
quartz 27	25.1	30.4		
quartz 36	24.5	29.7	quartz	26
calcite	62.6	68.9	calcite	66
dolomite	1.64	1.62	dolomite	2
K-feldspar	1.41	1	K-Feldspar	1
plagioclase 22	2	0.7	plagioclase	1
plagioclase 28	1	1.46	other	4

G3

Peak	measurement A	measurement B		mean proportions (%)
quartz 21	22.9	24.1		
quartz 27	24.3	23.2		
quartz 36	24.1	25.4	quartz	24
calcite	61	60.1	calcite	61
dolomite	1.29	2.01	dolomite	2
K-feldspar	1.18	2.22	K-Feldspar	2
plagioclase 22	2.4	1.5	plagioclase	2
plagioclase 28	1.12	1.2	other	11

H1

Peak	measurement A	measurement B		mean proportions (%)
quartz 21	12.2	12.3		
quartz 27	14.3	14.3		
quartz 36	14.3	14.1	quartz	14
calcite	55.1	55	calcite	55
dolomite	0.11	0.23	dolomite	0
K-feldspar	3.11	3.26	K-Feldspar	3
plagioclase 22	0	0	plagioclase	1
plagioclase 28	1.31	1.27	other	27

H2

Peak	measurement A	measurement B		mean proportions (%)
quartz 21	13.6	11.5		
quartz 27	14.9	15.9		
quartz 36	16.5	17	quartz	15
calcite	71.3	67.2	calcite	69
dolomite	0.66	0.07	dolomite	0
K-feldspar	2.06	2.35	K-Feldspar	2
plagioclase 22	0	0	plagioclase	1
plagioclase 28	1.1	0.96	other	13

H3

Peak	measurement A	measurement B		mean proportions (%)
quartz 21	13.3	13.9		
quartz 27	14.5	16.1		
quartz 36	15.6	15.6	quartz	15
calcite	57.8	59.3	calcite	59
dolomite	0.13	0.16	dolomite	0
K-feldspar	1.99	2.23	K-Feldspar	2
plagioclase 22	0	0	plagioclase	1
plagioclase 28	1.17	0.97	other	24

I1				
Peak	measurement A	measurement B		mean proportions (%)
quartz 21	11.6	9.4		
quartz 27	11.9	10.53		
quartz 36	11.4	9.4	quartz	11
calcite	103.3	85.9	calcite	86
dolomite	2.95	2.45	dolomite	2.700
K-feldspar	0.52	0.56	K-Feldspar	1
plagioclase 22	0.9	0	plagioclase	0
plagioclase 28	0.37	0.41		

I2				
Peak	measurement A	measurement B		mean proportions (%)
quartz 21	10.7	8.8		
quartz 27	10.47	9.17		
quartz 36	10.9	10.7	quartz	10
calcite	87.2	85.2	calcite	86
dolomite	2.72	2.76	dolomite	3
K-feldspar	0.53	0.73	K-Feldspar	1
plagioclase 22	0.8	0.5	plagioclase	1
plagioclase 28	0.49	0.49		

I3				
Peak	measurement A	measurement B		mean proportions (%)
quartz 21	9.3	10.4		
quartz 27	10.32	10.77		
quartz 36	9.8	11.6	quartz	10
calcite	84.3	89.6	calcite	86
dolomite	2.64	2.97	dolomite	3
K-feldspar	0.62	0.68	K-Feldspar	1
plagioclase 22	0.3	0.4	plagioclase	1
plagioclase 28	0.55	0.82		

J1				
Peak	measurement A	measurement B		mean proportions (%)
quartz 21	10.8	9.6		
quartz 27	9.47	12.6		
quartz 36	11.5	12.6	quartz	11
calcite	105.1	107.1	calcite	85
dolomite	3.73	2.16	dolomite	2.95
K-feldspar	0.14	0.29	K-Feldspar	0
plagioclase 22	1.6	0.6	plagioclase	1
plagioclase 28	0.39	0.58		

J2				
Peak	measurement A	measurement B		mean proportions (%)
quartz 21	8.1	8.7		
quartz 27	8.6	8.72		
quartz 36	14	10.3	quartz	10
calcite	97.6	98.6	calcite	87
dolomite	2.76	2.63	dolomite	3
K-feldspar	0.13	0.16	K-Feldspar	0
plagioclase 22	1	1	plagioclase	1
plagioclase 28	0.45	0.29		

J3				
Peak	measurement A	measurement B		mean proportions (%)
quartz 21	9.1	8.7		
quartz 27	9.31	9.59		
quartz 36	10.2	9.2	quartz	9
calcite	96.8	93.1	calcite	88
dolomite	1.87	2.38	dolomite	2
K-feldspar	0.17	0.46	K-Feldspar	0
plagioclase 22	0	0.1	plagioclase	0
plagioclase 28	0.34	0.34		

H1				
Peak	measurement A	measurement B		mean proportions (%)
quartz 21	12.2	12.3		
quartz 27	14.3	14.3		
quartz 36	14.3	14.1	quartz	14
calcite	55.1	55	calcite	55
dolomite	0.11	0.23	dolomite	0
K-feldspar	3.11	3.26	K-Feldspar	3
plagioclase 22	0	0	plagioclase	1
plagioclase 28	1.31	1.27	other	27

H2				
Peak	measurement A	measurement B		mean proportions (%)
quartz 21	13.6	11.5		
quartz 27	14.9	15.9		
quartz 36	16.5	17	quartz	15
calcite	71.3	67.2	calcite	69
dolomite	0.66	0.07	dolomite	0
K-feldspar	2.06	2.35	K-Feldspar	2
plagioclase 22	0	0	plagioclase	1
plagioclase 28	1.1	0.96	other	13

H3				
Peak	measurement A	measurement B		mean proportions (%)
quartz 21	13.3	13.9		
quartz 27	14.5	16.1		
quartz 36	15.6	15.6	quartz	15
calcite	57.8	59.3	calcite	59
dolomite	0.13	0.16	dolomite	0
K-feldspar	1.99	2.23	K-Feldspar	2
plagioclase 22	0	0	plagioclase	1
plagioclase 28	1.17	0.97	other	24

K				
Peak	measurement A	measurement B		mean proportions (%)
quartz 21	3.21	2.99		
quartz 27	3.08	3.39		
quartz 36	3	3.2	quartz	3.15
calcite	107.3	109.5	calcite	90.98
dolomite	5.25	5.24	dolomite	5.25
K-feldspar	0	0	K-feldspar	0.00
plagioclase 22	1.3	1	plagioclase	0.64
plagioclase 28	0.15	0.09		

L				
Peak	measurement A	measurement B		mean proportions (%)
quartz 21	4.16	3.71		
quartz 27	3.68	3.77		
quartz 36	5.4	3.5	quartz	4.04
calcite	119	117.5	calcite	90.28
dolomite	6.22	5.14	dolomite	5.68
K-feldspar	0	0	K-feldspar	0.00
plagioclase 22	1	0.2	plagioclase	0.36
plagioclase 28	0.11	0.12		

M				
Peak	measurement A	measurement B		mean proportions (%)
quartz 21	4.92	5.3		
quartz 27	4.98	5.26		
quartz 36	5.1	5.8	quartz	5.23
calcite	110.4	115.1	calcite	89.56
dolomite	5.11	4.36	dolomite	4.74
K-feldspar	0	0.01	K-feldspar	0.01
plagioclase 22	0.6	0.8	plagioclase	0.47
plagioclase 28	0.18	0.31		

N				
Peak	measurement A	measurement B		mean proportions (%)
quartz 21	3.84	3.76		
quartz 27	4.27	4.42		
quartz 36	4.8	4.5	quartz	4.27
calcite	106.7	109.3	calcite	91.69
dolomite	3.85	3.28	dolomite	3.57
K-feldspar	0	0.06	K-feldspar	0.03
plagioclase 22	0.1	0.8	plagioclase	0.46
plagioclase 28	0.72	0.2		

O				
Peak	measurement A	measurement B		mean proportions (%)
quartz 21	5.6	6.7		
quartz 27	7.09	7.63		
quartz 36	10.7	8.2	quartz	7.653
calcite	129	133	calcite	82.174
dolomite	8.29	10.1	dolomite	9.20
K-feldspar	0	0	K-feldspar	0.000
plagioclase 22	1.6	1.6	plagioclase	0.978
plagioclase 28	0.41	0.3		

Q				
Peak	measurement A	measurement B		mean proportions (%)
quartz 21	8.7	9.4		
quartz 27	8.67	8.67		
quartz 36	8.7	10.2	quartz	9
calcite	106.3	103.1	calcite	85
dolomite	5.29	5.46	dolomite	5.38
K-feldspar	0.34	0.05	K-feldspar	0
plagioclase 22	0.1	0.8	plagioclase	1
plagioclase 28	1.25	0.44		

R				
Peak	measurement A	measurement B		mean proportions (%)
quartz 21	8	7.6		
quartz 27	8.02	8.43		
quartz 36	9.2	9.2	quartz	8.41
calcite	106.5	111.4	calcite	84.00
dolomite	1.86	1.83	dolomite	1.85
K-feldspar	0.5	0.09	K-Feldspar	0.30
plagioclase 22	0	0.1	plagioclase	0.11
plagioclase 28	0.16	0.19	Clay minerals	5

Appendix B

Table B1: Raw ^{210}Pb and ^{137}Cs data

#	from (cm)	to (cm)	sample volume (cm^3)	sample weight (g)	water content (%)	Ra-226 [Bq/kg]	2s Err.	Cs-137 [Bq/kg]	2s Err.	Pb-210 [Bq/kg]	2s Err.
1	0	0.4	2.3	0.9	65.0	0	0	33.1	5.0	162.8	46.6
2	0.4	0.8	2.2	0.8	69.6						
3	0.8	1.2	2.6	0.4	85.7	8	3	34.7	4.7	90.3	34.3
4	1.2	1.7	4.0	1.8	63.1						
5	1.7	2.3	4.1	1.9	62.6	15.4	3.1	32.3	2.7	119.2	25.5
6	2.3	2.8	3.8	1.8	60.6						
7	2.8	3.4	3.9	2.0	59.2	14	5	41.3	3.9	164.8	32.8
8	3.4	3.8	2.7	1.6	55.0	18.0	4.0	43.4	4.2	186.5	34.1
9	3.8	4.3	3.5	1.9	57.7						
10	4.3	5.3	6.3	3.5	56.8	30.2	4.5	13.9	3.3	79.9	34.7
11	5.3	5.8	1.9	0.1	59.1						
12	5.8	7.7	3.3	1.7	58.4	34.5	1.2	25.6	1.3	112	16.6
13	7.7	8.2	3.1	2.0	51.9						
14	8.2	8.7	3.2	2.4	46.7	22	6	55.7	7.6	178.8	48.1
15	8.7	9.2	3.1	2.3	47.6						
16	9.2	9.8	2.4	1.8	47.3	33.7	4.9	13.7	2.5	40.4	25.2
17	9.8	11	2.8	2.0	47.9						
18	11	11.2	0.7	0.5	52.6	39.4	19.0	63.6	15.0	172.6	129.1
19	11	11.4	2.3	1.9	42.4						
20	11.4	12	3.6	2.5	49.2	38.4	4	60.6	4.0	114.1	25.4
21	12	13	5.0	3.1	53.1						
22	13	13.5	5.0	2.7	57.6	29.6	3.4	64.8	5.5	112.2	31.7
23	13.5	14	3.6	2.1	56.2						
24	14	14.5	4.9	3.3	50.2	29.9	3.2	31.7	3.8	76.1	23.8
25	14.5	17	17.5	9.7	56.7						
26	17	17.5	3.5	2.7	46.5	34.2	4	35.6	2.2	63.9	17.4
27	17.5	19.5	15.8	11.4	48.2	25.0		36.2	3.1	63.6	19.7
28	19.5	20.3	4.2	2.6	52.7	36.1	5.5	86.8	7.0	57.1	29.0
29	20.3	20.7	5.1	3.0	54.5	31.5	3.3	95.6	6.0	121.6	26.7
30	20.7	21.3	5.5	3.3	54.4	30.4	3.9	76.9	5.5	100	26.5
31	21.3	21.7	5.2	3.3	52.8						
32	21.7	22.5	3.3	2.1	52.4	36.4	3.7	41.5	2.9	75.5	19.8
33	22.5	23.2	5.6	4.0	48.8						
34	23.2	23.7	4.4	3.0	49.9	44.6	3.0	94.6	4.8	133.3	27.5
35	23.7	24.5	4.1	2.7	50.9						
36	24.5	25.2	7.0	4.1	54.8	36.1		74.2	3.8	83.5	17.8
37	25.2	25.9	5.8	3.7	51.8						
38	25.9	26.5	5.1	3.2	52.3	34	5	112.5	5.7	97.5	21.1
39	26.5	27.2	5.1	3.3	52.0	34.5	2.6	154.4	6.6	109.9	21.6
40	27.2	27.7	5.4	3.4	52.5	38.1	5	184	10.9	90.6	33.2

Table B1 continued

#	from (cm)	to (cm)	sample volume (cm^3)	sample weight (g)	water content (%)	Ra-226 [Bq/kg]	2s Err.	Cs-137 [Bq/kg]	2s Err.	Pb-210 [Bq/kg]	2s Err.
41	27.7	28.5	4.3	2.4	56.7	29.8	6.3	207.2	12.7	46.1	32.7
42	28.5	29.2	6.0	3.9	52.0	24.1	2.9	158.4	7.5	53.9	20.7
43	29.2	29.9	4.8	3.1	52.2	31.0	5.4	58.1	5.4	77.3	26.5
44	29.9	30.7	6.9	4.6	51.1						
45	30.7	31.2	4.9	3.1	52.9	29.9	1.9	72.9	3.1	87.7	15.1
46	31.2	31.8	5.8	3.1	57.7						
47	31.8	32.5	4.9	2.4	60.9	20.8	2.2	4.3	1.4	48.3	16.1
48	32.5	33.2	7.6	4.2	56.9						
49	33.2	34	6.0	3.3	57.2						
50	34	34.8	5.3	3.5	51.0	23.4	3.6	0	0	43.8	23.2
51	34.8	35.4	5.0	4.1	43.6	32.9	4.7	0	0	52.2	24.7
52	35.4	36.5	8.9	6.3	48.8						
53	36.5	37	1.9	1.0	56.8						
54	37	37.5	5.3	2.5	61.3						
55	37.5	38	5.5	2.8	59.6						
56	38	38.5	6.6	3.4	59.0						
57	38.5	39.5	6.3	3.3	58.1						
58	38.4	39	5.0	3.0	53.7						
59	39	39.5	5.0	3.2	52.4	31.7	5	0		35.2	15.4
60	39.5	40.1	3.2	2.0	52.7						
61	40.1	40.8	3.5	2.0	55.7	26.1	2.8	0		31.6	16.8
62	40.8	41.4	6.0	3.4	55.9						
63	41.4	42.1	4.1	2.6	52.0	27	5	0		36.9	31.9
64	42.1	43	8.1	5.2	52.2						
65	43	43.7	6.6	4.0	54.2	27.6	3.1	0		33.2	19.8
66	43.7	44.1	2.5	1.5	53.5						
67	44.1	44.8	8.1	5.2	52.1	41.2	3.5	0		49.5	17.2
68	44.8	45.2	1.3	0.7	59.9						
69	45.2	46	6.2	3.9	53.1	31.1	3.4	0		77.2	23.9
70	46	46.5	3.3	1.7	59.4						
71	46.5	47.3	4.8	3.1	52.2	41.5	8.1	0		37.5	34.2
72	47.3	48.2	4.3	2.6	54.2	29	5			55	25
73	48.2	49.1	7.5	4.4	54.7						
74	49.1	50	5.2	3.4	51.0	34.9	2.3	0		51.3	12.9
75	50	50.9	9.4	5.8	53.5						
76	50.9	51.9	5.9	3.4	55.4	30	4	0		37	21
77	51.9	52.5	6.4	3.5	57.0	28	7	0		52.9	29.4
78	52.5	53.5	8.5	4.6	57.2						
79	53.5	53.8	4.8	2.3	61.7	28.5	2.9	0		45.3	19.3
80	53.8	54.2	2.8	1.5	58.3	22	4			36	21
81	54.2	55.1	9.0	4.9	57.4	36.0	1.4	0		49.8	9.2
82	55.1	55.6	6.7	3.4	59.8	30	2	0		31	15

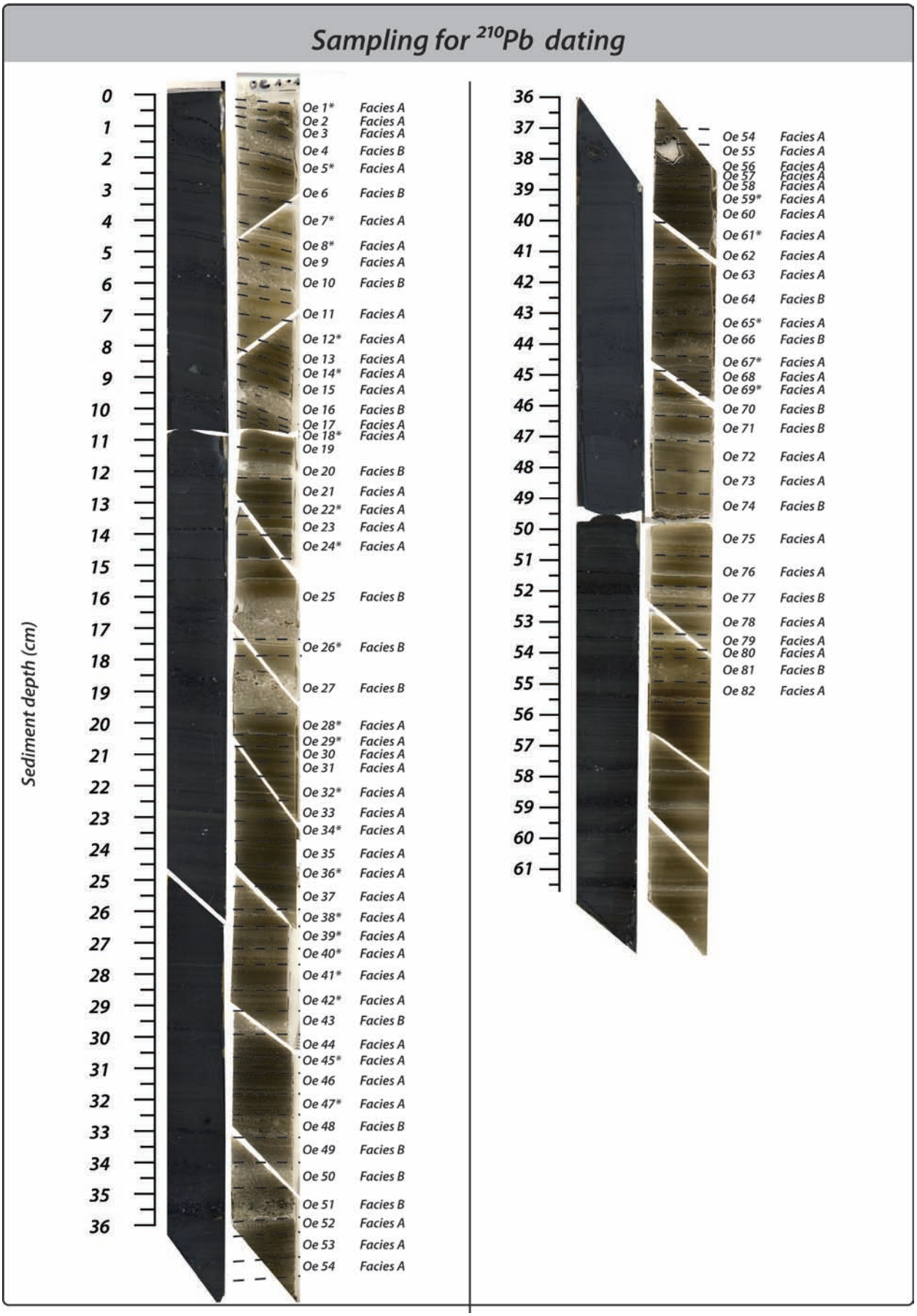

Figure 23: ^{210}Pb sampling of the mastercore. The top 55.6 cm were sampled according to homogenious sedimentary facies. Note that the dashed lines denote the boundaries between the individual samples. In addition, the samples were classified as facies A (varves) or facies B (turbidites). Samples marked with asterisk were used for the calculation of the CRS and composite CRS model.

Table B2: Raw data SCP counts

#	depth (cm)	sample (g)	tare E-flask [g]	tare E-flask+ sample [g]	tare + sample (-aliquot) [g]	SCP's per Petri dish	factor	number of SCP's per g dry sediment
1	0.2	0.0532	42.0885	96.7664	82.7502	16	3.901	1173
2	0.6	0.0538	41.875	90.0544	75.9261		3.410	
3	1	0.0564	42.0841	84.0105	69.8837	15	2.968	789
4	1.45	0.0537	45.7477	96.4952	83.532		3.915	
5	2	0.0539	44.3728	87.4368	73.8854	13	3.178	766
6	2.55	0.0576	42.2516	87.382	77.1069		4.392	
7	3.1	0.0555	45.6753	95.8631	85.8095	14	4.992	1259
8	3.6	0.0521	42.2355	91.1597	78.0695		3.737	
9	4.05	0.0518	42.1128	91.7921	77.532		3.484	
10	4.8	0.0577	44.3702	88.9959	73.8888	12	2.954	614
11	5.55	0.0542	42.2295	92.1923	76.5177		3.188	
12	6.75	0.0541	45.7518	95.8659	82.0323	15	3.623	1004
13	7.95	0.0558	41.8242	98.5358	83.6661		3.814	
14	8.45	0.0535	42.1079	96.603	80.5115	28	3.387	1772
15	8.95	0.0599	41.8119	84.5472	69.1371		2.773	
16	9.5	0.0504	44.4701	95.4067	81.2225		3.591	
17	10.4	0.0561	44.3455	88.5886	74.1954	31	3.074	1699
18	11.1	0.0595	45.828	89.0421	76.1036	32	3.340	1796
19	11.2	0.0552	44.4143	88.6372	74.4562	36	3.118	2034
20	11.7	0.0531	45.92	92.5204	77.0313	39	3.009	2210
21	12.5	0.0528	45.9082	85.3077	72.4432	50	3.063	2900
22	13.25	0.0572	45.8531	94.9355	80.7516	39	3.460	2359
23	13.75	0.0519	44.4419	87.11	72.9747	35	3.019	2036
24	14.25	0.0574	44.2728	86.9904	73.9647	30	3.279	1714
25	15.75	0.0569	44.3997	96.2041	82.6195	25	3.813	1676
26	17.25	0.055	124.8915	169.3302	155.4516		3.202	
27	18.5	0.0503	124.2918	166.5933	155.2886	18	3.742	1339
28	19.9	0.0513	124.6822	166.7359	152.8453		3.027	
29	20.5	0.0579	123.8628	167.4188	152.8281	5	2.985	258
30	21	0.0568	123.8038	167.508	149.9648		2.491	
31	21.5	0.0556	56.514	87.803	75.602	8	2.564	369
32	22.1	0.0576	61.059	91.565	78.986		2.425	
33	22.85	0.0529	58.87	89.807	78.079	9	2.638	449
34	23.45	0.0525	57.963	82.32	72.699		2.532	
35	24.1	0.0511	62.449	94.338	81.756	17	2.534	843
36	24.85	0.0552	62.47	91.609	77.967		2.136	
37	25.55	0.0553	57.748	85.288	72.885	15	2.220	602
38	26.2	0.0525	57.679	88.71	75.071		2.275	
39	26.85	0.0543	61.464	90.271	76.645	6	2.114	234
40	27.45	0.0526	57.185	89.179	74.696		2.209	
41	28.1	0.0558	57.834	84.262	70.752		1.956	
42	28.85	0.0504	61.433	92.666	79.401		2.355	
43	29.55	0.054	60.234	84.981	73.349		2.127	

Table B2 continued

#	depth (cm)	sample (g)	tare E-flask [g]	tare E-flask+ sample [g]	tare + sample (-aliquot) [g]	SCP's per Petri dish	factor	number of SCP's per g dry sediment
44	30.3	0.0537	60.858	91.683	79.679		2.568	
45	30.95	0.0543	61.013	89.713	76.921	1	2.244	41
46	31.5	0.0544	56.096	85.384	72.6		2.291	
47	32.15	0.0556	56.86	79.88	66.253		1.689	
48	32.85	0.0538	57.17	85.55	70.314		1.863	
49	33.6	0.0524	56.177	90.677	78.438	5	2.819	269
50	34.4	0.056	58.173	84.055	70.445		1.902	
51	35.1	0.0536	62.199	92.789	80.144	4	2.419	181
52	35.95	0.0538	58.114	83.998	68.132		1.631	
53	36.75	0.0532	57.555	86.731	72.941	3	2.116	119
54	37.25	0.0545	61.74	90.979	77.267		2.132	
55	37.75	0.0565	57.225	87.895	71.629	1	1.886	33
56	38.25	0.0553	57.466	88.796	76.571		2.563	
57	39	0.0524	60.76	90.983	77.877	6	2.306	264

Table B3: Varve thickness from AD 1907- 1986

year AD	varve thickness(mm)	year AD	varve thickness(mm)
1986	4.44	1946	2.078
1985	4.442	1945	2.006
1984	3.437	1944	3.295
1983	3.726	1943	1.505
1982	8.308	1942	2.507
1981	4.442	1941	6.518
1980	3.011	1940	2.868
1979	4.153	1939	1.065
1978	4.297	1938	4.454
1977	3.011	1937	1.955
1976	2.868	1936	3.652
1975	3.151	1935	2.364
1974	5.013	1934	3.222
1973	2.148	1933	2.507
1972	1.575	1932	2.364
1971	2.725	1931	4.942
1970	4.013	1930	2.078
1969	3.724	1929	3.08
1968	3.583	1928	3.51
1967	3.437	1927	4.727
1966	2.291	1926	3.366
1965	3.891	1925	4.082
1964	4.297	1924	4.156
1963	4.299	1923	3.526
1962	2.439	1922	2.221
1961	2.578	1921	1.808
1960	4.01	1920	2.293
1959	5.301	1919	1.575
1958	1.146	1918	1.003
1957	1.289	1917	1.564
1956	2.721	1916	1.307
1955	9.027	1915	0.871
1954	5.158	1914	1.084
1953	2.005	1913	0.871
1952	1.361	1912	1.155
1951	1.79	1911	2.167
1950	2.793	1910	1.945
1949	1.074	1909	4.097
1948	0.859	1908	1.564
1947	1.289	1907	2.816